A Kinetic Model for G protein-coupled Signal Transduction in Macrophage Cells

Patrick Joseph Flaherty

Electrical Engineering and Computer Sciences
University of California at Berkeley

Technical Report No. UCB/EECS-2007-4
http://www.eecs.berkeley.edu/Pubs/TechRpts/2007/EECS-2007-4.html

January 6, 2007

A Kinetic Model for G protein-coupled Signal Transduction in Macrophage Cells

by

Patrick Joseph Flaherty

B.S. (Rochester Institute of Technology) 2000
M.S. (University of California at Berkeley) 2003

A dissertation submitted in partial satisfaction of the
requirements for the degree of
Doctor of Philosophy

in

Engineering-Electrical Engineering and Computer Sciences
and the Designated Emphasis
in
Communication, Computation, and Statistics
and
Computational Biology

in the

GRADUATE DIVISION
of the
UNIVERSITY OF CALIFORNIA, BERKELEY

Committee in charge:
Professor Michael I. Jordan, Chair
Professor Adam P. Arkin
Professor Richard M. Karp

Fall 2006

The dissertation of Patrick Joseph Flaherty is approved:

Chair Date

Date

Date

University of California, Berkeley

Fall 2006

A Kinetic Model for G protein-coupled Signal Transduction in Macrophage Cells

by

Patrick Joseph Flaherty

Abstract

A Kinetic Model for G protein-coupled Signal Transduction in Macrophage Cells

by

Patrick Joseph Flaherty

Doctor of Philosophy in Engineering-Electrical Engineering and Computer Sciences

and the Designated Emphasis

in

Communication, Computation, and Statistics

and

Computational Biology

University of California, Berkeley

Professor Michael I. Jordan, Chair

Macrophage cells that are stimulated by two different ligands which bind to G protein-coupled receptors (GPCRs) usually respond as if the stimulus effects are additive, but for a minority of ligand combinations the response is synergistic. The G protein-coupled receptor system integrates multiple, perhaps conflicting, signaling cues from the environment in order to actuate cell morphology, gene expression, ion homeostasis and other physiological states. We study, in detail, the effects of the two signaling molecules complement factor 5a (C5a) and uridine diphosphate (UDP) on the intracellular second messenger calcium to elucidate

principals that govern the mechanism of G protein-coupled signal transduction. We have developed a formal hypothesis, in the form of a kinetic model, for the mechanism of action of this GPCR signal transduction system using data obtained from RAW264.7 macrophage cells. Bayesian statistical methods are employed to formally approach uncertainty and tie the model to experimental data. The model is entertained as a tool in the design of investigative experiments. The model accurately predicts a synergistic region in the calcium peak height dose response that results when cells are simultaneous stimulated by C5a and UDP. Though this model is not a complete representation of the G protein-coupled signal transduction system and contains many approximations, it is consistent with our experimental observations and is a useful substrate for further experimentation.

Finally, we address the problem of the design of robust experiments for the G protein-coupled signal transduction model. Classical optimal experiment design methods have not been widely adopted in practice for biological systems, in part because the resulting designs can be very brittle if the nominal parameter estimates for the model are poor, and in part because of computational constraints. We present a method for robust experiment design based on a semidefinite programming relaxation. We present an application of this method to the design of experiments for a complex calcium signal transduction pathway, where we have found that the parameter estimates obtained from the robust design are better than those obtained from an "optimal" design.

Professor Michael I. Jordan
Dissertation Committee Chair

To my family.

Acknowledgments

Many people have volunteered their aid through my work on projects in graduate school and deserve recognition for their selfless help. Though research involving a combination of statistics, engineering and biology is now common, my advisors Michael Jordan and Adam Arkin took a great risk years ago to mentor such research and should be recognized. They have guided, tutored, questioned, challenged and cheered me throughout my time in graduate school and their direction has helped me find my own place in the academic world. The students in the Jordan group were a constant source of learning. I have Alice Zheng to thank for telling me about the Jordan group and encouraging me to attend the group meetings. Dave Blei spent hours teaching me the details of his research so that I would be able to use it for my own.

Guri Giaever believed in me and used my research before I might have even used it myself. Guri's faith helped me to believe that my work can be useful and must meet the highest standards. My work with the Alliance for Cellular Signaling began with a short meeting with Mel Simon. Even since I have looked to Mel for guidance and advise in all of my work. He's the most insightful, idealistic and kind scientist I have known.

I first joined the Arkin lab after meeting with Denise Wolf and thank her for her inspiration and infectious, but playful thirst for knowledge. Tim Ham and Robin Osterhout were there even after hours of studying for prelim exams in room 214. Matt Onsum introduced me to the project of this thesis and deserves much of the credit for making the first, but most important steps that I followed. Leor Weinberger taught many of us in the Arkin lab the real meaning of doing good science and that success comes only after hard work.

Even as an undergraduate student Richie Koche showed his potential as a great scientist. He knew when to work late and when to drag me out of lab for a break after a full day.

I first met Shilpa Shroff in the Arkin Lab when I needed a place to live. Shilpa offered her apartment and years later I've found a best friend. Finally and most importantly, my family has always supported me with phone calls, cookies, trips home to the farm and constant reminders of the truly important things in life.

Contents

List of Figures

List of Tables

Chapter 1

Introduction

We have developed a formal hypothesis, in the form of a kinetic model, for the mechanism of action of the G protein-coupled receptor (GPCR) signal transduction system in macrophage immune cells. There are three main contributions of this work:

- a kinetic model for $G\alpha_q$ and $G\alpha_i$ coupled receptor pathways,
- the use of rigorous statistical methods to estimate uncertain parameters with heterogeneous data in a kinetic model,
- an experiment design method that uses a complex kinetic model and is robust to uncertain parameter estimates.

The G protein-coupled receptor system integrates, filters and responds to multiple, perhaps conflicting, signaling cues from the environment. Receptors in this superfamily respond to diverse intercellular signals such as: light, neurotransmitters, odorants, amino acids, hormones, nucleotides and chemokines (Kroeze et al., 2003). This receptor system

accounts for 40-50% of modern medicinal drug targets (Filmore, 2004) but only 10% of the known receptors are targeted by drugs (Kroeze et al., 2003). G protein-coupled receptors and associated extracellular messengers include: β-adrenergic receptors for epinephrine, rhodopsin receptors for photons, opioid receptors for endorphins and 5-hydroxytryptamine receptors for serotonin (Goodman et al., 2006).

Because the G protein signal transduction system is complex and involves many interacting species, we cannot at this time elucidate the entire mechanism of the system. Instead we study, in detail, the effects of two signaling molecules (C5a and UDP) on the intracellular second messenger calcium to elucidate underlying principals that govern the mechanism of G protein-coupled signal transduction.

C5a is part of the complement system which is part of the innate immune system. C5a, a 74 amino acid peptide whose precursor is produced in the liver, is activated at the site of infection (Alberts, 2002, Chapter 25). It is a potent anaphylotoxin and a strong chemoattractant for many immune system components including: neutrophils, basophils, eosinophils, leukocytes, monocytes and macrophages (Allegretti et al., 2005). The complement system is thus named because it was first discovered to "complement" and augment the opsonization activity of antibodies (Janeway and Travers, 1996, Chapter 2). Today, it is recognized that the complement system components have three main functions: (1) to aid opsonization, (2) as a chemoattractant for phagocytes such as macrophages and (3) as a damaging agent to certain bacterial membranes. For macrophages, which express the C5a receptor, the small peptide C5a functions both as a chemoattractant and as an opsonin to target certain pathogens for phagocytosis.

Extracellular nucleotides, such as UDP, function in autocrine and paracrine signaling systems. Macrophage cells and their precursors, monocytes, express several receptors that are specific to extracellular nucleotides, but the physiological role of the signal is not entirely known. Warny et al. (2001) showed that the P2Y6 receptor, which is sensitive to UDP, regulates the production and secretion of the chemokine interleukin 8 (IL-8) in monocytes.

The C5a and P2Y receptor systems are expressed in macrophage cells and the derivative cell line, RAW264.7, used in this study. Macrophage cell are a central component of the adaptive and innate immune system in humans. These cells have a long life, reside in tissue and are usually the first to encounter invasive pathogens (Alberts, 2002, Chapter 25). Their primary role is to engulf by phagocytosis pathogens and recruit other phagocytic cells such as neutrophils from the blood stream by secreting chemokines and cytokines. If the pathogen is too large, phagocytes may also surround it and secrete their lysosomal products by exocytosis.

To use the model as a predictive tool in the design of experiments, rigorous statistical methods are employed to approach uncertainty in the model and data. These statistical methods allow us to build a bridge between scientific models and experimental data. Since we have significant prior information about the system, we have chosen to use Bayesian methods which allow use to naturally incorporate this information. The choice is a matter of appropriateness for this problem. Each scientific problem is unique and requires careful consideration of the application. At the end we obtain a posterior distribution for model parameters and predictions. These distributions represent our posterior uncertainty in our

model predictions and parameter values after observing experimental data.

The experimental design method presented here is a step towards a practical method for using the complex kinetic model to inform the design of future experiments. Locally optimal experiment design methods make use of the nonlinear differential equation model by maximizing a function of the first derivatives of the model with respect to the parameters. However, these parameter estimates are themselves uncertain which makes the function to be optimized uncertain. We formulate and solve the problem efficiently using semidefinite programming. This method is demonstrated on a simple chemical model and a calcium signaling model.

The common thread through this dissertation is the formal application of statistical methods to complex uncertain biological systems. The model structure functions as a formal hypothesis of the G protein-coupled receptor signal transduction mechanism. That hypothesis is refined by incorporating experimental data, with proper accounting for uncertainty, using Bayesian statistical methods. The refined model is used to predict the outcome of novel experiments and experimental data are used to check the validity of the model. If the model prediction and observed outcome differ significantly, the model may be further revised. The process of prediction and revision is continued until a reasonably complete understanding of the mechanism is obtained. This classical methodology is applied using modern statistical technology to a system and data set that are too complex to reason about without these computational aids. The methods we have developed for this task are demonstrated on a scientifically important system and are scalable to more complex biological systems.

Scientific ideas earn their validity not necessarily only because they are correct, but because they are developed and tested in the right way. There is still much to be learned about these systems and the story told here is not complete. However, we draw useful scientific conclusions by properly applying rigorous methods. Therefore, the methods and the answers to which they lead are complementary and necessarily presented together.

Chapter 2

G protein-coupled Receptor Signal Transduction Model

Receptors that couple to heterotrimeric GTP-binding regulatory proteins (G proteins) make up a large superfamily of drug targets. Roughly half of all nonantibiotic prescription drugs target this family of receptors (Goodman et al., 2006).

G protein-coupled receptors (GPCRs) are composed of seven α-helices that span the plasma membrane. GPCRs contain an extracellular domain that is activated by an agonist. The intracellular domain binds a guanine nucleotide associated heterotrimer made up of α, β and γ subunits. As a signaling unit, the G protein complex effectively acts as a heterodimer. The β and γ units are bound *in-vivo* and only dissociate in detergent. The G protein subunits remain bound to the cytoplasmic side of the plasma membrane through the pleckstrin homology (PH) domain of the β unit.

There is significant diversity in the G protein isoforms. One review reports that there are 21 gene products known to encode α units, five that encode β units and 11 that

encode γ units (Quitterer and Lohse, 1999). It has also been reported that the distribution is 15, 5 and 10 respectively (Berg et al., 2002). These numbers are likely to change as more is learned about the system. In theory there are approximately 1000 different combinations of heterotrimers. It is unlikely that all combinations occur in nature (Berg et al., 2002). It is thought that the α unit has specificity to the receptor and allows the cell to respond to different stimulus while the $\beta\gamma$ dimer confers membrane localization (Goodman et al., 2006). Whether the $\beta\gamma$ units are completely interchangeable among α units is still a matter of debate (Krumins and Gilman, 2006).

The seven transmembrane spanning α-helix receptor changes conformation upon binding a ligand. The bound receptor induces a conformational change in the associated G protein heterotrimer which reduces the α subunit's affinity for GDP and increases its affinity for GTP resulting in an exchange of GDP for GTP. The α-GTP dissociates from the $\beta\gamma$ subunits and both can bind to and modify other proteins. The α subunit has intrinsic GTPase activity which hydrolyzes the GTP nucleoside to GDP and P_i, inactivating the α subunit. Other GTPase proteins such as phospholipase C β (PLCβ) and regulators of G protein signaling (RGS) can accelerate the hydrolysis. The α-GDP has a high affinity for $\beta\gamma$ and the two subunits associate returning the complex to its initial state. A simplified schematic of this switch is shown in Figure 2.1. The signaling "off" state is Gα-GDP and the signaling "on" state is Gα-GTP. The hydrolysis step is relatively slow and takes seconds to minutes (Berg et al., 2002; Bourne et al., 1991).

Adenylate cyclase and phospholipase C β are the main effectors for active G protein α-GTP and $\beta\gamma$ subunits. Adenylate cyclase converts ATP into cyclic AMP (cAMP)

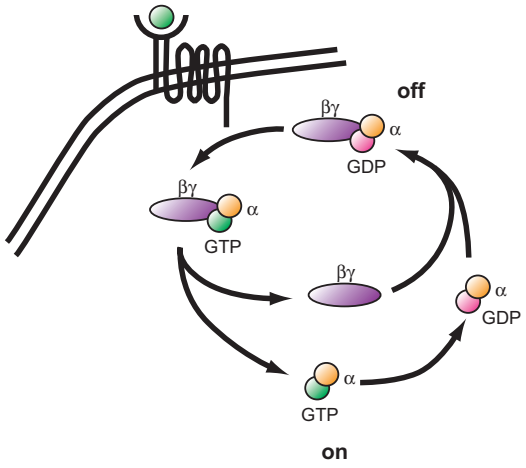

Figure 2.1: G proteins act as molecular switches. The G protein signal transduction system is turned "on" when an agonist is bound to an associated receptor and "off" by a timing mechanism controlled by the rate of GTP hydrolysis.

and phospholipase C converts phosphatidyl inositol 4,5-biphosphate (PIP2) into inositol 1,4,5-triphosphate (IP3) and diacylglycerol (DAG). IP3 activates IP3-gated channels in the endoplasmic reticulum (ER) to release calcium into the cytosol. Calcium and cAMP are two important second messengers because they can bind to many other proteins and affect gene transcription levels, protein phosphorylation states, protein localization and other cellular processes. In this work, we have focused on the G protein signal transduction system from agonist binding to calcium release.

Many G protein-coupled receptors become desensitized to a sustained agonist concentration. The receptor system appears to respond to a change in the relative amount of agonist, not the absolute amount within a certain dynamic range. The primary mechanism for adaptation appears to be covalent modification (e.g. phosphorylation or methylation). G protein receptor kinases and other specific protein kinases phosphorylate serine or threonine residues on receptor proteins that are bound to agonist, but not receptor proteins

that are not bound to agonist. Phosphorylated receptors are usually targeted for recycling in the lysosome by β-Arrestin. In the lysosome, the receptor and ligand are decoupled, the receptor is returned to the cellular membrane and the ligand is returned to the extracellular region (Lauffenburger and Linderman, 1993, section 5.4). Protein kinase C (PKC) phosphorylates and inactivates downstream proteins such as PLCβ and prevents them from being activated by Gα-GTP or G$\beta\gamma$. A second mechanism for adaptation is competitive binding at the inositol tri-phosphate (IP3) receptor on the endoplasmic reticulum membrane. The receptor acts as a channel for Ca^{2+} flux from the ER to the cytosol upon binding IP3, but is inactivated if Ca^{2+} binds to the receptor. This mechanism was elegantly modeled as an *adaptation box* module by Segel et al. (1986).

2.1 Model Structure

Models of cellular biochemical systems can broadly be classified as either phenomenological or kinetic. Phenomenological models attempt to capture salient features in the data without particular regard to the physical mechanisms which may give rise to those features. This type of model is useful when the physical mechanism is unknown or too complicated to realistically represent dynamically. Mendelian inheritance and the coin tossing probability models are good examples of such phenomenological models. Kinetic models are useful in other ways. By directly representing the physical laws that give rise to a phenomena we can check the validity of our hypothesis and search for missing components in that hypothesis - refining our model until it is both representative of the mechanism and adequately fits the experimental evidence. Familiar kinetic models include those for billiard ball dy-

namics based on Newtonian mechanics and Kirchoff's current and voltage laws based on Maxwell's equations for conservation of charge. In practice most models are a mix of the two philosophies, but lean more towards one.

We have opted for the latter methodology, a kinetic model, in this work. This model is based on the law of mass action which can be derived from thermodynamic equilibrium arguments (Nelson et al., 2004). We have primarily maintained this approach except in some specific instances where too little mechanistic information is available. We judge the utility of our model using quantitative and rigorous statistical analysis of the fit to experimental data. In the end we judge our effort by the idea that "Not all models are correct, but some are useful." (Box et al., 1978).

2.1.1 Background

One of the first models for IP3-induced calcium release was proposed by Meyer and Stryer (1988). In their model, calcium enhances its own release by positive feedback on PLC. Upon exhausting the stores of calcium (e.g. the endoplasmic reticulum), they are replenished by ATPase pumps and IP3 is hydrolyzed to restore PIP2. This model still serves as a core for most modern models of the system as reviewed in (Lauffenburger and Linderman, 1993, pp. 206).

The model by Keizer and De Young (1992) uses a mechanism of IP3 receptor adaptation by which calcium inhibits its own release. In their model, calcium also enhances its own release, as in the Meyer and Stryer (1988) model, by enhancing the activity of PLC. The model by Cuthbertson and Chay (1991) includes the effect of PKC on G protein signaling. By including positive and negative feedback components, their model was shown

to have dynamics that permit oscillations and pulses in the calcium concentration. The Swillens and Mercan (1990) model includes IP4 (inositol 1,3,4,5-tetrakiphosphate) as an inhibitor of calcium release.

Each of these models and others were justified and derived on the basis of different data in different cell types. In some very important experiments Harootunian et al. (1991) tested the predictions made by several models in REF52 fibroblasts. They found the model that included calcium enhancement of its own release through PLC and calcium store depletion agreed with their experiments.

Three recent models have improved the quality of these initial models. Lukas (2004a,b) used available literature data and new experimental results on the calcium response to bradykinin stimulation. Their work compares the calcium response over a range of doses predicted by the model to experimentally measured values and finds good agreement. The Mishra and Bhalla (2002) model investigates the role of IP4 as a signal coincidence detector in the GPCR pathway. The focus of this model is mainly on inositol phosphate metabolism. Their work investigates the interesting question of model sensitivity, but does not compare the model predictions to experimental data. The model by Lemon et al. (2003) predicts the calcium response to UTP stimulation. The model is compared to some experimental data, but the final model involves several questionable linearizations and the comparison to experimental data is limited.

None of the previously reviewed models addresses multiple ligand signals. Furthermore, most analyses of the models address dynamical issues such as oscillations, but neglect a careful and rigorous comparison of the model to data.

2.1.2 Overview

Figure 2.2 shows the overall structure of our model. The two main motifs at work in this model are: (1) combinatorial control and (2) multiple feedback regulation loops.

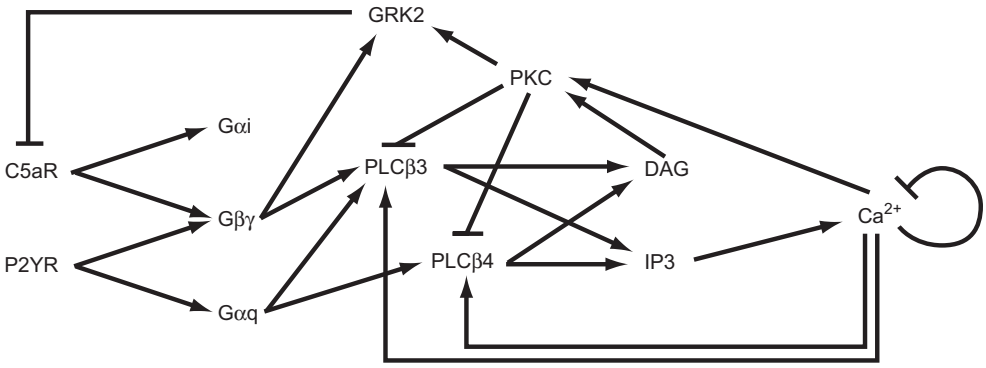

Figure 2.2: Simplified schematic of GPCR signal transduction pathway for C5a and P2Y receptors. Upon specific ligand binding to the receptor, the G protein heterotrimer dissociates to free Gα-GTP and G$\beta\gamma$. Both are able to bind specific isoforms of PLCβ and catalyze the synthesis of IP3 and DAG from PIP2. PLCβ acts as a GTPase for Gα-GTP and G$\beta\gamma$ has a high affinity for Gα-GDP. IP3 binds to specific receptor-channels on the membrane of the ER to release Ca^{2+} in to the cytosol. DAG and Ca^{2+} bind to and activate PKC which phosphorylates and inactivates PLCβ. GRK is activated once it is phosphorylated by PKC and is localized to the cellular membrane by G$\beta\gamma$. GRK phosphorylates the C5a receptor which inactivates it.

Combinatorial Control The molecular diversity in key signaling isoforms leads to a combinatorial control structure from receptor activation to calcium release. In our model, $G\alpha_q$ activates both PLCβ3 and PLCβ4 which means that UDP signaling goes through both of these isoforms. $G\alpha_i$ does not activate PLCβ, but G$\beta\gamma$ does activate PLCβ3. Both $G\alpha_q$ and $G\alpha_i$ have a G$\beta\gamma$ subunit that can activate PLCβ3. Because specific Gα subunits activate specific PLCβ isoforms, there is the capacity for the signaling network to integrate co-incident signals such that specific ligand combinations yield unique calcium responses.

Multiple Feedback Regulation Loops Calcium participates in processes that both enhance and inhibit its own release. Calcium enhances its own release by binding to the EF-hand domain on PLCβ and is required for PLCβ to hydrolyze PIP2 into IP3 and DAG. Calcium inhibits its own release by binding to and inactivating the IP3-gated channel in the ER and by binding to PKC, which inactivates PLCβ. The dynamic change in calcium concentration depends on the kinetic constants of these feedback reactions. In this model, protein kinases PKC and GRK2 inhibit the production of IP3 when the cell is stimulated with C5a. However, when the cell is stimulated with UDP, activated GRK2 is generated even though the C5a receptor is inactive. This process precharges the GRK2-mediated feedback inhibition for C5a in the model.

The details of the model, which are shown in a less simplified form in Figure 2.3, are both important and informative. We have attempted to synthesize and represent experimental information reported in scientific literature over approximately the past 20 years. In many instances exact molecular concentrations or rate constants are unknown and we have made informed guesses as to the true parameter values. In other cases, we have drastically simplified the complexity of the system in order to focus on the mechanisms that are central to our model. Population measurements on the calcium response are used to estimate the posterior distribution of the parameters in the system.

Even with judicious simplifications, this model is still quite complex. We detail the kinetic equations that form the substance of the reactions diagramed in Figure 2.3 in the following sections.

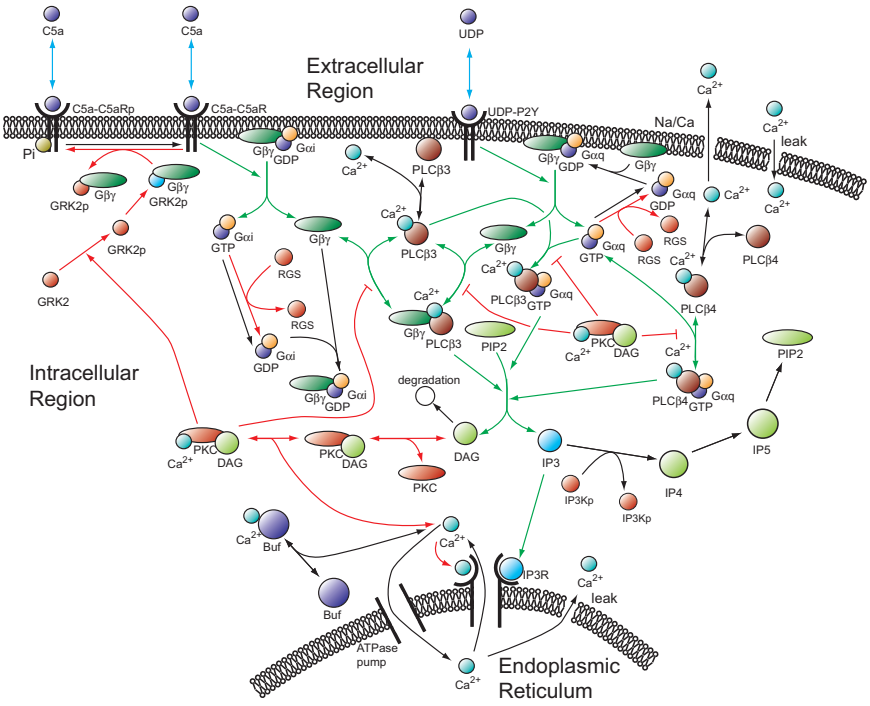

Figure 2.3: Detailed schematic of GPCR signal transduction pathway for C5a and P2Y receptor systems. Small molecules including GTP, GDP ligands and Pi are colored blue. Membrane bound proteins are colored light green. Protein kinases and RGS's are colored red. Gα subunits are orange. G$\beta\gamma$ subunits are colored dark green. Phospholipase isoforms are colored maroon. Calcium ions are turquoise. Reaction occurring in the extracellular medium are colored turquoise. Feedback reaction arrows are colored red and forward reactions are colored green.

2.2 Receptor Reactions

Table 2.1 shows the receptor-ligand binding reactions for C5a and UDP. The constant k_f is the effective forward reaction rate constant and k_r is the reverse reaction rate constant in the standard mass action kinetics formulation (Segel, 1991; Nelson et al., 2004).

Reaction			k_f (μM^{-1}s^{-1})	k_r (s^{-1})	References
UDP + P2Y	$\rightleftharpoons$	UDPC	13.20*	3.62*	
C5a + C5aR	$\rightleftharpoons$	C5aC	92.41*	0.38*	

Table 2.1: Receptor activation reaction rate constants.

2.2.1 P2Y Receptor

The P2Y class of receptors bind to purine nucleotides. For example, the P2Y1 receptor has affinity for ADP, the P2Y6 receptor is activated by UDP and the P2Y2 receptor is activated by UTP (Siegel et al., 2006). At least 5 members of the P2Y family of receptors are expressed in RAW264.7 cells as assayed by rtPCR and microarray experiments. Knockdown (shRNAi) experiments for the P2Y6 show very little change in population calcium response but a knockdown of P2Y2 does show a decrease in the response[1]. Assuming that the P2Y6 receptor is in fact a sensing component for UDP in this cell type, this evidence suggests that more than one isoform of the P2Y receptor is involved in signaling upon binding UDP. Rather than model each isoform separately, we has chosen to model a generic P2Y receptor and acknowledge that more information is needed to disambiguate the contributions of multiple receptor isoforms.

While we do not have much kinetic data for the P2Y6 receptor, the P2Y2 receptor has been studied in detail. We use the information from this similar receptor to inform our model parameter priors. Garrad et al. (1998) measured the EC50 for Ca^{2+} response to UTP in 1321N1 cells to be 250nM. Lukas (2004a) reports the equilibrium binding constant is $K_d \approx 5\mu$M.

P2Y receptors have been shown to form hetromeric complexes (Yoshioka et al., 2001). In particular P2Y2 and the adenosine receptor 1 were shown to coimmunoprecipitate. While the implication for diversity of signal recognition is interesting, the functional significance of this result for Ca^{2+} signaling is not clear and we have not modeled this

[1] http://www.signaling-gateway.org/data/fxm/query?type=class&classID=P2YR

dynamic.

2.2.2 C5a Receptor

There is only one known isoform of the C5a receptor in RAW264.7 cells[2]. A directed shRNAi knockdown of the receptor shows a decrease in signaling in population calcium assays. For these reasons, we have modeled the concentration of C5a receptors assuming only one isoform. It has been estimated that there are approximately 30,000 receptor molecules in RAW cells[3] The forward and reverse receptor-ligand binding rate constants are unknown and we have estimated the prior values from similar receptors (Lauffenburger and Linderman, 1993).

Molecule	Initial Concentration	
	(μM)	(molecules)
C5aR	0.05	30,100
P2Y	0.1	60,200

Table 2.2: Receptor initial concentrations.

2.3 G Protein Reactions

The role of G proteins in signal transduction has been studied from a structural and mechanistic perspective (Bourne et al., 1991). The two main mechanisms of the switch is the activation of Gα subunits by ligand-bound receptors and the GTPase activity of some effector proteins. These features yield a unidirectional molecular switch (see Figure 2.1) that serves to integrate and amplify extracellular signals. The diversity of roles of G$\beta\gamma$ subunits

[2]http://www.signaling-gateway.org/data/fxm/query?type=class&classID=C5AR
[3]L. Jiang personal communication.

in signal transduction is reviewed more recently in Clapham and Neer (1997). We have represented this molecular switch as a system of mass-action kinetic equations described in Table 2.3.

The first three rows of Table 2.3 describe the reactions involving $G\alpha_i$ and the activated C5a receptor and the last three rows describe the reactions involving $G\alpha_q$ and the activated P2Y receptor. Both $G\alpha$ isoforms have intrinsic GTPase (GAP) activity and the rate constant for the hydrolysis has been measured to be approximately 0.03-0.06s^{-1}(Ross and Wilkie, 2000). $G\alpha$ subunits associate with $G\beta\gamma$ with high affinity when bound to GDP and with low affinity when bound to GTP. We have modeled this dynamic by selecting a fast rate constant for the reassociation of $G\alpha$-GDP with $G\beta\gamma$; enforcing the constraint that when $G\alpha$ is bound to GTP it cannot reassociate with $G\beta\gamma$ (Berg et al., 2002).

Reaction			k_f ($uM^{-1}s^{-1}$)	References
C5aC + $G\beta\gamma$-$G\alpha_i$-GDP	$\rightarrow$	C5aC + $G\beta\gamma$ + $G\alpha_i$-GTP	0.0129*	
$G\alpha_i$-GTP	$\rightarrow$	$G\alpha_i$-GDP	0.022 (s^{-1})	
$G\alpha_i$-GDP + $G\beta\gamma$	$\rightarrow$	$G\beta\gamma$-$G\alpha_i$-GDP	7000	
UDPC + $G\beta\gamma$-$G\alpha_q$-GDP	$\rightarrow$	UDPC + $G\beta\gamma$ + $G\alpha_q$-GTP	0.137*	
$G\alpha_q$-GTP	$\rightarrow$	$G\alpha_q$-GDP	0.022 (s^{-1})	
$G\alpha_q$-GDP + $G\beta\gamma$	$\rightarrow$	$G\beta\gamma$-$G\alpha_q$-GDP	7000	

Table 2.3: G protein reaction rate constants.

It is a main assumption of this part of the model that there is a homogeneous pool of $G\beta\gamma$ that binds to $G\alpha_q$ and $G\alpha_i$ unpreferentially. It is not clear from available literature whether specific isoform combinations of the $G\beta\gamma$ dimer bind preferentially to specific $G\alpha$ isoforms (Casey and Gilman, 1988).

Though little is known about G protein binding order and cooperativity at the

effector, some research has illuminated the concentration changes that occur for different G protein subunits. Krumins and Gilman (2006) showed that if the $G\alpha_i$ subunit is decreased in concentration, the $G\alpha_q$ concentration is increased to compensate. Further, it was shown that $G\beta$ subunits are required for the stability of α subunits *in vivo* (Krumins and Gilman, 2006).

Molecule	Initial Concentration	
	(μM)	(molecules)
$G\beta\gamma$	7.14	4,300,000
$G\alpha_i$	6.64	4,000,000
$G\alpha_q$	0.50	300,000

Table 2.4: G protein initial concentrations.

The G protein initial concentrations are shown in Table 2.4. The $G\alpha_i$ and $G\alpha_q$ amounts were measured[4] in RAW264.7 cells and converted to μM concentrations assuming a 1pl cell volume.

2.3.1 $G\alpha_i$ Activation

The C5a response couples through the $G\alpha_i$ protein. $G\alpha_i$ is activated by the 7 α-helix transmembrane C5a receptor. Upon activation GDP is exchanged for GTP and the $G\alpha_i$-GTP dissociates from $G\beta\gamma$. Two of the three known $G\alpha_i$ isoforms exist in RAW cells as measured by antibody binding assay and rtPCR[5]. It is not yet clear which isoforms of $G\alpha_i$ are activated by bound C5a receptors (Ali et al., 1999; Fudenberg, 1980). Knockdown experiments on the $G\alpha_{i2}$ isoform show the unexpected phenotype that the peak height of the calcium response to C5a is increased over the control wild-type cell line. This result

[4]S. Mumby personal communication
[5]http://www.signaling-gateway.org/data/fxm/query?type=class&classID=GNAI.

has been attributed to off-target and nonspecific effects in the shRNAi hairpin design and subsequent lentiviral infection[6].

2.3.2 Gα_q Activation

The UDP response is not PTx-sensitive and the P2Y receptor class has been shown to couple to Gα_q isoform (Yoshioka et al., 2001). In these RAW264.7 macrophage cells, the population calcium response to UDP is decreased in Gα_q knockdown cell lines[7]. The Gα_q activation rate constant has been optimized from wild-type and knockdown data since the *in-vivo* rates are unknown. The activation mechanism for Gα_q is the same as Gα_i with different kinetic rates shown in Table 2.3.

2.4 Phosphoinositide Cascade Reactions

There are four known subfamilies of phosphoinositide-specific phospholipase C (PLC): β, γ, δ and ϵ. Of these four, we are mainly interested in PLCβ of which there are four known isozymes (numbered 1-4) because this subfamily has the greatest catalytic properties for hydrolyzing PIP2 and is activated through the G protein pathway (Berg et al., 2002). PLCγ is activated by tyrosine kinases, PLCδ is activated by Ca^{2+} and PLCϵ is activated by Ras (Berridge et al., 2003). Several reviews of all four subfamilies with a discussion of their regulation and effectors are available (Noh et al., 1995; Litosch, 2002; Rhee, 2001).

PLCβ contains five functional domains. At the amino terminus is a pleckstrin homology (PH) domain that localizes the protein to the membrane. EF hand domains bind

[6] I. Fraser personal communication.
[7] http://www.signaling-gateway.org/data/fxm/query?type=class&classID=GNAQ

calcium ions. A catalytic domain is in the center next to a C2 domain (phospholipase C domain 2) that binds to a phospholipid. Finally, at the carboxyl terminus, a G protein binding domain lends PLCβ its specific activity only upon activation by a G protein (Berg et al., 2002).

Activated phosphoinositide-specific PLC catalyzes the hydrolysis of phosphatidylinositol 4,5-bisphosphate (PIP2) and generates inositol 1,4,5-triphosphate (IP3) and diacylglycerol (DAG). IP3 binds to IP3-gated calcium channels on the membrane of the endoplasmic reticulum causing a net efflux of calcium into the cytosol. DAG binds to and activates protein kinase C (PKC) which is an important feedback mechanism (see section 2.6) (Noh et al., 1995).

The C5a receptor activates the Gα_{i} subfamily of G proteins. Activated Gα_{i} inhibits cAMP synthesis by adenylyl cyclase, but Gα_{i} has not been shown to activate any isoforms of PLCβ. Therefore, signal transduction driven by C5a is thought to be exclusively through G$\beta\gamma$ stimulation of PLCβ. G$\beta\gamma$ activates PLCβ2/3 but not PLCβ4 (Sternweis and Smrcka, 1993; Jiang et al., 1994, 1996). It may activate PLCβ1 weakly. A partial ordering of signaling efficiency by G$\beta\gamma$ is: PLCβ3 $\geq$ PLCβ2 $\geq$ PLCβ1 (Park et al., 1993a).

The P2Y receptor activates the Gα_{q} subfamily of G proteins. Gα_{q} activates all 4 isozymes of PLCβ. A partial ordering of PLCβ1-3 sensitivity to Gα_{q} PLCβ3 $\geq$ PLCβ1 $\gg$ PLCβ2 according to Smrcka and Sternweis (1993). According to Rhee (2001, p. 289) the partial ordering is PLCβ1 $\geq$ PLCβ3 $\gg$ PLCβ2 and cites Smrcka and Sternweis (1993) and Jhon et al. (1993) but actually derives the ordering from Jhon et al. (1993). Gα_{q} also activates PLCβ4, but it is not known to what degree relative to the other isozymes

(Lee et al., 1994; Jiang et al., 1994). The basal activity of PLCβ4 is inhibited by ribonucleotides, though not by ribonucleosides, including GTP-γ-S; a non-hydrolyzable GTP analog (Lee et al., 1994). Since GTP-γ-S is used in the experiments to determine activity of PLCβ this experimental technique cannot be used for PLCβ4 and an alternative experiment has not yet been found.

These experimental observations generally match those obtained through shRNAi perturbations. PLCβ2, PLCβ3 and PLCβ4 have been targeted using shRNAi. PLCβ1 is not expressed in RAW264.7 cells as measured by rtPCR. The PLCβ3 knockdown resulted in a decreased Ca^{2+} response to C5a and the PLCβ4 knockdown resulted in a decrease in the Ca^{2+} response to UDP[8].

While a great deal is known about the regulators and effectors of the various isoforms of PLCβ, comparatively little is known about their molecular concentrations *in vivo* because binding studies are much easier to accomplish *in vitro*. PLCβ2 and PLCβ3 are expressed in this cell line and those isoforms are both activated by $G\alpha_q$ and $G\beta\gamma$. We suppose that some PLCβ2 molecules are involved in the signal transduction cascade and they respond similarly to PLCβ3 for these experiments (Wu et al., 1993; Park et al., 1993a). So, we have selected a concentration for PLCβ3 to be roughly twice that of PLCβ4. We have set the number of PLCβ4 molecules to be roughly 10-fold smaller than the number of $G\alpha_q$ molecules so that all the PLCβ4 molecules are likely to find a $G\alpha_q$ rapidly when the cell is stimulated by UDP. Table 2.5 shows the initial concentrations for the PLCβ isoforms and associated phospholipids.

Calcium and magnesium are important activators of PLCβ. Many binding studies

[8]http://www.signaling-gateway.org/data/fxm/query?type=class&classID=PLCB

Molecule	Initial Concentration	
	(μM)	(molecules)
PLCβ3	0.116	70,000
PLCβ4	0.066	40,000
PIP2	0.5	301,000
IP3	0.0018	1,083
DAG	0.001	602

Table 2.5: PLCβ initial concentrations.

involving PLCβ found that the affinity of PLCβ for G protein subunits changes as a function of the Mg^{2+} concentration (Clapham and Neer, 1997). While Mg^{2+} is an important catalytic ion, it is not a central focus of our study and we have chosen to neglect its dynamics for this model. Calcium, however, is of central concern to our model. We use this second-messenger to assay significant changes in G protein mediated signal transduction. It has been shown in HEK-293 that Gα_{i}-derived $\beta\gamma$ subunits and Ca^{2+} are required for potentiation of PLC-mediated signaling cells (Schmidt et al., 2000). The EF-binding domain in PLCβ requires a calcium ion bound to confer activity to the protein. In this model, the dissociation constant for the Ca^{2+} activation is set close to the physiological concentration of cytosolic calcium ($K_d \approx 400$nM). Otherwise, we would find that the reaction would not matter in our model and it could be removed to make a more parsimonious model.

Smrcka and Sternweis (1993) suggested that there are separate sites on the PLCβ3 isoform that may independently bind G$\beta\gamma$ and Gα_{q}-GTP. It is argued that the activity of the enzyme is increased when both G$\beta\gamma$ and Gα_{q}-GTP are bound. They observed that Gα_{i} concentration usually exceeds Gα_{q} concentration in cells and this dual binding may be a signal integration site. They suggest that when the Gα_{q} pathway is stimulated the concentration of G$\beta\gamma$ is not high enough to appreciably lead to dual occupancy of PLCβ3 by

$G\alpha_q$-GTP and $G\beta\gamma$. But when the $G\alpha_i$ and $G\alpha_q$ pathway are stimulated, there is sufficient levels of $G\beta\gamma$ and $G\alpha_q$-GTP to cause PLCβ3 to be dually occupied and thus increase the efficiency of PIP2 hydrolysis. PLCβ3 then operates as a coincident detection mechanism for $G\alpha_i$ and $G\alpha_q$ pathway stimulation.

This hypothesis has not been implemented in our model. We consider that PLCβ3 can only be bound to $G\beta\gamma$ *or* $G\alpha_i$-GTP but not both. This strong mutual exclusivity assumption has allowed us to test the hypothesis of whether this is sufficient to explain $G\alpha_i$ and $G\alpha_q$ pathway convergence effects in our data. This issue will be revisited in the section on ligand synergy (section 3.7).

2.4.1 IP3 synthesis by $G\alpha_q$ activated PLCβ3

The dissociation constant for $G\alpha_q$ binding to PLCβ1 is 0.6nM (Park et al., 1993b) and the dissociation constant for $G\alpha_q$ binding to PLCβ3 is approximately 40-60nM (Rhee, 2001; Runnels and Scarlata, 1999). In this model, the K_d for PLCβ3 binding to $G\alpha_q$-GTP is approximately 2nM; between the measured PLCβ1 and PLCβ3 rates.

Reaction			k_f	k_r	References
PLCβ3 + Ca^{2+}	$\rightleftharpoons$	PLCβ3-Ca^{2+}	20	8	(Berg et al., 2002) (Ryu et al., 1987) (Meyer and Stryer, 1988) (Ellis et al., 1998)
$G\alpha_q$-GTP + PLCβ3-Ca^{2+}	$\rightleftharpoons$	PLCβ3-Ca^{2+}-$G\alpha_q$-GTP	50	0.1	(Jiang et al., 1996) (Rhee, 2001)
PLCβ3-Ca^{2+}-$G\alpha_q$-GTP + PIP2	$\rightleftharpoons$	PLCβ3-Ca^{2+}-$G\alpha_q$-GTP-PIP2	70.88*	1	(Jiang et al., 1996)
PLCβ3-Ca^{2+}-$G\alpha_q$-GTP-PIP2	$\rightarrow$	PLCβ3-Ca^{2+} +$G\alpha_q$-GDP + IP3 + DAG	27.90*		(Jiang et al., 1996)

Table 2.6: $G\alpha_q$ and PLCβ3 reaction rate constants.

It is known that PLCβ3 has independent binding sites for $G\alpha_q$ and $G\beta\gamma$ (Zhu and Birnbaumer, 1996; Clapham and Neer, 1993). But it is not known to what extent

the effects of simultaneous occupancy lead to changes in PLC activity. The C-terminus of PLCβ3 binds Gα_{q} and acts as a GAP (GTPase-activating protein). Removal of C-terminus abolishes activation by Gα_{q} and increases the activation by G$\beta\gamma$ (Banno et al., 1994). We have assumed, in this model, that PLCβ3 may only be bound to G$\beta\gamma$ *or* Gα_{q}, but not both. This is an important assumption in our model, if the model is still able to explain the calcium peak height synergy between C5a and UDP then we have a counter-example showing that it is possible that simultaneous binding is not necessary for a synergistic interaction.

2.4.2 IP3 synthesis by G$\beta\gamma$ activated PLCβ3

G$\beta\gamma$ is a weak activator of both PLCβ2 and PLCβ3 (Katz et al., 1992). Since neither C5a nor UDP differentially regulate PLCβ2 and PLCβ3 we modeled these two isoforms as a lump sum of PLCβ3. PLCβ3 is active when bound by G$\beta\gamma$ and a calcium ion. Since G$\beta\gamma$ does not require a bound GTP to be active, it is not subject to the same molecular timing mechanism as Gα_{q}-GTP. We have assumed the affinity of free G$\beta\gamma$ for Gα-GDP is higher than for PLCβ3 so that G$\beta\gamma$ preferentially reassociates with a Gα-GDP subunit. Park et al. (1993b) measured the half-maximal concentration of G$\beta\gamma$ required to active PLCβ3 to be 25nM in the presence of 200nM free Ca^{2+}. In this model we have taken $K_d \approx 500$nM for the reaction: G$\beta\gamma$ + PLCβ3-Ca^{2+} $\rightleftharpoons$ G$\beta\gamma$-PLCβ3-Ca^{2+}. For simple monovalent binding reactions, K_d is the concentration required to activate half of enzyme, but the measurement in (Park et al., 1993b) is the fraction of PIP2 converted to IP3; and therefore does not directly report the K_d of the enzyme activation.

Reaction			k_f	k_r	References
G$\beta\gamma$ + PLCβ3-Ca^{2+}	$\rightleftharpoons$	PLCβ3-Ca^{2+}-G$\beta\gamma$	8.35	0.39	(Wu et al., 1993) (Murthy et al., 1996) (Jiang et al., 1996) (Katz et al., 1992)
PLCβ3-Ca^{2+}-G$\beta\gamma$ + PIP2	$\rightleftharpoons$	PLCβ3-Ca^{2+}-G$\beta\gamma$-PIP2	165.83*	8	(Wu et al., 1993) (Murthy et al., 1996) (Jiang et al., 1996) (Katz et al., 1992)
PLCβ3-Ca^{2+}-G$\beta\gamma$-PIP2	$\rightarrow$	PLCβ3-Ca^{2+}-G$\beta\gamma$ + IP3 + DAG	5.42*		(Wu et al., 1993) (Murthy et al., 1996) (Jiang et al., 1996) (Katz et al., 1992)

Table 2.7: G$\beta\gamma$ and PLCβ3 reaction rate constants.

2.4.3 IP3 synthesis by Gα_q activated PLCβ4

PLCβ4 was discovered relatively recently compared to other PLCβ isoforms. However, it is important to the mechanism of this model because it was found that a PLCβ4 knockdown cell line had a reduced response to UDP[9]. PLCβ4 is activated by Gα_q, but is not responsive to G$\beta\gamma$ (Lee et al., 1994). We have used the same kinetic constants as PLCβ3 for the Gα_q mediated activation of PLCβ4 due to the sparsity of information on this new isoform. The relevant rate constants used in the model are shown in Table 2.8.

Reaction			k_f	k_r	References
PLCβ4 + Ca^{2+}	$\rightleftharpoons$	PLCβ4-Ca^{2+}	20	8	(Berg et al., 2002) (Ellis et al., 1998)
Gα_q-GTP + PLCβ4-Ca^{2+}	$\rightleftharpoons$	PLCβ4-Ca^{2+}-Gα_q-GTP	62.55	10.63	(Lee et al., 1994) (Jiang et al., 1994)
PLCβ4-Ca^{2+}-Gα_q-GTP + PIP2	$\rightleftharpoons$	PLCβ4-Ca^{2+}-Gα_q-GTP-PIP2	1238.79*	1	(Lee et al., 1994) (Jiang et al., 1994)
PLCβ4-Ca^{2+}-Gα_q-GTP-PIP2	$\rightarrow$	PLCβ4-Ca^{2+} + Gα_q-GDP + IP3 + DAG	22.85*		(Lee et al., 1994) (Jiang et al., 1994)

Table 2.8: Gα_q and PLCβ4 reaction rate constants.

[9] http://www.signaling-gateway.org/data/fxm/query?type=target&afcsID=A001806

2.5 IP3 Receptor Reactions

Our IP3 receptor model is adapted from Keizer and De Young (1992). This model assumes the tetrameric IP3 receptor opens cooperatively upon binding four IP3 molecules and closes upon binding one or more calcium ions. The Keizer and De Young (1992) model also assumes that receptor affinity for calcium is increased upon binding to IP3. This provides a rapid, threshold specific, negative feedback mechanism for calcium release. This mechanism does not explain the reduction of cytosolic calcium concentration, only the termination of its increase. The restoration of equilibrium is accomplished through specific ATPase pumps (SERCA pumps) and Ca^{2+}/Na^{2+} pumps. The model presented in Keizer and De Young (1992) is simplified in that it does not explicitly account for the concentration of IP3 receptors in the cell; calcium release is proportional to the fraction active receptors. Since we would like to simulate IP3 receptor knockdown experiments, we have modeled the receptor concentration explicitly. We have assumed on the order of 10,000 tetrameric receptor complexes per cell.

Molecule	Initial Concentration	
	(μM)	(molecules)
IP3R	0.0208	12,522
IP3R-IP3	0.00175	1,053
IP3R-IP3-Ca^{2+}	0.0023	1,384
IP3R-Ca^{2+}	0.0002	120

Table 2.9: IP3 receptor initial concentrations.

The kinetic diagram for one subunit of the tetrameric IP3 receptor can be represented as shown in Figure 2.4 (Keizer and De Young, 1992).

Table 2.10 shows the relevant rate constants for the IP3 receptor model module.

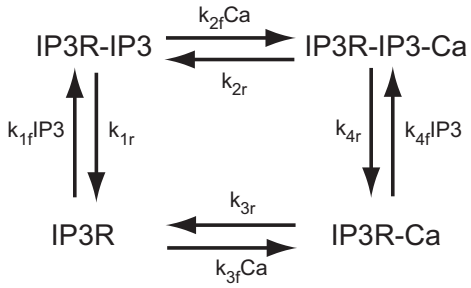

Figure 2.4: A kinetic diagram for one subunit of the tetrameric IP3 receptor.

Since this module is a cycle of reversible reactions, one of the rate constants is thermodynamically constrained. We have taken k_{r4} to the the constrained rate constant.

Reaction			k_f	k_r	References
IP3R + IP3	$\rightleftharpoons$	IP3R-IP3	177.47	2.2	(Keizer and De Young, 1992)
IP3R-IP3 + Ca^{2+}	$\rightleftharpoons$	IP3R-IP3-Ca^{2+}	0.411	0.0434	(Keizer and De Young, 1992)
IP3R + Ca^{2+}	$\rightleftharpoons$	IP3R-Ca^{2+}	0.9	0.806	(Keizer and De Young, 1992)
IP3R-Ca^{2+} + IP3	$\rightleftharpoons$	IP3R-IP3-Ca^{2+}	20	0.029233	(Keizer and De Young, 1992)

Table 2.10: IP3 receptor reaction rate constants.

Thermodynamic Constraint Since the four reactions in Table 2.10 form a cycle of reversible reactions, one of the reaction rates must be constrained by the others according to the second law of thermodynamics. Consider the system to be a Markov chain with states: $s_0 \triangleq \text{IP3R}$, $s_1 \triangleq \text{IP}_3\text{R} \cdot \text{IP}_3$, $s_2 \triangleq \text{IP}_3\text{R} \cdot \text{IP}_3 \cdot \text{Ca}^{2+}$, $s_3 \triangleq \text{IP}_3\text{R} \cdot \text{Ca}^{2+}$. The system can be rewritten as

$$s_0 + \text{IP}_3 \rightleftharpoons s_1 + \text{Ca}^{2+} \rightleftharpoons s_2 \rightleftharpoons s_3 + \text{IP}_3 \rightleftharpoons s_0 + \text{Ca}^{2+}. \tag{2.5.1}$$

The net chemical force or change in Gibbs free energy (ΔG) for this reaction must be zero since the reactants and products are the same at either end of the chain

(Nelson et al., 2004). We define ΔG^0 to be the standard free energy with all species concentrations standardized and converted to non-dimensional quantities by dividing by c_0. Generally, the reference concentration $c_0 \triangleq 1\text{M}$, but we will make the definition $c_0 \triangleq 1\mu\text{M}$ to match the concentration reference for our model. This is a common modification in biochemical systems where the absolute concentration levels are much smaller than in bulk chemical systems.

The change in free energy for the system is

$$\Delta G^0 = \Delta G_1^0 + \Delta G_2^0 + \Delta G_3^0 + \Delta G_4^0 = 0 \tag{2.5.2}$$

where the subscript on the standardized free energy terms refers to the reaction in the corresponding row in Table 2.10.

The mass action rule can be written

$$\begin{aligned} \exp\left\{\frac{\Delta G^0}{k_B T}\right\} &= \exp\left\{\frac{\Delta G_1^0 + \Delta G_2^0 + \Delta G_3^0 + \Delta G_4^0}{k_B T}\right\} \\ &= \frac{K_{eq1} K_{eq2}}{K_{eq3} K_{eq4}} \\ &= \frac{k_{1r}}{k_{1f}} \frac{k_{2r}}{k_{2f}} \frac{k_{3f}}{k_{3r}} \frac{k_{4f}}{k_{4r}} \\ &= 1. \end{aligned} \tag{2.5.3}$$

The constrained rate constant is then

$$k_{4r} = k_{4f} \left(\frac{k_{1r}}{k_{1f}}\right) \left(\frac{k_{2r}}{k_{2f}}\right) \left(\frac{k_{3f}}{k_{3r}}\right). \tag{2.5.4}$$

Calcium Flux Our model includes an outward leak of Ca^{2+} from the ER to the cytosol because of the steep concentration gradient, and an ATPase Ca^{2+} pump (Carafoli, 1987).

Part of the calcium flux equation is

$$\frac{d[\mathrm{Ca}^{2+}]}{dt} = c_2\left(v_1[IP3R \cdot IP3]^4 + v_8\right)\left([\mathrm{Ca}^{2+}_{ER}] - [\mathrm{Ca}^{2+}]\right) - v_4\frac{[\mathrm{Ca}^{2+}]^2}{[\mathrm{Ca}^{2+}]^2 + k_4^2} - \frac{V_{ex}[\mathrm{Ca}^{2+}]}{K_{ex} + [\mathrm{Ca}^{2+}]} + a_1 + \cdots . \tag{2.5.5}$$

The first term is the IP3-dependent flux. The flux of calcium through the IP3-mediated channel is proportional to the number of open channels and the difference in Ca^{2+} concentration in the ER and the cytosol. An IP3-mediated channel is only considered open when all four subunits are bound with IP3, but not Ca^{2+}. The probability that one subunit is bound is proportional to $[IP3 \cdot IP3R]$ (Meyer et al., 1988). If each subunit is independent, the probability that the channel is open is proportional to $[IP3 \cdot IP3R]^4$. The calcium flux constant in the Keizer and De Young (1992) model is $v_1 = 800\mathrm{s}^{-1}$. But, in that model, v_1 multiplies the ratio $x_1^4 = \left(\frac{[\text{IP3R-IP3}]}{R_{TOT}}\right)^4$, where the denominator is the total amount of IP3R in any state. To convert v_1 to and equivalent flux rate for this model which multiplies $([\text{IP3R-IP3}])^4$ we must divide v_1 by R_{TOT}^4. This gives an equivalent flux rate constant of $v_1 \approx 2e9\mu\mathrm{M}^{-4}s^{-1}$ which is approximately within an order of magnitude of the value used in this model, $v_1 = 1e8\mu\mathrm{M}^{-4}\mathrm{s}^{-1}$.

The second term in equation (2.5.5) is for the ATPase-pump. The hill coefficient in this Michaelis-Menten style approximation is two because two Ca^{2+} ions are pumped out of the cytosol for every ATP consumed (Keizer and De Young, 1992). The third term is used for the Ca^{2+}/Na^{2+} exchanger and the last term models the calcium leak from the extracellular medium into the cytosol due to a strong concentration gradient. These mechanisms are discussed in the following sections and the initial concentrations for relevant species are shown in Table 2.11. The rate constants are shown in Table A.2.

Molecule	Initial Concentration (μM)	(molecules)
Ca^{2+}	0.0786	47,317
$Ca^{2+}{}_{ER}$	10.35	6,231,302
Buffer	0.5	270,600
Ca^{2+}-Buffer	0.0505	30,400

Table 2.11: Calcium initial concentrations.

2.5.1 ATPase Pumps and Na^{2+}/Ca^{2+} Exchangers

Four main pumping mechanisms that maintain the intracellular calcium concentration at equilibrium (Berridge et al., 2003) are:

- Plasma membrane Ca^{2+}-ATPase pumps (PMCA)
- Na^{2+}/Ca^{2+} exchangers (NCX)
- Sarco(endo)plasmic reticulum ATPase pumps (SERCA)
- Mitochondrial uniporters.

Of these, we have modeled the SERCA pump and the NCX exchanger. The SERCA pump plays a role in muscle contraction in the sarcoplasmic reticulum and in all nucleated cells at the endoplasmic reticulum interface (Berridge et al., 1999). There are several isoforms of the SERCA pump (1, 2a, 2b and 3). We have assumed that our cells contain the 2b isoform of the pump because these pumps have been shown to be present in all non-muscle cells and function as a "housekeeping" calcium pump (East, 2000). The equilibrium concentration of calcium in most cells is approximately 100nM (Berridge et al., 2003). We have chosen rate constants for these transporters such that the resting equilibrium Ca^{2+} concentration is 80nM.

According to Berridge et al. (2003), the PMCA and SERCA pumps have lower transport rates, but higher affinities which implies they respond to modest changes in Ca^{2+} concentration, but have a limited capacity. The NCX and mitochondrial uniporters have much greater transport rates, but lower affinities and confer the ability of the cell to respond over a greater dynamic range in Ca^{2+} concentration.

ATPase Pump The SERCA ATPase pump transports Ca^{2+} from the cytosol to the ER using an energy driven process. Two Ca^{2+} ions are pumped out of the cytosol for every ATP consumed, so the process has been approximated by a hill function (Keizer and De Young, 1992) with $v_4 = 20\mu\text{Ms}^{-1}$ and hill coefficient $k_4 = 0.65\mu\text{M}$. The flux term that adds into Equation (2.5.5) is

$$v_4^2 \frac{[\text{Ca}^{2+}]^2}{k_4^2 + [\text{Ca}^{2+}]^2}. \tag{2.5.6}$$

The values in Keizer and De Young (1992) for this reaction is $v_4 = 0.5\mu\text{M}s^{-1}$ and $k_4 = 0.09\mu\text{M}$. The values for these rate constants in our model are within an order of magnitude.

Na^{2+}/Ca^{2+} Exchanger There is a low-affinity high capacity Na^{2+}/Ca^{2+} exchanger that is engaged when the cytosolic calcium concentration becomes unhealthy for the cell. Three sodium ions are exchanged for one calcium ion. We have modeled this as a Michaelis-Menten reaction with constants $K_{ex} = 0.25\mu\text{M}$ and $V_{ex} = 0.023\mu\text{Ms}^{-1}$. The reported value of K_m for the exchanger is in the 2-5μM range (Carafoli, 1987).

Extracellular to cytosol leak The concentration of calcium in the extracellular medium is physiologically and experimentally approximately 2-5mM. Because of this large concentra-

tion gradient from the extracellular volume to the intracellular volume, we have included a term for the leakage of calcium into the cell. We have considered this rate to be constant because all of our experiments were done in the same extracellular conditions. Had we the need to model different extracellular calcium concentrations, this term could be made dependent on the difference between the intracellular concentration and the extracellular concentration. The leak term in our model is $a_1 = 0.0055\mu\text{Ms}^{-1}$.

2.5.2 Calcium Buffers

There are over 200 known calcium binding proteins (effectors or buffers) in the human genome. Carafoli et al. (2001) has reported that at equilibrium 20μM of intracellular calcium is complexed to proteins. The most obvious buffers include calmodulin and other EF-hand proteins. Fura-2 proteins that we have used to measure the cytosolic calcium concentration themselves act as a buffer for calcium. Cellular processes that may proceed without the dye may be modified when the dye is introduced because of this buffering. This complexity is outside the scope of this model so we have made approximations in modeling buffering proteins. We assume a simple mass-action binding rule for buffering: Ca^{2+} + Buf $\rightleftharpoons$ Ca^{2+}-Buf with kinetic rate constants $k_f = 10\mu\text{M}^{-1}\text{s}^{-1}$ and $k_r = 7\text{s}^{-1}$. These constants give a relatively high, but still physiological K_d value of 0.7μM.

Volume Correction In this model all the differential equations have been written in μM concentration referenced to the volume of the cell except for the ER calcium concentration which is discussed in section 2.5. The ER calcium concentration requires a volume correction when a Ca^{2+} ion flows from the ER into the cytosol through the IP3-gated channel because

the ER is approximately 20% the volume of the cytosol. The volume correction constant is $c_2 = 0.185$ in this model (Alberts, 2002).

ER to cytosol leak Since the concentration of Ca^{2+} in the ER is higher than in the cytosol, a mechanism for Ca^{2+} leak from the ER into the cytosol is included in the model, v_8. We have set $v_8 = 0.15s^{-1}$, which is the same value as in Keizer and De Young (1992).

Single or Multiple Stores There are two main competing theories regarding stored calcium in the cell. One holds that the ER contains stores that are functionally or physically discrete (Bootman et al., 1992). These stores have differing sensitivities to IP3 and release all of their stored calcium in quantal amounts when the receptors have been activated beyond their individual thresholds. The other theory holds that the ER is essentially one store of calcium and through a process of Ca^{2+}-mediated feedback inhibition, the receptor closes thus leading to a quantal release (Segel et al., 1986).

Strong evidence in favor of both theories exist and the true story is likely to be some combination of the two (Bootman et al., 1992). A more complete model would likely include aspects of both theories as well as details regarding the spatial effects of nearby channel openings. We have opted to use an ordinary differential equation framework to model the system, so we are able to consider compartmental systems, but not the spatial detail that is likely required for a more accurate representation of our understanding of this aspect of the system. Our interest lies more in the details of cross-talk among GPCR components, so we have chosen to more roughly model this aspect of the system and use the Ca^{2+}-mediated adaptation model.

Mitochondrial Stores The role of mitochondria in calcium release has not been shown to be significant in this cell type. It has been shown that the mitochondria are a store for calcium and release their stored calcium in some cases, but this seems to occur only under conditions of extreme distress for the cell. It has been reported that the K_m for the mitochonrial uniporter is 10μM (Carafoli, 1987). Since the experimental observations for this system indicate the maximum ligand-induced intracellular calcium concentration is approximately 300nM, we have chosen not to include mitochondrial stores in this model.

2.6 Feedback Reactions

We have modeled four mechanisms of Ca^{2+} dependent feedback:

- Ca^{2+} inactivation of IP3-gated Ca^{2+} channels.
- Covalent modification of PLCβ by PKC.
- Covalent modification of C5a receptor by GRK.
- PLCβ requires Ca^{2+} to hydrolyze PIP2.

The first form has already been discussed as part of the Keizer and De Young (1992) model for the IP3 receptor in Section 2.5. A calcium ion bound to one or more subunits of the tetrameric IP3 receptor will shut down the IP3-mediated channel. This negative feedback mechanism is the fastest acting and closest to the calcium release - the end point in our model of the signal transduction cascade.

Initial concentrations for the other three mechanisms of Ca^{2+}-mediated feedback are shown in Table 2.12. A discussion of each mechanism follows.

Molecule	Initial Concentration (μM)	(molecules)
RGS_a	0.023	13,879
PKC	0.025	15,000
GRK	0.023	13,879

Table 2.12: Protein kinase and GTPase initial concentrations.

2.6.1 Protein Kinase C

Protein kinase C (PKC) is an immunological defense regulatory molecule found in both mammals and plants (Spitaler and Cantrell, 2004). The conserved structure of PKC contains two regulatory domains and two catalytic domains. The C1 regulatory domain binds DAG and the C2 regulatory domain binds calcium. The C3 catalytic domain binds ATP and the C4 regulatory domain confers substrate specificity (Newton, 1995).

PKC is localized to the plasma membrane by binding to DAG. The K_d of PKC for Ca^{2+} is much greater than physiological calcium levels. However, upon binding DAG, the affinity of the PKC-DAG complex for Ca^{2+} is at physiological levels. Taken together, these observations indicate a cooperativity between DAG and Ca^{2+} to activate PKC (Berg et al., 2002).

PKC has a substrate binding domain at the C-terminus and a pseudo-substrate at the N-terminus. In the inactive state (not bound to DAG and Ca^{2+}) the pseudo-substrate is near the substrate binding domain. When DAG and Ca^{2+} are bound the conformation changes and the substrate binding domain is free to bind other effector molecules such as PLCβ or G protein-coupled receptors (Berg et al., 2002).

2.6.2 Calcium and DAG are required for PKC activation

Ca^{2+} and DAG are required for PKC activation. Activated PKC phosphorylates serine/threonine residues on effector proteins (Berg et al., 2002). We have modeled the mechanism of PKC activation as a thermodynamic cycle because both Ca^{2+} and DAG are required for activation and the order of binding is not known. The parameter associated with the reaction PKC-DAG + Ca^{2+} ← PKC-DAG-Ca^{2+} is thermodynamically constrained in this model. We have chosen the rates in this thermodynamic cycle such that once DAG is bound, the PKC-DAG complex has a higher affinity for Ca^{2+} than PKC alone (Shinomura et al., 1991). Table 2.13 shows the kinetic rates selected for the mechanism of activation of PKC.

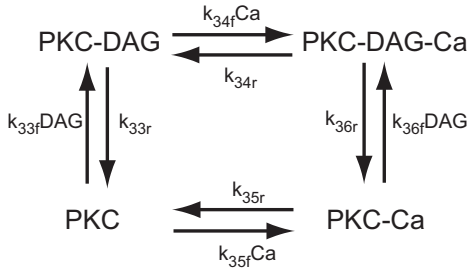

Figure 2.5: A kinetic diagram for the activation of PKC by DAG and Ca^{2+}.

The dissociation constant for the PKC-DAG complex binding Ca^{2+} has been measured to be 700nM and the dissociation constant for PKC binding Ca^{2+} has been measured to be 3mM (Newton, 1995). The model parameter values for these rates are 600nM and 3mM respectively. It has been reported that Ca^{2+} bound to PKC has no effect on the PKC's affinity for a C1 domain ligand such as DAG (). However, setting the forward and reverse rate constants for DAG binding to PKC and DAG binding to PKC-Ca^{2+} would constrain the dissociation constant for PKC-DAG binding Ca^{2+} to be equal to the dissoci-

ation constant for PKC binding Ca^{2+}. But it has been observed that these values are very different. This apparent measurement contradiction is resolved in our model by assuming the dissociation constants for PKC binding DAG and PKC-Ca^{2+} binding DAG are different, but both very small in absolute value. This choice causes an apparent equivalence between the measured binding affinities while still allowing for different binding affinities for Ca^{2+}.

Reaction			k_f	k_r	References
PKC + DAG	$\rightleftharpoons$	PKC-DAG	100	0.05	(Ananthanarayanan et al., 2003) (Shinomura et al., 1991)
PKC-DAG + Ca^{2+}	$\rightleftharpoons$	PKC-DAG-Ca^{2+}	10	6	(Ananthanarayanan et al., 2003) (Shinomura et al., 1991)
PKC + Ca^{2+}	$\rightleftharpoons$	PKC-Ca^{2+}	0.01	30	(Ananthanarayanan et al., 2003) (Shinomura et al., 1991)
PKC-Ca^{2+} + DAG	$\rightleftharpoons$	PKC-DAG-Ca^{2+}	1000	0.0001	(Ananthanarayanan et al., 2003) (Shinomura et al., 1991)

Table 2.13: Protein kinase C activation thermodynamic cycle.

The thermodynamic constraint in this cycle is

$$k_{34r} = k_{34f}\left(\frac{k_{33f}}{k_{33r}}\right)\left(\frac{k_{35r}}{k_{35f}}\right)\left(\frac{k_{36r}}{k_{36f}}\right). \tag{2.6.1}$$

PKC phosphorylates PLCβ3/4 PLCβ isoforms are covalently modified by protein kinase C (PKC) (Litosch, 2002; Yue et al., 2000). PKC inhibits the Gα_q mediated activity of PLCβ3 by phosphorylating the Ser^{1105} residue of PLCβ3. PKC also inhibits the G$\beta\gamma$ mediated activity of PLCb3, but the mechanism is not related to the Ser^{1105} residue (Yue et al., 2000).

It is unclear what effect the order of binding Gα_q or G$\beta\gamma$ and phosphorylation by PKC has on the activity of PLCβ. We have assumed in this model that PLCβ3/4 must be bound to only Ca^{2+} to be rendered inactive by phosphorylation. We have also assumed that only active forms of PKC (bound to both DAG and Ca^{2+}) are able to phosphorylate

PLCβ. In this model, the rate constants for PKC-mediated inhibition are the same for PLCβ3 and PLCβ4 as shown in Table 2.14.

Reaction			k_f	k_r	References
PKC-DAG-Ca^{2+} + PLCβ3-Ca^{2+}	$\rightleftharpoons$	PKC-DAG-Ca^{2+}-PLCβ3-Ca^{2+}	830.44*	111	
PKC-DAG-Ca^{2+}-PLCβ3-Ca^{2+}	$\rightarrow$	PKC-DAG-Ca^{2+} + PLC$\beta 3_p$-Ca^{2+}	11.70* (s^{-1})		
PKC-DAG-Ca^{2+} + PLCβ4-Ca^{2+}	$\rightleftharpoons$	PKC-DAG-Ca^{2+}-PLCβ4-Ca^{2+}	5.90*	11	
PKC-DAG-Ca^{2+}-PLCβ4-Ca^{2+}	$\rightarrow$	PKC-DAG-Ca^{2+} + PLC$\beta 4_p$-Ca^{2+}	0.93* (s^{-1})		

Table 2.14: PLCβ phosphorylation by PKC rate constants.

2.6.3 G protein Receptor Kinase

There are two main classes of kinases that phosphorylate G protein-coupled receptor complexes: PKC and G protein receptor kinase (GRK). The commonality among these signal control molecules is that they inactivate the receptor through phosphorylation of serine or threonine residues. PKC also covalently modifies PLCβ. The inactive receptors are targeted for recycling through the lysosomes by β-arrestin (Lefkowitz, 1998).

Lefkowitz (1998) has suggested that PKC acts on the G protein-coupled receptor itself, but it has also been shown that PKC acts at the level of PLCβ and is able to completely abolish signaling through PLCβ (Yue et al., 2000). We have modeled GRK as the only mechanism for direct receptor desensitization.

The G protein receptor kinase (GRK) family contains six isoforms (1-6). The most extensively studied are the rhodopsin kinase (GRK1) and the βARK (GRK2). GRK2 is the focus of our model because a change in the calcium response is observed for a GRK2 shRNAi knockdown line. GRK2 is activated and recruited to the plasma membrane when bound to G$\beta\gamma$ and a membrane phosphatidyl biphosphate.

GRK desensitizes active C5a receptors G protein-coupled receptors are phosphorylated at serine / threonine residues by G protein-coupled receptor kinases (Shenoy and Lefkowitz, 2003). However, the assertion that GRK2 phosphorylates and desensitizes agonist-occupied C5a receptors is controversial. There is evidence in fetal calf serum cells that this process does not occur (Milcent et al., 1999). There is contradictory evidence in rat basophilic leukemia cells that GRK2 or GRK3 does phosphorylate C5a receptors (Langkabel et al., 1999). We have assumed in this model that GRK2 does phosphorylate and desensitize the C5a receptor.

Table 2.15 shows the rate constants for GRK activation and desensitization of the C5a receptor. It has been reported that the K_m for GRK phosphorylation by active PKC is 6nM, compared to the model value of $K_m = 120$nM (Chuang et al., 1995).

Reaction			k_f	k_r	References
PKC-DAG-Ca^{2+} + GRK	$\rightleftharpoons$	PKC-DAG-Ca^{2+}-GRK	77.52*	10	(Chuang et al., 1995)
PKC-DAG-Ca^{2+}-GRK	$\rightarrow$	PKC-DAG-Ca^{2+} + GRK_p	18.34* (s^{-1})		(Chuang et al., 1995)
GRK_p + G$\beta\gamma$	$\rightleftharpoons$	GRK_p-G$\beta\gamma$	4.98*	0.05	(Penela et al., 2003) (Daaka et al., 1997)
GRK_p-G$\beta\gamma$ + C5aC	$\rightleftharpoons$	GRK_p-G$\beta\gamma$-C5aC	591.54	12.37	
GRK_p-G$\beta\gamma$-C5aC	$\rightarrow$	GRK_p-G$\beta\gamma$ + $C5aC_p$	199.31 (s^{-1})		

Table 2.15: GRK activation and phosphorylation rate constants.

The GRK2 shRNAi knockdown cells show an increase in the peak height of the calcium pulse[10] when the cell is stimulated by C5a in some experiments. An increase in calcium peak height does not occur for the knockdown cells when stimulated by UDP. Inaccurate targeting of the shRNAi or off-target effects or other causes not directly attributable to GRK2 mediated phosphorylation of C5aR may cause the shift in peak height observed. However, in the absence of a convincing alternative hypothesis, we assume that GRK2

[10]http://www.signaling-gateway.org/data/fxm/query?type=target&afcsID=A001094

phosphorylates the C5a receptor in this macrophage cell line.

2.6.4 G$\beta\gamma$ and PKC are required for GRK activation

Langkabel et al. (1999) has shown that C5a receptor phosphorylation is abolished when rat basophilic leukemia cells are pretreated with a PKC inhibitor and the receptors become hyperphosphorylated when GRK is overexpressed. A similar finding was achieved in human mononuclear leukocytes (Chuang et al., 1995). Free G$\beta\gamma$ must also bind to GRK to make it active (Lefkowitz, 1998).

This activation mechanism leaves open the questions of order and cooperativity with respect to PKC and G$\beta\gamma$. We have assumed in this model that PKC must first phosphorylate GRK2 because PKC and GRK2 are found in the cytosol (Lefkowitz, 1998). Once phosphorylated we assume GRK2 translocates to the membrane where it can bind to a free G$\beta\gamma$ and become active. In our model, the K_d for G$\beta\gamma$ binding to GRK2 is small, so there is opportunity for the G$\beta\gamma$ to become free again and reassociate with Gα-GDP.

Arrestin Agonist-bound receptors are internalized by β-arrestin (Shenoy and Lefkowitz, 2003). Phosphorylated receptors have a higher affinity for β-arrestins than unphosphorylated receptors (Lefkowitz, 1998). While important for the recovery of signaling capacity, we have chosen not to model receptor internalization and recycling because the time frame of our experimental measurements $\sim$ 3min is short compared to the time frame of receptor recycling. We have taken the dephosphorylation time constant for the C5a receptor to be $k_f = 0.001s^{-1}$ which causes makes the half time for receptor resensitization to be 16 min.

2.6.5 RGS is a GAP for Gα_{q}-GTP and Gα_{i}-GTP

Regulators of G protein signaling (RGS) control the ability of G protein subunits to signal downstream effectors. The RGS exerts its GTPase activity by binding to a free Gα-GTP molecule and hydrolyzing the GTP to GDP + $\mathrm{P_i}$ (Ross and Wilkie, 2000). Since knowledge of the mechanisms of action of RGSs is so sparse, we have modeled these molecules as constitutively active. When more definitive experimental knowledge of this system develops we will be able to fill in the missing mechanistic details - especially regarding its regulation.

Reaction			k_f	k_r	References
RGS_a + Gα_{i}-GTP	$\rightleftharpoons$	RGS_a-Gα_{i}-GTP	100	0.1	
RGS_a-Gα_{i}-GTP	$\rightarrow$	RGS_a + Gα_{i}-GDP	100 (s^{-1})		
RGS_a + Gα_{q}-GTP	$\rightleftharpoons$	RGS_a-Gα_{q}-GTP	100	0.1	(Kehrl and Sinnarajah, 2002)
RGS_a-Gα_{q}-GTP	$\rightarrow$	RGS_a + Gα_{q}-GDP	100 (s^{-1})		(Kehrl and Sinnarajah, 2002)

Table 2.16: RGS reaction rate constants.

2.7 Dephosphorylation and Degradation Reactions

Receptors and PLCβ molecules that have been phosphorylated must return to their unphosphorylated states. We have assumed that the necessary phosphotases exist and operate by a first order mechanism. An alternative approach is to fix a concentration of phosphotase for each dephosphorylation reaction and assume Michaelis-Menten enzyme kinetics for the reaction. However, this approach would require us to specify another molecular concentration and two more rate constants. Our current approach only requires one rate constant. We have opted for the less accurate, but simplified approach at this stage of the model.

2.7.1 C5aR and PLCβ3/4 dephosphorylation

An active C5a receptor that has been phosphorylate by GRK is returned to an unphosphorylated state with the C5a agonist decoupled. The true mechanism likely involving β-arrestin but we have simplified our model and left out arrestin because of the short time frame of the experimental measurements compared to the long time frame of receptor recycling. The C5a receptor and PLCβ3/4 dephosphorylation mechanism is modeled by a first order reaction.

As Table 2.17 shows, we have set the recovery rate for phosphorylated PLCβ to be approximately 8 seconds and the recovery rate for C5aR to be approximately 16 min.

Reaction			k_f	k_r	References
PLC$\beta 3_p$-Ca^{2+}	$\rightarrow$	PLCβ3-Ca^{2+}	0.12 (s^{-1})		
PLC$\beta 4_p$-Ca^{2+}	$\rightarrow$	PLCβ3-Ca^{2+}	0.12 (s^{-1})		
$C5aC_p$	$\rightarrow$	C5aR + C5a	0.001 (s^{-1})		

Table 2.17: Resensitization reaction rate constants

2.7.2 DAG degradation and PIP2 synthesis

It is possible that PIP2 availability is a limiting factor in IP3 generation and thus Ca^{2+} signaling. The initial concentration of PIP2, in our model, is 0.5μM. In a cell with 1 pl volume, this amounts to approximately 300,000 molecules. Willars et al. (1998) measured the absolute PIP2 basal level to be 1×10^8 per cell. They also estimated that 15,000 molecules of PLCβ are required to achieve the maximum hydrolysis rate they measured *in-vivo* which is within the same order of magnitude as the chosen model values in Table 2.5.

We have modeled the PIP2 replenishment pathway to be $IP3 \rightarrow IP4 \rightarrow IP5 \rightarrow$

$PIP2$. We do not find the effect of PIP2 depletion to be a significant cause for loss of Ca^{2+} signaling on the time scales of our experiments in our model. The endoplasmic reticulum is depleted of calcium before PIP2 availability becomes a limiting factor.

We have included the conversion of IP3 to IP4 because some evidence has suggested that IP4 also acts as a signaling molecule for Ca^{2+} release from the ER. The conversion of IP5 to PIP2 as a first order reaction simply models the replenishment of PIP2 and IP3 or IP4 could have been substituted for IP5 in this mechanism for the purposes of this model. Table 2.18 shows the initial concentrations of these molecular species and Table 2.19 shows the rate constants.

Molecule	Initial Concentration (μM)	(molecules)
$IP3K_a$	0.00166	1000
IP4	0.1	60,200
IP5	0.1	60,200

Table 2.18: IP recycling initial concentrations.

Reaction			V_{max}/k_f	K_m/k_r	References
DAG	$\rightarrow$	$\emptyset$	0.35 (s^{-1})		
IP3 + $IP3K_a$	$\dashrightarrow$	IP4 + $IP3K_a$	13.9	0.0557	(Xia and Yang, 2005)
IP4	$\dashrightarrow$	IP5	100	1.4	(Berg et al., 2002)
IP5	$\rightarrow$	PIP2	0.008		

Table 2.19: DAG degradation and PIP2 synthesis reaction rate constants.

This completes a detailed discussion of the model parameters, initial conditions and the relevant literature. We conclude this section with an overview of the mechanism of crosstalk that arises in the G-protein signal transduction pathway when these assumptions are made.

Chapter 3

Model and Data Analysis

In this analysis, we used 15 experiments spanning 9 doses of C5a and 14 experiments spanning 11 doses of UDP on wild-type cells. We also measured the calcium response to C5a and UDP in 5 different shRNAi knockdown cell lines. An experiment is a time series of measurements of a particular well in a 96 well plate and each experiment consists of multiple treatments. Most experiments have 3-4 samples per treatment. Table 3.1 shows a summary of the training data used for statistical parameter estimation for this model. The parameters that have been estimated using this data set are denoted with a star in Section 2 and in Table A.2.

	Knockdown Fraction(qRT-PCR) %	Knockdown Fraction(western) %	**C5a** dose count	**C5a** exp't count	**C5a** sample size	**UDP** dose count	**UDP** exp't count	**UDP** sample size
Wild-type			9	15	58	11	14	53
GRK2	90 ± 7	40 ± 6	5	16	69	3	9	40
$G\alpha_{i2}$	83 ± 5	73 ± 6	2	5	17	2	12	50
$G\alpha_{q}$	70 ± 8	66 ± 23	1	3	13	2	4	19
PLCβ3	-	83 ± 15	1	3	12	1	3	12
PLCβ4	87 ± 6	-	1	4	16	2	8	39

Table 3.1: Data set used for parameter estimation.

In the following sections we show a detailed comparison of this experimental data set to model simulations. Since it is unreasonable to show all 96 experiments, we will select representative experiments to demonstrate the quality of fit or use summary features such as peak height where appropriate.

3.1 Experimental Protocol

Intracellular free calcium in cultured adherent RAW264.7 cells is measured in a 96-well plate format using the fluorescent dye Fura-2 (Tsien, 1989; Grynkiewicz et al., 1985). The Ca^{2+}-sensitive fluorescent dye, Fura-2, permeates the cell membrane as an ester and is hydrolyzed in the cell to its Ca^{2+}-sensitive form. A FLEXstation scanning fluorometer is used to measure fluorescence using a bottom read of a 96-well plate. Because scanning a column is very rapid, sets of 8 wells in each column are effectively read simultaneously. Each well is sampled approximately every 4 seconds.

For calibration purposes, the time series is divided into three stages. To calibrate a baseline, fluorescence measurements are taken for 20-40 seconds before the ligand is added. The Ca^{2+} response is monitored for 170 seconds after ligand addition. After 190 seconds F_{min} solution is added and at 320 seconds F_{max} solution is added. The F_{min} and F_{max} solutions are used to calibrate the concentration of Ca^{2+} using

$$[Ca^{2+}] = K_d Q \frac{R - R_{min}}{R_{max} - R}, \tag{3.1.1}$$

where $R \triangleq F_{L1}/F_{L2}$ and $Q \triangleq F_{min}/F_{max}$. In this experimental protocol $L1 \approx 340$nm is the wavelength used to detect ion-bound Fura-2 and $L2 \approx 380$nm is the wavelength for ion-free

Fura-2. K_d is the dissociation constant for Fura-2 + $Ca^{2+} \rightleftharpoons$ Fura-2 • Ca^{2+} [1].

It is common practice to subtract the baseline Ca^{2+} concentration from measurements and report only the change in cytosolic Ca^{2+} concentration since the baseline measurement depends on the amount of loading dye used and other experimental variations. However, to compare our model predictions to the experimental data we require an estimate of the baseline calcium concentrations. We have normalized the measurements to have an average baseline concentration of 80nM in each time series. This concentration corresponds to a generally agreed upon level from several investigators and literature.

3.2 Simulation Method

The system of ordinary differential equations was solved using the SUNDIALS Suite (v2.3.0) (Hindmarsh et al., 2005). The software was configured to use backward differentiation formulas (BDF) for the linear multistep method and Newton iterations because the system is likely to be stiff. The Markov chain monte carlo algorithm was implemented in C because the MATLAB implementation performed to slowly. In the future, it may prove advantageous to use the parallel options in the SUNDIALS software to take advantage of a distributed computing environment to improve the time required to solve the system.

3.3 Input Model

Because the ligand concentration at the cellular lipid membrane does not transition instantaneously from zero to some fixed positive concentration, we measured and modeled the

[1] AfCS protocol #PP00000211.

expected ligand concentration as a function of time.

From the vantage point of an average cell, the concentration of ligand is at first zero, then as the ligand molecules diffuse in the media the concentration asymptotes to constant. We propose the following model for the ligand concentration at the cellular interface as a function of time

$$y(t) = \begin{cases} \frac{a_1(t-t_0)}{(t-t_0)+a_2} + a_3 & \text{if } t > t_0, \\ a_3 & \text{if } t \leq t_0. \end{cases} \tag{3.3.1}$$

The ligand introduction time is t_0. The parameters of the model, $\{a_1, a_2, a_3\}$ were fit using a Levenberg-Marquardt algorithm and a weighted least-squares cost function to 31 time points which are each an average of 96 experiments. The weights for each time point are inversely proportional to the sample standard error at the time point.

The measurements were made by robotically adding 25μL of 400nM FITC solution to wells containing 75μL of water leaving 100μM FITC solutions in each of the 96 wells at 30 seconds. The time series was observed at $\sim$ 2 second intervals for 40 seconds. The fluorescence measurement was approximately stable after 40 seconds.

Figure 3.1 shows the input model and data for the FITC calibration. It is clear that a step function model for ligand concentration is not appropriate for this experimental system. The ligand concentration is not expected to reach 95% of the asymptotic concentration until 38.5s after t_0. Since the time-scale of the calcium pulse is approximately 30s, an accurate model of the ligand concentration as a function of time is significant component of the model.

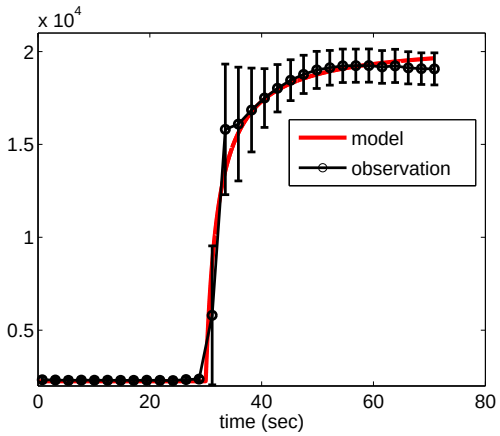

Figure 3.1: The input model prediction (red) and experimental data (black). Ligand was introduced at $t_0 = 30s$.

3.4 Wild-type Data

Observations of the intracellular calcium concentration over time indicate that stimulation of the cell by C5a or UDP leads to a pulse in calcium concentration. Figure 3.2 shows the response of the wild-type cell to stimulation with C5a and UDP. The C5a response adapts, but the UDP response has a sustained elevated calcium level that slowly decays.

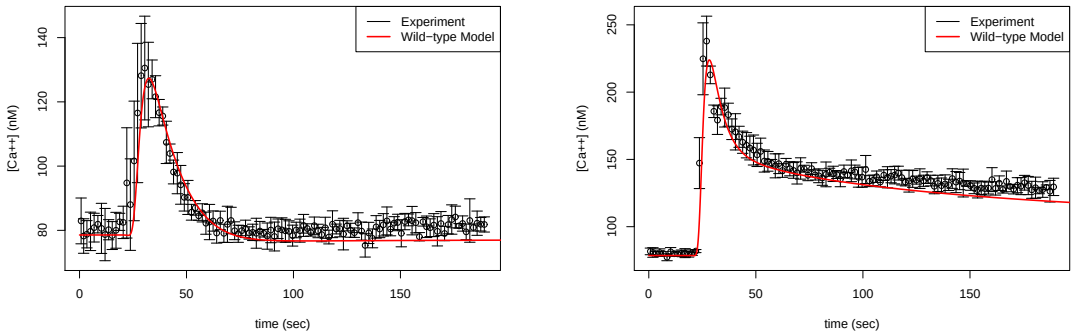

Figure 3.2: (left) Wild-type C5a 250nM calcium response. (right) Wild-type UDP 25μM calcium response.

Figure 3.3 shows the peak height of the calcium pulse as a function of C5a or UDP

dose. The dose response profile has the usual saturating characteristic, but the EC50 for the two ligands are different. The peak height EC50 for C5a is approximately 0.6nM and the EC50 for UDP is approximately 250nM. The UDP EC50 is in close agreement to that for the P2Y2 receptor measured by Garrad et al. (1998).

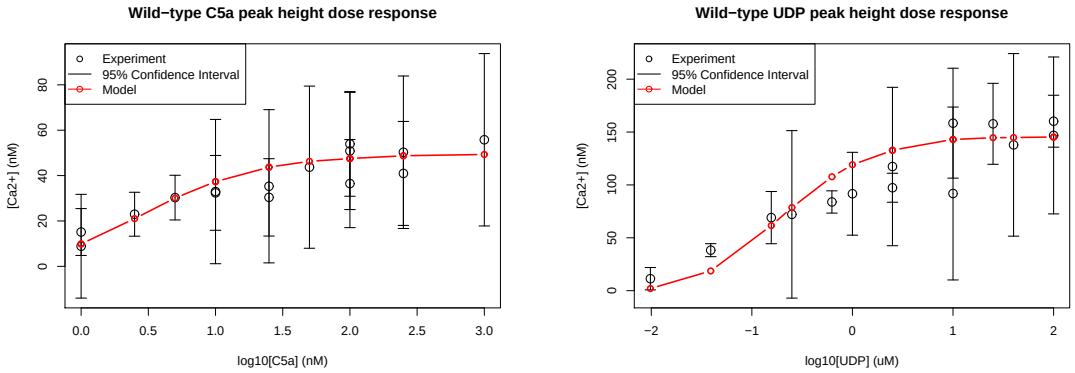

Figure 3.3: Calcium pulse peak height dose response to C5a and UDP. The 95% confidence intervals are the measured confidence intervals based on a Gaussian error at the peak value. (left) C5a peak height dose response. (right) UDP peak height dose response.

3.5 Knockdown Data

We have used five shRNAi knockdown cell lines and the wild-type cell line data to infer 20 parameter values in our model. In general it is inappropriate to use the same data for inference and validation, but we keep in mind that we will only formally use the data for inference and will use other experimental data for formal validation. Our test data does not look "like" our training data because it is composed of different experiment - simultaneous ligand stimulation.

The model predictions for the knockdown experiments include an estimation of uncertainty. The upper and lower 99% confidence intervals for the the model predictions are

based on the assumption that the uncertainty in knockdown fraction is well approximated by a normal distribution with the standard error given in Table 3.1 for the western blot data. These upper and lower confidence intervals are shown in each figure as UCI and LCI respectively.

Krumins and Gilman (2006) observed a compensatory effect for Gα subunits and G$\beta\gamma$ subunits. If the amount of Gα is reduced experimentally, the amount of G$\beta\gamma$ is reduced by the cell to compensate. Accordingly, the model simulations for Gα_{i} and Gα_{q} knockdown experiments also adjust the G$\beta\gamma$ concentration by an equal amount to ensure the following initial condition equality is satisfied, $[G\alpha_{\mathrm{i}}] + [G\alpha_{\mathrm{q}}] = [G\beta\gamma]$.

3.5.1 GRK2 Knockdown

The G-protein receptor kinase is an important feedback protein that phosphorylates the active C5a receptor, but not the active P2Y receptor in the model. The Ca^{2+} peak height for C5a stimulated cells is higher in the GRK2 knockdown line compared to the wild-type cells upon stimulation by C5a in some experiments.

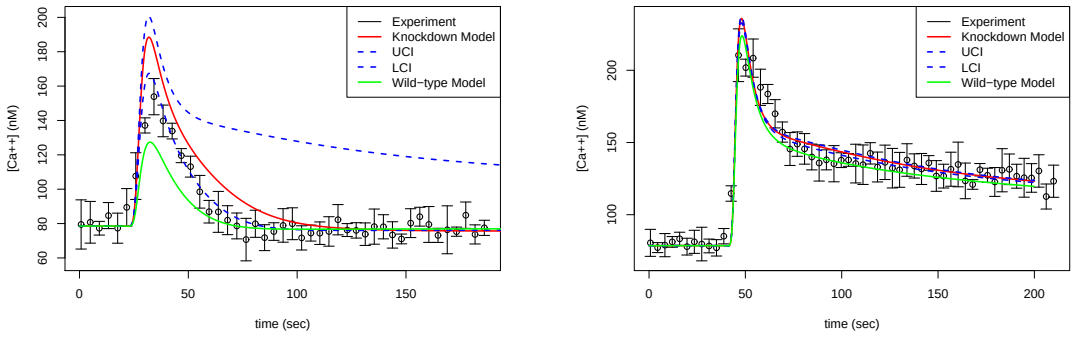

Figure 3.4: (left) GRK2 knockdown C5a 250nM calcium response. (right) GRK2 knockdown UDP 25μM calcium response.

Figure 3.4 shows the GRK2 knockdown cells stimulated by C5a and UDP. The model predicts the calcium peak height for 250nM [C5a] stimulation of GRK2 knockdown cells is 188nM compared to the 127nM for the wild-type cells. The model predicts the peak height is higher than the actual experimental peak height, but the lower 99% confidence interval based on the knockdown uncertainty shown in Table 3.1 fits the experimental data well.

3.5.2 Gα_i Knockdown

The trimeric G-protein with a Gα_i subunit is activated by the C5a receptor. Cell lines with a Gα_i knockdown respond poorly to C5a stimulation, but the effect on UDP stimulation is minimal. Both the experimental data and the model simulation show a diminished pulse for C5a and an unaffected pulse for UDP stimulation (Figure 3.5).

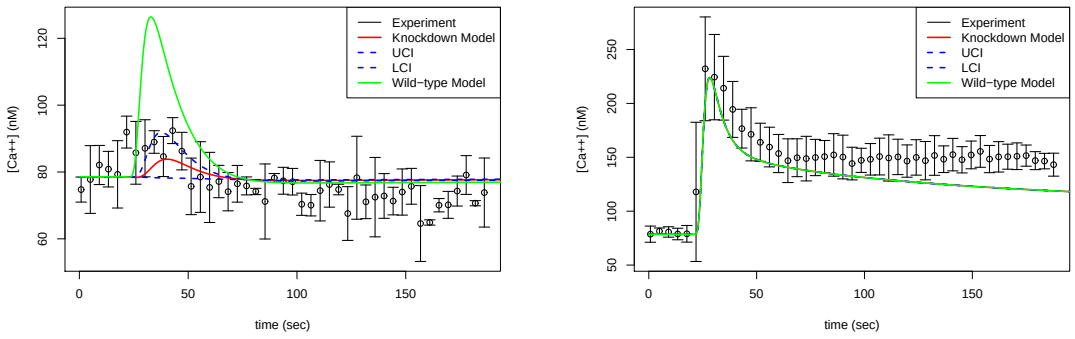

Figure 3.5: (left) Gα_i Knockdown C5a 100nM calcium response. (right) Gα_i knockdown UDP 25μM calcium response.

3.5.3 Gα_q Knockdown

Figure 3.6 shows the model and experimental data from a representative Gα_q knockdown experiment. Gα_q is associated with the P2Y6 receptor which is activated by UDP. As expected, the calcium response to UDP shows a diminished peak height. However, the characteristic incomplete adaptation is still evident. The response to C5a is unchanged by the knockdown.

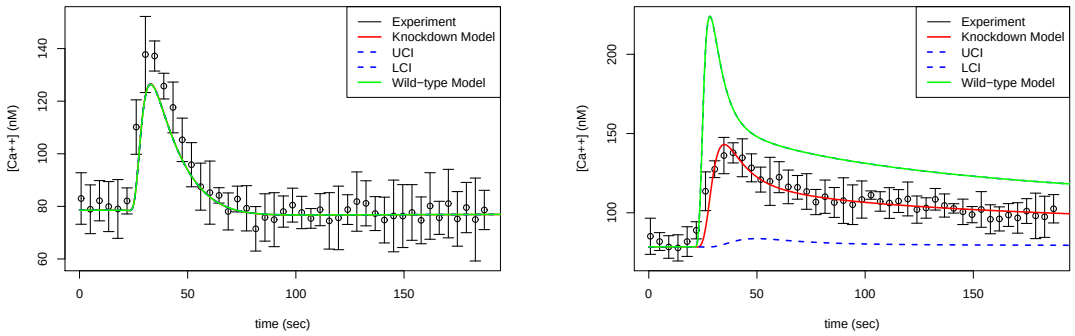

Figure 3.6: (left) Gα_q knockdown C5a 100nM calcium response. (right)Gα_q knockdown UDP 25μM calcium response.

Though the model fits the experimental data well, the prediction confidence intervals are large. This is due to the large uncertainty in the true knockdown of Gα_q which, from Table 3.1, is 66% $\pm$ 23%.

3.5.4 PLCβ3 Knockdown

Figure 3.7 shows a representative PLCβ3 knockdown experiment. PLCβ3 is activated by both Gα_q and G$\beta\gamma$ which means that it is activated upon stimulation by both UDP and C5a in our model.

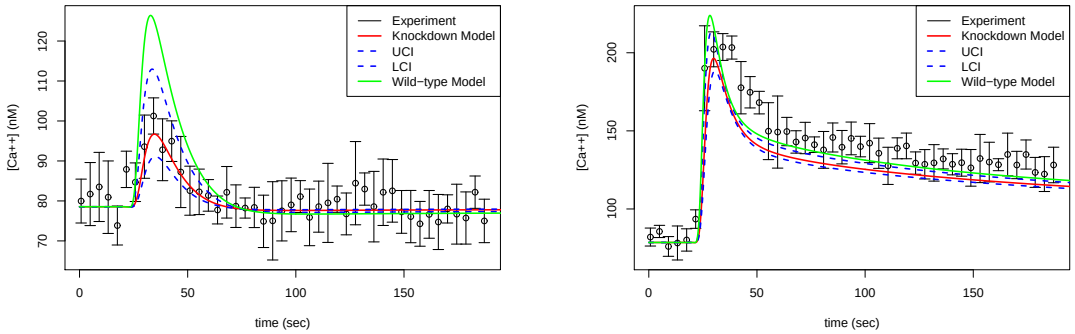

Figure 3.7: (left) PLCβ3 knockdown C5a 100nM calcium response. (right) PLCβ3 knockdown UDP 25μM calcium response.

The prediction confidence intervals are larger for the C5a response than for the UDP response for two reasons. First, the C5a response is only mediated by PLCβ3, while the UDP response is mediated by both PLCβ3 and PLCβ4. Second, the absolute magnitude of cytosolic calcium is lower for the C5a response than for the UDP response, which makes the relative size of the confidence intervals look bigger in side-by-side comparison.

3.5.5 PLCβ4 Knockdown

Figure 3.8 shows an example PLCβ4 knockdown experiment. PLCβ4 is only activated by Gα_{q}-GTP which is 10-fold less abundant than Gα_{i}. The contribution of PLCβ4 to the production of IP3 is not great in the model. The knockdown simulation does decrease the calcium response from UDP, but only by a relatively small amount.

3.6 Toxins

Bacterial and synthetic toxins are important tools in the investigation of signal transduction networks because the effect of toxins is different than the effect of knockdowns. If the

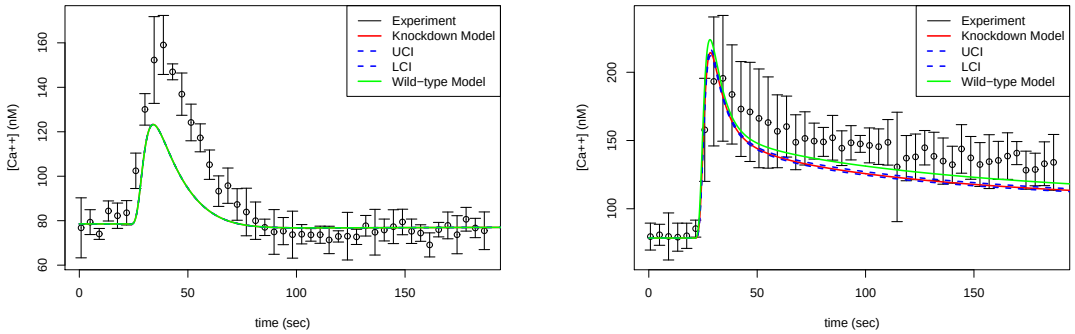

Figure 3.8: (left) PLCβ4 knockdown C5a 20nM calcium response. (right) PLCβ4 knockdown UDP 25μM calcium response.

reaction network is viewed as a connected graph, knockdowns remove nodes and toxins remove edges. Table 3.2 shows the three toxins that are effective in perturbing the GPCR systems we have modeled. The affected reaction in our model is shown beside the toxin. In simulation, we have considered the effect of the toxin to be to reduce the kinetic rate constant by 80%.

Toxin	Affected Reaction
Pertussis	(k105f) C5aC+G$\beta\gamma$-Gα_{i}-GDP $\rightarrow$ C5aC+G$\beta\gamma$ +Gα_{i}-GTP
U-73122	(k15bf) PLCb4-Ca^{2+} +Gα_{q}-GTP-PIP2 $\rightarrow$ PLCβ4-Ca^{2+} +Gα_{q}-GDP+IP3+DAG
	(k21bf) PLCβ3-Ca^{2+}-G$\beta\gamma$-PIP2 $\rightarrow$ PLCβ3-Ca^{2+}-G$\beta\gamma$ +IP3+DAG
Calphostin-C	(k33f) PKC+DAG $\rightarrow$ PKC-DAG

Table 3.2: Several toxins are used to probe the system. These toxins inhibit specific reactions.

U-73122 and pertussis toxins inhibit IP3 synthesis, but Calphostin-C inhibits the PKC-mediated feedback pathway. It is interesting to investigate the net effect on calcium release when a Gα_{i}, Gα_{q} or PLCβ knockdown cell line, which inhibit IP3 synthesis, is combined with a toxin that inhibits a negative feedback mechanism. We also explore the effect of pertussis toxin and U73122 in combination with GRK2 knockdown cells to investigate the net effect of a forward and feedback pathway perturbation.

Pertussis Toxin Pertussis toxin (PTx) is an exotoxin secreted by the pathogenic Gram-negative bacterium *Bordetella pertussis*. The toxin molecule consists of two subunits. The B subunit binds the complex to the cellular membrane and the A subunit confers the biological activity. Pertussis toxin ADP-ribosylates the Cys^{352} residue of $G\alpha_i$ (Finger and Koenig, 1996, chap. 31). This ADP-ribose causes the $G\alpha_i$ to have a lower affinity for GTP than normal, effectively trapping the $G\alpha_i$ in the "off" state (Berg et al., 2002, pp. 419). This toxin is an effective method for classification of ligand response as either PTx-sensitive or PTx-insensitive, narrowing the set of possible α-units involved in the transduction mechanism. Interacting pathways can be interrogated using multiple perturbations by pretreating wild-type and knockdown cells with PTx. The model simulations for this experiment are shown in Figure B.1 and Figure B.2.

U-73122 U-73122 is an aminosteroid that inhibits agonist-induced PLCβ activity (Jin et al., 1994)(Biosciences, 2006, pp. 62). The model simulations for this experiment are shown in Figure B.3 and Figure B.4.

Calphostin-C Calphostin-C (CPC), isolated from *Cladosporium cladosporioides*, is a specific inhibitor of PKC. It is 1000× more inhibitory to PKC than to other protein kinases (Kobayashi et al., 1989; Tamaoki et al., 1990). It acts by competitively binding to the DAG regulatory domain on PKC. DAG is then unable to bind and activate PKC (Biosciences, 2006, pp. 21).

Figure 3.10 shows the predicted response for five knockdown and the wild-type cell lines when pretreated for 30 min with CPC and then stimulated with 100nM C5a. A

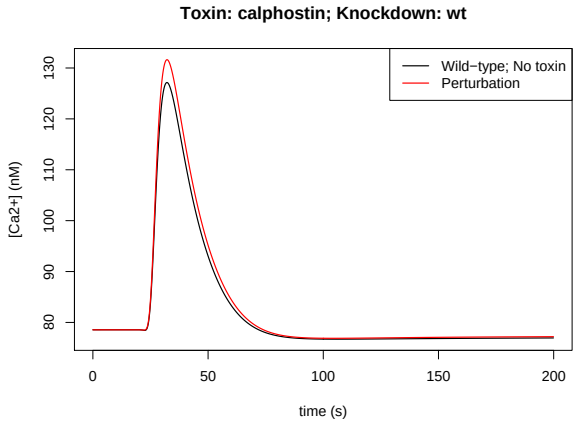

Figure 3.9: 100nM C5a Calphostin-C Wild-type Response

full complement of simulation results are shown in Figure B.5 and Figure B.6.

3.7 Synergistic Interaction between C5a and UDP

Preliminary experiments shown in Figure 3.11 show that the simultaneous addition of both ligands gives a higher peak height and faster decay than expected from a model in which the contribution from the UDP and C5a stimulation is additive.

A test of the usefulness of a model is whether it is able to predict the outcome of a novel experiment. Usually, a held-out data set that is similar to the training data set is used for this purpose. However, we test this model on an experiment which subjects the cells to both ligands (C5a & UDP) simultaneously for a variety of concentrations. Our training data only includes single ligand stimulation experiments.

A "synergy ratio" is computed for each ligand dose pair. The numerator of the ratio is the peak offset from baseline of the intracellular calcium concentration. The denominator of the ratio is the sum of the peak offsets when the cell or model is only stimulated with

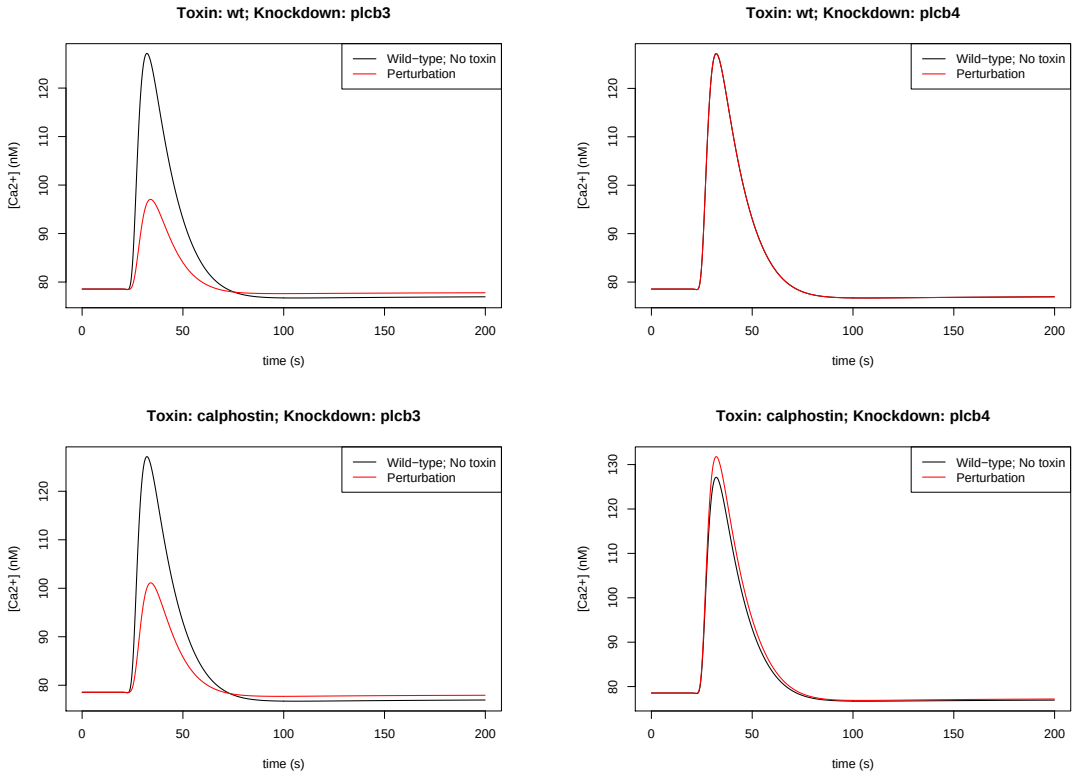

Figure 3.10: Predicted response for cell lines pretreated with Calphostin-C (a PKC inhibitor) and stimulated with 100nM C5a.

one ligand. A ratio greater than one indicates that the peak height is greater than expected from an additive combination of ligand effects; the combination is synergistic. According to the model simulations there is a ridge of synergistic calcium release for a moderate dose of UDP (shown in the upper-left panel of Figure 3.12).

In order to test this model prediction, an experiment design was constructed to measure the synergy ratio at the points denoted as black open circles in the upper-left panel of Figure 3.12. The results of these experiments for three fixed doses of C5a as a function of UDP dose are shown in the remaining three panels. The model predictions for the experiments with 90% prediction confidence intervals are shown in red with black error

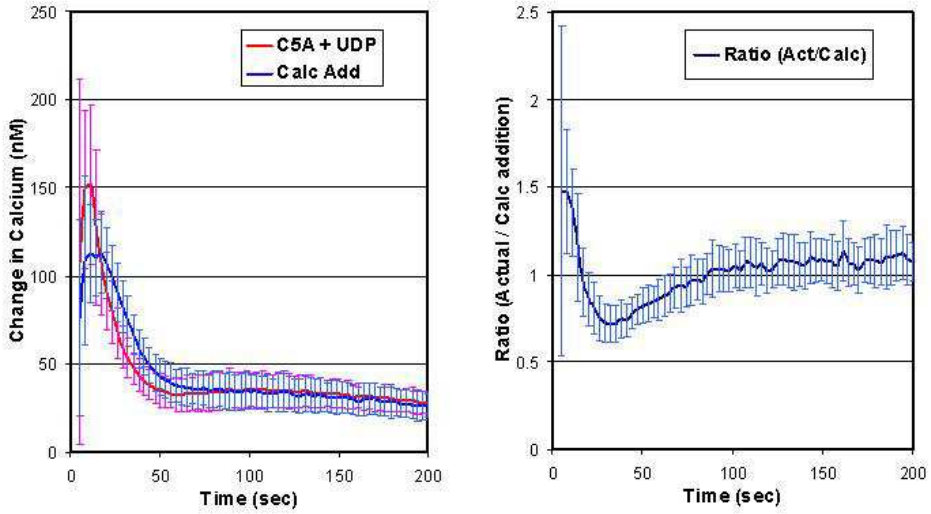

Data are compiled from 6 experiments. The left panel shows the average stimulation of calcium when RAW cells were exposed simultaneously to C5a and UDP (red). The linear addition of stimulations produced by C5a and UDP alone are shown in blue. The left panel shows an average of ratios of the actual calcium response with simultaneous addition of the two ligands to the calculated addition of both responses alone. In this case, ratios were calculated for each experiment before averaging. This reduces experimental variability due to changes in absolute calcium signals. Errors are standard deviations.

Figure 3.11: Observed C5a - UDP Synergy

bars. The filled black circles show the measured synergy ratio. While the model predictions based on only the nominal parameter values shows a region of synergy, when the uncertainty in the parameters and measurement error is taken into account, the model predicts that the observed data will not reject the possibility that the experimentally measured ratio is equal to or less than one by chance. Indeed, the spread in the experiment observations span a synergy ratio of one in most cases. The model-based Monte Carlo confidence intervals inform us in the design of experiments stage as to the expected value and the variance in the experimental data. Without accounting for uncertainty, we may be misled to believe that the experimental data rejects to possibility of a synergistic interaction between C5a and UDP. Instead, our conclusion from these data must be that the data are consistent

with the mechanism for GPCR signal transduction hypothesized by the model.

3.7.1 Crosstalk Mechanism

While the quantitative differences between the calcium response to C5a and UDP can be attributed, at least in part, to the specificity of Gα isoforms and G$\beta\gamma$ for PLCβ isoforms, the synergistic response is not obviously due to the same mechanism. The synergy mechanism in our model cannot be due simultaneous binding of $G\alpha_q$ and G$\beta\gamma$ binding to PLCβ3 because we have explicitly assumed both cannot be bound to PLCβ3 simultaneously. The flexibility of the model provides us the unique opportunity to perturb the system to analyze the mechanism and then design targeted experiments to test the mechanism.

In our simulation studies, if the $G\alpha_q$-PLCβ3-Ca^{2+} and $G\alpha_q$-PLCβ4-Ca^{2+} binding reactions are inhibited, the system still exhibits synergy indicating the crosstalk mechanism is mediated by G$\beta\gamma$. If binding reaction of G$\beta\gamma$ to phosphorylated GRK2 is removed, the synergy is eliminated. Furthermore, if the GRK2-mediated phosphorylation of complexed C5a receptors is removed, the double ligand response is additive. We deduce then that the synergy mechanism also involves GRK2 phosphorylation of complexed C5a receptors.

A formal sensitivity analysis of the role of each reaction is possible in this model, but is computationally intensive and less informative than a targeted probe of the model. A manual exploration of the model structure allows us to observe the effects of each perturbation at any model state. We are able to isolate and prune the exploration more efficiently than an automated method at this time. An exhaustive exploration of model perturbations would be computationally intensive because it would require and investigation of each model state for each perturbation. Even then we may miss an important and unexpected

effect.

The concentration time series of active PKC, active GRK and phosphorylated C5a receptor indicates that the amount of time required for the feedback signal to propagate through and finally desensitize the C5a receptor is approximately the same whether the system is stimulated by UDP and C5a or C5a alone. However, rate of change of the concentration of PLCβ3 is much faster with UDP and C5a compared to C5a or UDP alone.

Furthermore, as a negative control, we have stimulated the model with a two fixed doses of either C5a or UDP and then simulated the additive combination of those doses to assess whether C5a or UDP can self-synergize. In all cases examined, C5a and UDP were unable to self-synergize indicating that heterogenous receptor activation is necessary for synergistic calcium release in this model. This observation implies that the mechanism of synergy is dependent upon the differences between subsets of reactions for each receptor system.

Since the system, even in the more simplified form of our model compared to the real cell, is complex, a complete understanding of the mechanism will require further simplification. We have shown that the synergy in the model is mediated by G$\beta\gamma$. We have also shown that GRK feedback plays a role in the synergy mechanism. Finally, neither C5a nor UDP can self-synergize in this model. No doubt a more detailed analysis with appropriate simplified models of the proposed mechanisms will be required for a full understanding of synergy. Nevertheless, as a tool to aid in reasoning and representing complex biological systems and as a tool for the design of experiments, this model has proved useful.

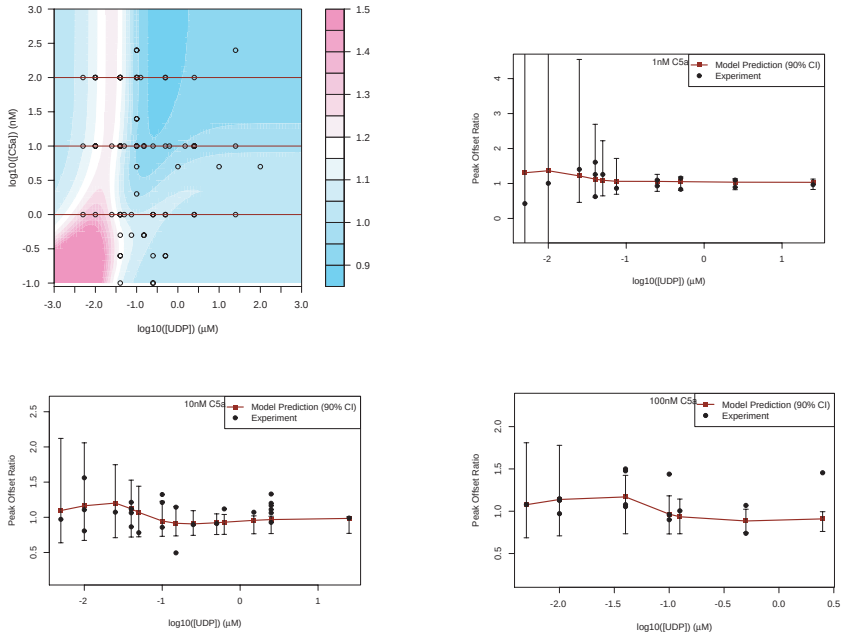

Figure 3.12: The model is used as a predictive tool to infer the expected effect of stimulating the cell simultaneously with UDP and C5a which signal through the $G\alpha_q$ and $G\alpha_i$ pathways respectively. Synergy is measured as the ratio of peak height offset from baseline attained from simultaneous stimulation to the peak height offset calculated by the sum of the responses to each ligand individually. The upper-right panel shows the expected synergy ratio as a function of UDP and C5a dose (truncated at 1.5). The simulations show a ridge of synergy at a moderate UDP dose for most C5a doses. The black circles indicate dose combinations points for which experiments were conducted to test the model. The remaining three panels show the synergy ratio as a function of UDP dose for three fixed C5a doses indicated by the red lines in the upper-left panel. While the synergy ratio is expected to be greater than one for a moderate dose of UDP, when parameter and measurement uncertainty is taken into account the magnitude of the effect is not sufficient to conclude that the experimental observations would be significantly different than one. The model-based point estimates are shown as red squares and the actual experimental measurements are shown as black dots. While the pattern of the experimental measurements fits the model predictions, we find, as predicted, that the magnitude of the effect on the calcium peak offset ratio in this cell type is not sufficient to conclude that synergy is present. Without the prediction confidence intervals, we would be lead to wrongly expect a synergy ratio that is significantly different than one.

Chapter 4

Statistical Inference

Statistical inference is fundamentally about making decisions, on the basis of observed data, about features of the physical system that gave rise to the data (Kendall et al., 1994). In the case of hypothesis testing the features of the system may be the model and our inferential objective is to reject inappropriate models. More often, however, the features are the unknown parameters of the model. A model is asserted and statistical inference methods are used to estimate the physical constants as they appear in the model.

As a statistical problem, the inference problem presented by the GPCR model falls in the area of nonlinear regression problems. The model for us is a system of nonlinear differential equations. The state of the system will be called s, the controllable conditions of the system (e.g. knockdown fraction) will be called x and the measured data will be called y. The model can be written

$$y(t) = g(x, \theta, s_0, t) + \varepsilon(x), \qquad \varepsilon \sim \mathcal{N}(0, \sigma(x, t)). \tag{4.0.1}$$

We have explicitly written the model as a function of the initial conditions s_0 and

the parameters θ. For notational simplicity we will suppress some of these terms where needed. Equation (4.0.1) is a statistical model which can now be used to bridge the divide between a deterministic simulation model and experimental data. Because we have made an assumption on the error term, we can write the likelihood of the experimental data under this model as

$$f(y|\theta) = \prod_{n=1}^{N} \prod_{t=1}^{T_n} f(y|t, x_n, \theta) \tag{4.0.2}$$

where a y is a sample containing T_n time points. The likelihood for one experiment and one time point is the probability density function based on (4.0.1)

$$f(y|t, x_n, \theta) = \frac{1}{\sqrt{2\pi\sigma^2(x_n, t)}} \exp\left\{ -\frac{(y(t) - g(x_n, \theta, t))^2}{2\sigma^2(x_n, t)} \right\}.$$

But this is the likelihood of the data under the model. We really would like the likelihood of the model given the data. Bayes rule allows us to reverse this conditioning and compute the function we are interested in from the likelihood.

4.1 Bayesian Inference

In the Bayesian framework, the parameters of the model $\theta \in \Theta$ are regarded as random variables. Prior to observing data, the joint distribution over the parameters will be denoted $\pi(\theta)$. After observing a sample, y_n, we update our prior distribution and obtain the posterior distribution $p(\theta|y_n)$. Bayes Theorem links these two quantities

$$p(\theta|y_n) = \frac{f(y_n|\theta)\pi(\theta)}{\int_\Theta f(y_n|\theta)\pi(\theta)d\theta}. \tag{4.1.1}$$

Bayes theorem provides a direct method for parameter updating. As more data is accumulated, the user need only update the posterior distribution and only carry that along instead of all of the data. This property is very valuable in a situation such as this where follow-up experiments are expected.

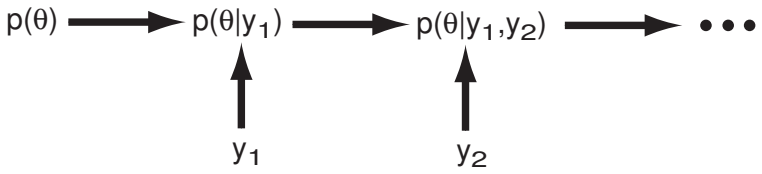

Figure 4.1: The posterior data is updated and becomes the new prior as new data is accumulated.

In some cases, the posterior distribution can be computed analytically and inference is computationally simple. However, often the parameter space is complex or high-dimensional (e.g. $\Theta = \Theta_1 \times \Theta_2 \times \cdots \times \Theta_n$) and the resulting high dimensional integration in the denominator is not trivial. This subject will be addressed in section 4.2. The remainder of this section will deal with useful distributions derived from the posterior distribution.

4.1.1 Parameter Confidence Intervals

Estimating parameter confidence intervals is somewhat broader than obtaining point estimates of parameters. The goal is to report a set, $\mathcal{A}$, which contains the true value of the parameter with high probability. In a sense, a point parameter estimate is a confidence interval with measure zero.

Classical confidence intervals are statements about the probability that a *random* interval *covers* the true parameter θ since the data is considered random and the parameter is fixed but unknown (Casella and Berger, 2002). The classical confidence interval statement

can be written

$$\mathbb{E}_\theta\left(\mathbf{1}_{\{\theta\in[L(Y),U(Y)]\}}\right) = P_\theta(\theta \in [L(Y), U(Y)]) = \int_{L(Y)}^{U(Y)} f(X|\theta)dX \tag{4.1.2}$$

where the expectation is with respect to the data generating distribution $F(y|\theta)$.

The interpretation of (4.1.2) is important. It says that the interval $[L(Y), U(Y)]$, which depends on the random variable representing the sample, Y, covers the true parameter with a particular probability. Had we drawn a different sample, the intervals would be different, but the fixed parameter would not change. The statement says that over repeated draws of samples, we can expect that for example 90% of the intervals that we calculate actually do contain the true parameter. In general (4.1.2) is impossible to compute since it requires the true θ. However, in some cases, the intervals can be expressed in terms of a quantity with a distribution that is independent of the parameter. In these cases, the distribution is called a *pivot* and the interval can be found. Modern statistical techniques, such as the bootstrap, have been developed to get around this problem.

The Bayesian setup allows us to make the statement, "The true value of the parameter is inside the interval with 90% probability." at the cost of more assumptions. This is possible because the data is fixed (it has been observed) and the parameter (or our belief of it) is random. To distinguish the two, very different, concepts the Bayesian form is called a credible interval

$$\mathbb{E}\left(\mathbf{1}_{\{\theta\in\mathcal{A}\}}|y\right) = P(\theta \in \mathcal{A}|y) = \int_{\mathcal{A}} p(\theta|y)d\theta \tag{4.1.3}$$

where $p(\theta|y)$ is the posterior density function. Notice that the averaging distribution

in (4.1.2) is $f(y|\theta)$ and the averaging distribution in (4.1.3) is $p(\theta|y)$. Unlike pivots, Bayesian credible sets can always be found and they are not necessarily convex.

4.1.2 Prediction Confidence Intervals

As more replicate data is collected it is reasonable that the parameter confidence intervals should concentrate on the true parameter assuming the data can provide such information. But because there is variability in the measurements, the confidence intervals on the model prediction of an observed sample should concentrate to fixed, but non-empty interval.

Consider a newdata point Y_{n+1}; written in upper case because it is an as yet unobserved random variable. The distribution can be written

$$P(Y_{n+1}|y_n) = \int f(Y_{n+1}|\theta)p(\theta|y_n)d\theta \tag{4.1.4}$$

since Y_{n+1} is independent of Y_n given θ.

Approximation by Maximum A-posteriori Estimate Rather than obtaining the entire prediction distribution, we can settle for a point estimate. Equation (4.1.4) is then simplified by replacing the integral by a max,

$$\begin{aligned} P(Y_{n+1}|y_n) &\approx \max_{\theta} f(Y_{n+1}|\theta)p(\theta|y_n) \\ &= f(Y_{n+1}|\hat{\theta}_{\text{MAP}})p(\hat{\theta}_{\text{MAP}}|y_n). \end{aligned} \tag{4.1.5}$$

We have effectively collapsed the entire posterior distribution over the parameters to a point mass at $\hat{\theta}_{\text{MAP}}$. This approximation is common and very computationally efficient,

but unsatisfying since we have disregarded the uncertainty in the parameter in the computation of our prediction. However, if the variation in the parameter is small or the prediction does not change appreciably in the neighborhood of $\hat{\theta}_{\text{MAP}}$ then this approximation is useful.

Approximation by Monte Carlo If we can take an independent sample of size M from (4.1.1) then we can sample from the predictive posterior distribution to approximate (4.1.4). We replace the true posterior distribution by "plugging-in" the empirical posterior distribution to get the mixture distribution with finite mixing components,

$$\begin{aligned} P(Y_{n+1}|y_n) &\approx \int f(Y_{n+1}|\theta) dP_{n,M}(\theta) \\ &= \frac{1}{M}\sum_{i=1}^{M} f(Y_{n+1}|\theta_i), \end{aligned} \tag{4.1.6}$$

where $P_{n,M}(\theta|y_n) = \sum_{i=1}^{M} \frac{1}{M}\delta_{\theta_i}$ is the empirical cdf and

$$\delta_x \triangleq \begin{cases} 0 & \text{if } \theta < x, \\ 1 & \text{if } \theta \geq x. \end{cases}$$

If $f(Y_{n+1}|\theta)$ is simple (which it is in our case since $f(Y_{n+1}|\theta) \sim \mathcal{N}(\mu_{\text{MOD}}, \sigma)$, where μ_{MOD} is the model prediction and σ is the sample standard deviation of an observation from (4.0.1)) the prediction distribution can be computed by Monte Carlo sampling the mixture distribution (4.1.6).

4.2 Markov Chain Monte Carlo

Analytical forms for Bayes estimates do not often exist except in special situations when the prior is said to be conjugate to the likelihood, so they must be computed numerically in many practical applications. The difficult component is often the normalization constant in (4.1.1). The integral can be interpreted generally as the expected value of some function $g(\cdot)$ where $g = f(y|\theta)$ is the likelihood function for the model in (4.1.1),

$$\mathbb{E}_\pi(g) = \int_\Theta g(\theta)\pi(\theta)d\theta.$$

Some classes of methods for computing this integral are:

- Gaussian-Hermite Quadrature
- Laplace Approximations
- Markov Chain Monte Carlo (MCMC).

Of these classes of methods, MCMC is by far the most general purpose and widely used in practice.

4.2.1 Gauss-Hermite Quadrature

Numerical integration, as it is usually taught in calculus is also called *quadrature*. In general an integral to be approximated can be written

$$I = \int_a^b f(x)dx. \tag{4.2.1}$$

The integral can be approximated by calculating f at a set of points $\{x_1, \ldots, x_n\}$ and using a weighted combination of those function evaluations to approximate the integral,

$$I \approx \hat{I} = \sum_{i=1}^{n} w_i f(x_i). \tag{4.2.2}$$

This approximation algorithm separates into two components: (1) selecting design points $\{x_1, \ldots, x_n\}$ and (2) selecting weights $\{w_1, \ldots, w_n\}$. Simple quadrature approximates an integral on an interval by selecting equal intervals for the design points and equal weights (Kendall et al., 1994). The approximation in (4.2.2) becomes a sum of rectangles.

Gauss-Hermite quadrature handles the situation when the limits of integration are $(-\infty, \infty)$. The design points and weights are chosen such that the approximation is exact if $\exp(x^2/2)f(x)$ is a polynomial of order $(2n-1)$ or less (Kendall et al., 1994).

4.2.2 Laplace Approximation

The Laplace Approximation is useful if the quantity $g(\theta)\pi(\theta) \geq 0, \quad \forall\theta$. Then it can be written $g(\theta)\pi(\theta) = \exp\{nh(\theta)\}$ where n can be taken to go to infinity (Casella and Berger, 2002).

$$h(\theta) \approx h(\theta_0) + (\theta - \theta_0)h'(\theta_0) + \frac{(\theta - \theta_0)^2}{2}h''(\theta_0) \tag{4.2.3}$$

If θ_0 is chosen to be at a maximum (e.g. $\hat{\theta}_{MAP}$) then the $h'(\theta_0) = 0$ and the Laplace approximation becomes the normalization term from a Gaussian density function

$$\int_\Theta g(\theta)\pi(\theta)d\theta \approx \int_\Theta \exp\left\{n\frac{(\theta - \theta_0)^2}{2}h''(\theta_0)\right\} d\theta. \tag{4.2.4}$$

4.2.3 Markov Chain Monte Carlo

Twenty of the 84 parameters in the GPCR model were chosen to be estimated from data based on relevance to the experimental data. Only those parameters that related to the knockdown experiments in Table 3.1 were estimated and are denoted with a star in Table A.2. We used data to estimate only the two forward rate constants in the enzymatic mass-action equations because the forward and reverse rate constants for a given reaction will be highly correlated in the posterior distribution making estimation by Markov chain methods computationally expensive.

For each estimated parameter we constructed an independent Gaussian prior on a log scale with a mean chosen based on literature data and a standard deviation of 0.25. We found that this prior variance was sufficiently permissive for the exploration of the parameter space while still constraining the rates to be physically reasonable.

The Metropolis-Hastings algorithm (Robert and Casella, 2004) was used to estimate the posterior density of the parameters $\Pr(\theta|y)$ where y is the observed data. Since the posterior density of the parameters has significant correlation structure, three independent chains were simulated from different initial parameter values. Each chain was simulated for a burn-in period of 50,000 iterations and then a sample size of 29906 was taken with a thinning factor of 10. To assess convergence of the posterior distribution estimate, we used the Gelman-Rubin potential scale reduction factor (PSRF) (Gelman and Rubin, 1992). The multivariate PSRF is 2.44 and 95% of the individual PSRFs were less than 1.5. A PSRF value of one indicates that the distribution has converged.

The observed standard deviation, in (4.0.1), for each calcium measurement was

Algorithm: Metropolis-Hastings

Initialize $\theta^{(0)}$

for *i = 0 to M-1* **do**

Sample $u \sim \text{Uniform}[0, 1]$.

Sample $\theta^* \sim q(\theta^*|\theta^{(i)})$.

if $u < \mathcal{A}(x^{(i)}, x^*) = \min\left[\frac{p(x^*)}{p(x^{(i)})}, 1\right]$ **then**

$x^{(i+1)} = x^*$

else

$x^{(i+1)} = x^{(i)}$

end

end

Figure 4.2: Metropolis-Hastings Algorithm

estimated from 3-4 replicates on the same plate. By chance the replicate measurements for some time points were nearly identical causing the standard deviation estimate to be close to zero. Since the log of the likelihood for a Gaussian distribution contains the standard deviation estimate in the denominator, a near-zero value will force the likelihood to be large unless a parameter value is selected which causes the simulation value to be very close to the measured value in the numerator. This effectively causes only a few terms in the likelihood to have a disproportionate importance in the model fit. We implemented a common remedy for this situation. A small constant factor (1nM) was added to the estimate of the standard deviation to prevent this degeneracy in the solution.

4.3 Posterior Density Analysis

Posterior prediction confidence intervals were constructed using the percentiles from the predictive distribution approximated with 2000 Monte Carlo samples from $\Pr(Y_{new}|\theta)$ at each of 100 simple random samples from according to

$$\Pr(Y_{new}|y) = \int \Pr(Y_{new}|\theta)\Pr(\theta|y)d\theta \approx \sum_{i=1}^{100} \Pr(Y_{new}|\theta_i)\Pr(\theta_i|y) \tag{4.3.1}$$

where $\Pr(Y_{new}|\theta_i) \sim \mathcal{N}(0, \hat{s}^2)$ and $\hat{s}^2$ is the pooled variance. The pooled variance is estimated by taking the average of the variances of all the time points in each for the 29 wild-type experiments. These average variances are weighted by the number of technical replicates in each experiment and then averaged to yield the estimate of $\hat{\sigma}^2$ from (4.0.1). Figure 4.3 shows prediction confidence intervals for two experiments on wild-type cells. The predictive confidence intervals were computed using equation (4.1.6).

Figure 4.4 shows the posterior probability $\Pr(\theta|y)$ for the three MCMC chains as a function of the sample number. Figure 4.5 shows a comparison of the prior and posterior densities. The posterior density has a smaller variance than the prior density indicating that some information about the parameter has been gained from the calcium measurements. The marginal samples from the three independent chains overlap considerably indicating that the sampling algorithm has converged to the true posterior distribution.

Credible intervals based on the marginal densities are generally conservative. It is possible a point can be inside the joint credible intervals constructed from say the 90% marginal intervals, but not in the true joint interval. Even so, the marginal distribution of the parameters are informative for assessing the improvement in parameter accuracy due

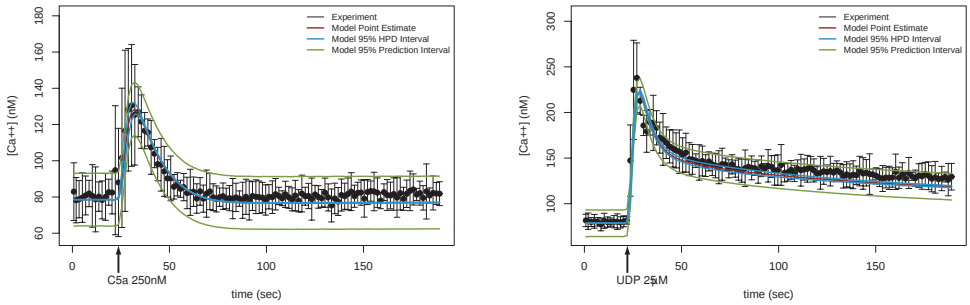

Figure 4.3: Model simulations are compared to experimental data. The point estimate is computed using the posterior parameter distribution estimated by Markov chain Monte Carlo given the data from 96 experiments on C5a and UDP at various doses in combination with 5 different shRNAi knockdown cell lines. The 95% HPD interval simulations are computed using parameters from the component-wise 95% confidence intervals of the posterior distribution on parameters. The 95% posterior predictive intervals are estimated by Monte Carlo simulations including both parameter and measurement uncertainty. The measured mean of four replicates is shown by a black dot and the error bar, computed as 1.96 times the standard deviation, approximates the 95% confidence interval for the data assuming normally distributed errors. (left) C5a at 250nM was introduced at 20s and the experimentally observed pulse in cytosolic calcium concentration is shown. (right) The qualitative shape of the calcium pulse for UDP is different than for C5a. The pulse does not completely adapt and return the prestimulated level. For both ligands, the model prediction confidence intervals overlap the data error bars which indicate the model fit is consistent with the data within the measurement uncertainty.

to observing data.

The 95% credible intervals for all the estimated parameters based on one of the chains are in Table 4.3.

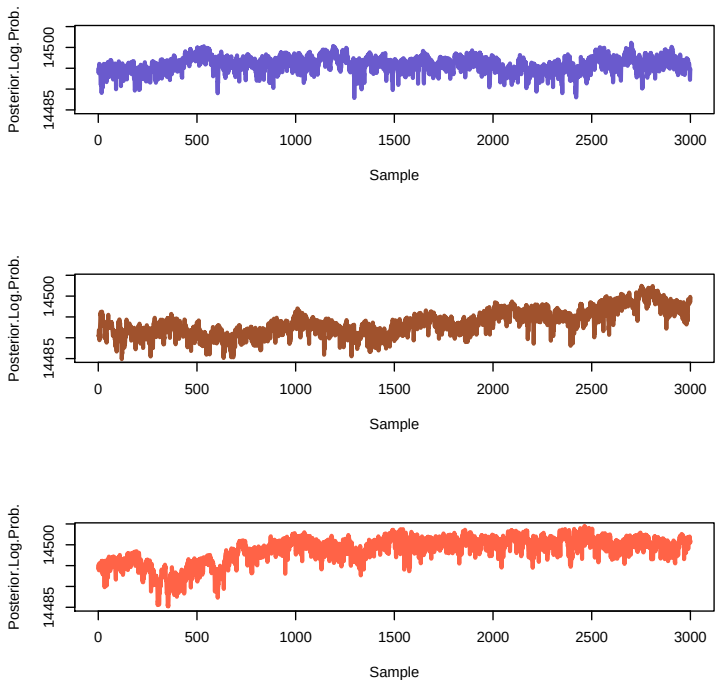

Figure 4.4: The posterior probabilities of the sampled parameter vector is plotted as a function of the sample number for three independent MCMC chains. The posterior probabilities are relatively stable and consistent between chains after a considerable burn-in period.

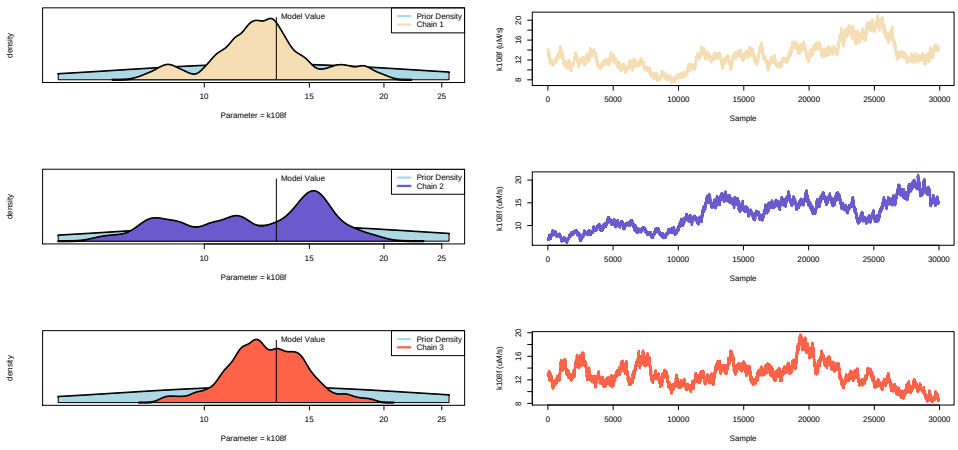

Figure 4.5: (left) The prior and posterior density for the parameter in the reaction UDP + p2yr → UDPC. (right) Sample paths for the parameter from three independent MCMC chains.

	Marginal Mean	**Lower 95% HPD**	**Upper 95% HPD**	**Model**
k108f	12.79	8.09	18.46	13.20
k108r	3.51	2.07	5.00	3.61
k101f	110.47	32.33	197.76	92.41
k101r	0.50	0.043	0.98	0.37
k102bf	293.35	118.54	494.92	199.31
k105f	0.01	0.010	0.017	0.012
k109f	0.13	0.12	0.15	0.13
k15af	1424.34	764.53	2331.21	1238.78
k15bf	33.34	16.99	55.39	22.85
k19af	123.54	51.11	191.00	70.87
k19bf	32.01	16.42	56.67	27.89
k21af	163.77	149.73	179.55	165.83
k21bf	5.49	5.08	5.89	5.41
k24af	8.38	3.073	12.55	5.89
k24bf	0.65	0.22	1.02	0.93
k25af	662.20	513.98	819.13	830.44
k25bf	20.56	10.63	32.18	11.69787
k37f	5.14	3.96	6.93	4.98
k28af	184.86	49.53	349.19	77.52
k28bf	7.56	2.95	14.92	18.34

Table 4.1: Highest posterior density intervals for estimated parameters.

Chapter 5

Experiment Design

We consider the general problem of statistical experiment design as it arises in the context of the G protein-coupled receptor model. Experiments to measure rate constant parameters are expensive, time-consuming and inaccurate for complex systems. So, it is valuable to use cheap, but indirect or noisy measurements on calcium concentration to infer the values of certain critical rate constants. We are interested in using the kinetic model to guide our experimental design to infer the values of rate constants.

Suppose we have a nonlinear model $y = f(x, \theta) + \varepsilon, \quad \varepsilon \sim \mathcal{N}(0, \sigma^2)$ where $x \in \mathcal{X}$ represents the controllable conditions of the experiment, y is the experimental measurement and $\theta \in \mathbb{R}^p$ are the parameters of the model. We consider a finite menu of available experiments $\mathcal{X} \in \{x_1, \ldots, x_m\}$ but in general $\mathcal{X}$ may be a countably infinite set. The objecive of experiment design is to select the best set of n experiments from the menu (with repeats) in the sense of some criterion of the estimate $\hat{\theta}$. We can relax this combinatorial problem by instead optimizing the probability distribution over $\mathcal{X}$. This distribution can

then be multiplied by n and rounded appropriately to give an approximately optimal design in the original sense (Boyd and Vandenberghe, 2003). Let $\xi(dx)$ be a probability measure over design points such that

$$\xi(x) = \left\{ \begin{array}{c} x_1, \ldots, x_m \\ \\ w_1, \ldots, w_m \end{array} \right\} \tag{5.0.1}$$

when x is discrete.

We adopt a standard least-squares framework for parameter estimation. In the nonlinear setting this is done by making a Taylor series expansion of the model about an estimate θ_0 (Seber and Wild, 2003).

$$f(x, \theta) = f(x, \theta_0) + V(\theta - \theta_0) + O(\|\theta - \theta_0\|), \tag{5.0.2}$$

where V is the Jacobian matrix of the model; the i^{th} row of V is $v_i^T = \left.\frac{\partial f(x_i, \theta)}{\partial \theta}\right|_{\theta_0}$.

The least-squares estimate of θ is $\hat{\theta} = \theta_0 + \left(V^T W V\right)^{-1} V^T W x \left(y - f(x, \theta_0)\right)$, where $W = \text{diag}(w)$. The covariance matrix for the parameter estimate is $\text{cov}(\hat{\theta}|\xi) = \sigma^2 \left(V^T W V\right)^{-1}$, which is the inverse of the observed Fisher information matrix.

The aim of optimal experiment design methods is to minimize the covariance matrix of the parameter estimate (Atkinson and Donev, 1992; Boyd and Vandenberghe, 2003; Box et al., 1978). There are two well-known difficulties that must be surmounted in the case of nonlinear models (Box et al., 1978):

- The optimal design depends on an evaluation of the derivative of the model with respect to the parameters at a particular parameter estimate. Given that our goal is parameter estimation, this involves a certain circularity.

- Simple optimal design procedures tend to concentrate experimental weight on only a few design points (Silvey, 1980). Such designs are overly optimistic about the appropriateness of the model, and provide little information about possible lack of fit over a wider experimental range.

There have been three main responses to these problems: sequential experiment design (Silvey, 1980), Bayesian methods (Lindley, 1956), and maximin approaches (Pronzato and Walter, 1988).

In the sequential approach, a working parameter estimate is first used to construct a tentative experiment design. Data are collected under that design and the parameter estimate is updated. The procedure is iterated in stages. While heuristically reasonable, this approach is often inapplicable in practice because of costs associated with experiment set-up time.

In the Bayesian approach exemplified by (Lindley, 1956), a proper prior distribution is constructed for the parameters to be estimated. The objective function is the KL divergence between the prior distribution and the expected posterior distribution; this KL divergence is *maximized* (thereby maximizing the amount of expected information in the experiment design). Sensitivity to priors is a serious concern, however, particularly in the biological setting in which it can be quite difficult to choose priors for quantities such as bulk rates for a complex process.

The maximin approach considers a bounded range for each parameter and finds the optimal design for the worst case parameters in that range. The major difficulties with this approach are computational, and its main applications have been to specialized

problems (Silvey, 1980).

The approach that we present here is close in spirit to the maximin and the bayesian approach. We view both of the problems discussed above as arguments for a *robust* design. One which is insensitive to the linearization point and to model error. We work within the framework of E-optimal design (see below) and consider perturbations to the rank-one Fisher information matrix for each design point. An optimization with respect to such perturbations yields a robust semidefinite program (Vandenberghe and Boyd, 1996; El Ghaoui et al., 1998; El Ghaoui and Lebret, 1997). In a special case, these rank-one perturbations can be considered equivalent to a full-rank pertubation on the resultant information matrix. A Bayesian design arises when that perturbation matrix is specified a-priori (Chaloner and Verdinelli, 1995).

5.1 Locally Optimal Experiment Design

Most optimization methods minimize a scaler function of the decision variables subject to constraints. The three most common scalar measures of the size of the parameter covariance matrix in optimal experiment design are:

- *D-optimal design*: determinant of the covariance matrix.
- *A-optimal design*: trace of the covariance matrix.
- *E-optimal design*: maximum eigenvalue of the covariance matrix.

We adopt the E-optimal design criterion, and formulate the design problem as follows:

$$\mathcal{P}_0 : p_0^* = \min_w \lambda_{\max} \left[\left(\sum_{i=1}^m w_i v_i v_i^T \right)^{-1} \right] \quad s.t. \ \sum_{i=1}^m w_i = 1 \qquad (5.1.1)$$
$$w_i \geq 0, \forall i,$$

where $\lambda_{\max}[M]$ is the maximum eigenvalue of a matrix M. The induced 2-norm is equivalent to the spectral norm this problem can also be written as

$$\mathcal{P}_0 : p_0^* = \min_w \left\| \left(\sum_{i=1}^m w_i v_i v_i^T \right)^{-1} \right\|_2 \quad s.t. \ \sum_{i=1}^m w_i = 1 \qquad (5.1.2)$$
$$w_i \geq 0, \forall i.$$

This problem can be recast as the following semidefinite program (Boyd and Vandenberghe, 2003):

$$\mathcal{P}_0 : p_0^* = \max_{w,s} s \quad s.t. \ \sum_{i=1}^m w_i v_i v_i^T \geq s I_p \qquad (5.1.3)$$
$$\sum_{i=1}^m w_i = 1, \quad w_i \geq 0, \forall i,$$

which forms the basis of the robust extension that we develop in the following section. Note that the optimal value of the semidefinite program is the inverse of the original problem, but the optimizer is the same.

5.2 Robust Experiment Design

The uncertain parameters appear in the experiment design optimization problem through the Jacobian matrix, V. We consider additive unstructured perturbations on the Jacobian in this problem. The uncertain observed Fisher information matrix is $F(w, \Delta) =$

$\sum_{i=1}^{m} w_i(v_i v_i^T - \Delta_i)$, where Δ_i is a $p \times p$ matrix for $i = 1, \ldots, m$. We consider a spectral norm bound on the magnitude of the perturbations such that $\|\mathbf{blkdiag}(\Delta_1, \ldots, \Delta_m)\| \leq \rho$.

Incorporating the perturbations, the E-optimal experiment design problem with uncertainty based on (5.1.3) can be cast as the following minimax problem:

$$\begin{aligned} \mathcal{P}_\rho : p_\rho^* = \quad & \max_w \min_\Delta s \\ \text{subject to} \quad & \textstyle\sum_{i=1}^{m} w_i(v_i v_i^T + \Delta_i) \geq s I_p \\ & \Delta = \mathbf{blkdiag}(\Delta_1, \ldots, \Delta_m), \|\Delta\| \leq \rho \\ & \textstyle\sum_{i=1}^{m} w_i = 1, \quad w_i \geq 0, \forall i. \end{aligned} \tag{5.2.1}$$

We will call equation (5.2.1) an *E-robust experiment design.*

To implement the program efficiently, we can recast the linear matrix inequality in (5.2.1) in a linear fractional (LFT) representation:

$$F(w, s, \Delta) = F(w, s) + L\Delta R(w) + R(w)^T \Delta^T L^T \geq 0,$$

where

$$F(w, s) = \sum_{i=1}^{m} w_i v_i v_i^T - s I_p, \qquad R(w) = \tfrac{1}{\sqrt{2}} (w \otimes I_p)$$
$$L = \frac{-1}{\sqrt{2}} \left(\mathbf{1}_m^T \otimes I_p \right), \quad \Delta = \mathbf{blkdiag}(\Delta_1, \ldots, \Delta_m).$$

However, the constraints in (5.2.1) are not enough. Each Δ_i can be chosen to minimize the term in which it is involved independently of the others. This will simply scale all of the $vivi^T$ by the same constant and the optimizing w is unchanged.

A further constraint is $\Delta_1 = \cdots = \Delta_m$. This forces each $v_i v_i^T + \Delta_i$ to lie within a norm bounded neighborhood of the same size and shape. With this constraint the robust

SDP with structured uncertainty becomes a robust SDP with unstructured uncertainty.

$$\begin{aligned} \mathcal{P}_\rho : p^*_\rho = \quad & \max_w \min_{\|\Delta\| \le \rho} s \\ \text{subject to} \quad & \textstyle\sum_{i=1}^m w_i v_i v_i^T + \Delta \ge s I_p \\ & \textstyle\sum_{i=1}^m w_i = 1, \quad w_i \ge 0, \forall i. \end{aligned} \tag{5.2.2}$$

Employing a special case of the S-procedure (El Ghaoui et al., 1998) the robust SDP can be cast as a normal SDP

$$\begin{aligned} \mathcal{P}_\rho : p^*_\rho = \quad & \min_{w,\tau} -s \\ \text{subject to} \quad & \begin{bmatrix} \sum_{i=1}^m w_i v_i v_i^T - s I_p - \frac{1}{2}\tau I_p & \frac{\rho}{\sqrt{2}} I_p \\ \frac{\rho}{\sqrt{2}} I_p & \tau I_p \end{bmatrix} \ge 0 \\ & \textstyle\sum_{i=1}^m w_i = 1, \quad w_i \ge 0, \forall i. \end{aligned} \tag{5.2.3}$$

If $\rho = 0$ we recover (5.1.3). Using the Schur complement the first constraint in (5.2.3) can be further simplified to

$$\sum_{i=1}^m w_i v_i v_i^T - \rho I_p \ge s I_p, \tag{5.2.4}$$

which makes the regularization of the optimization problem (5.1.3) explicit. The uncertainty bound, ρ, serves as a weighting parameter for a regularization term. Finally, the original objective criterion can be rewritten $\min_w \lambda_{\max}\left[\left(V^T W V - \rho I_p\right)^{-1}\right]$ which is no harder to solve than an eigenvalue problem. However, equation (5.2.1) is much more general than this simplification and the general form will be used to intrduce other convex constraints that provide better designs.

5.3 Application to G protein-coupled Receptor Model

We demonstrate the robust experiment design on two models of biological systems. The first model is the Michaelis-Menten model of a simple enzyme reaction system. This model, derived from mass-action kinetics, is a fundamental building block of many mechanistic models of biological systems. The second example is a model of a complex calcium signal transduction pathway in macrophage immune cells. In this example we consider RNAi knockdowns at a variety of ligand doses for the estimation of receptor level parameters.

5.3.1 Michaelis-Menten Reaction Model

The Michaelis-Menten model is a common approximation to an enzyme-substrate reaction (Segel and Slemrod, 1989). The basic chemical reaction that leads to this model is $E + S \underset{k_{-1}}{\overset{k_{+1}}{\rightleftharpoons}} C \xrightarrow{k_2} E + P$, where E is the enzyme concentration, S is the substrate concentration and P is the product concentration. We employ mass action kinetics to develop a differential equation model for this reaction system (Segel and Slemrod, 1989). The velocity of the reaction is defined to be the rate of product formation, $V_0 = \frac{\partial P}{\partial t}\big|_{t_0}$. The initial velocity of the reaction is

$$V_0 \approx \frac{\theta_1 x}{\theta_2 + x}, \tag{5.3.1}$$

where

$$\theta_1 = k_{+2} E_0, \quad \theta_2 = \frac{k_{-1} + k_{+2}}{k_{+1}}. \tag{5.3.2}$$

We have taken the controllable factor, x, in this system to be the initial substrate concentration S_0. The parameter θ_1 is the saturating velocity and θ_2 is the initial substrate

concentration at which product is formed at one-half the maximal velocity. In this example $\theta_1 = 2$ and $\theta_2 = 2$ are the total enzyme and initial substrate concentrations. We consider six initial substrate concentrations as the menu of experiments, $\mathcal{X} = \left\{\frac{1}{8}, 1, 2, 4, 8, 16\right\}$.

Figure 5.1 shows the robust experiment design weights as a function of the uncertainty parameter with the Jacobian computed at the true parameter values. When ρ is small, the experimental weight is concentrated on only two design points. As $\rho \to \rho_{\max}$ the design converges to a uniform distribution over the entire menu of design points. In a sense, this uniform allocation of experimental energy is most robust to parameter uncertainty. Intermediate values of ρ yield an allocation of design points that reflects a tradeoff between robustness and nominal optimality.

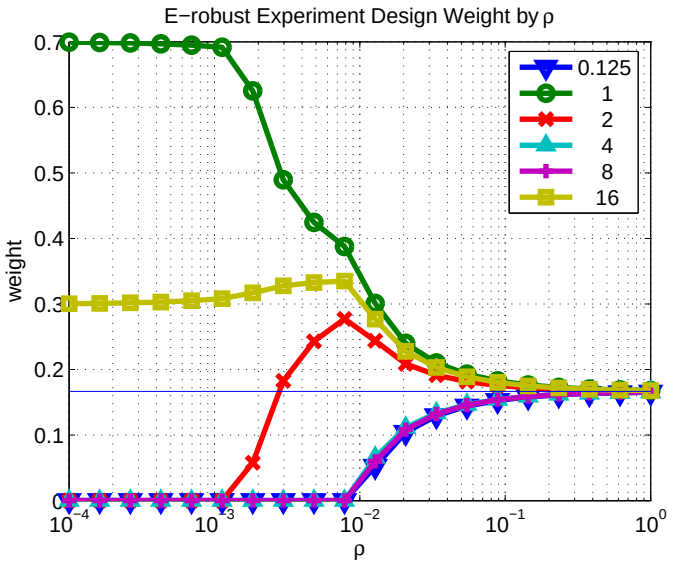

Figure 5.1: Michaelis-Menten model experiment design weights as a function of ρ.

For moderate values of ρ we gain significantly in terms of robustness to errors in $v_i v_i^T$, at a moderate cost to maximal value of the minimum eigenvalues of the parameter

estimate covariance matrix. Figure 5.2 shows the efficiency of the experiment design as a function of ρ and the prior estimate θ_{02} used to compute the Jacobian matrix. The E-efficiency of a design is defined to be

$$\text{efficiency} \triangleq \frac{\lambda_{\max}\left[\text{cov}\left(\hat{\theta}|\theta,\xi_0\right)\right]}{\lambda_{\max}\left[\text{cov}\left(\hat{\theta}|\theta_0,\xi_\rho\right)\right]}. \tag{5.3.3}$$

If the Jacobian is computed at the correct point in parameter space the optimal design achieves maximal efficiency. As the distance between θ_0 and θ grows the efficiency of the optimal design decreases rapidly. If the estimate, θ_{02}, is eight instead of the true value, two, the efficiency of the optimal design at θ_0 is 36% of the optimal design at θ. However, at the cost of a decrease in efficiency for parameter estimates close to the true parameter value we guarantee the efficiency is better for points further from the true parameters with a robust design. For example, for $\rho = 0.001$ the robust design is less efficient for the range $0 < \theta_{02} < 7$, but is more efficient for $7 < \theta_{02} < 16$.

5.3.2 Calcium Signal Transduction Model

When certain small molecule ligands such as the anaphylatoxin C5a are introduced into the environment of an immune cell a complex chain of chemical reactions leads to the transduction of the extracellular ligand concentration information and a transient increase in the intracellular calcium concentration. This chain of reactions can be mathematically modeled using the principles of mass-action kinetics and nonlinear ordinary differential equations. We consider specifically the model presented in (Lemon et al., 2003) which was developed for the P2Y2 receptor, modifying the model for our data on the C5a receptor.

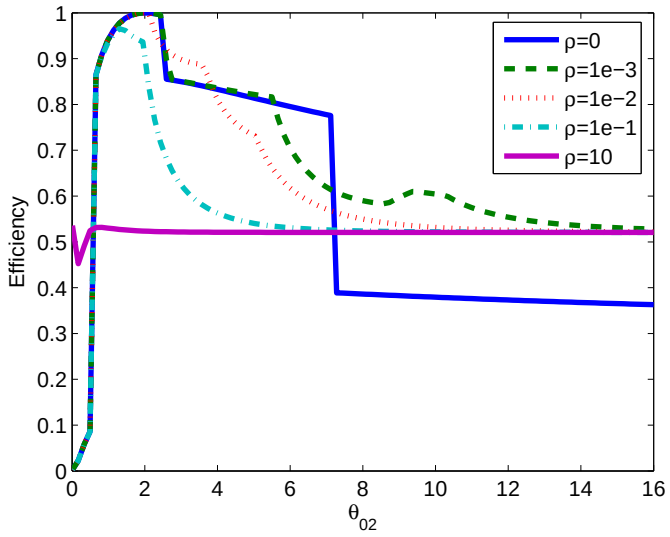

Figure 5.2: Efficiency of robust designs as a function of ρ and perturbations in the prior parameter estimate θ_{02}.

The menu of available experiments is indexed by one of two different cell lines in combination with different ligand doses. The cell lines are: wild-type and a *GRK2* knockdown line. *GRK2* is a protein that represses signaling in the G-protein receptor complex. When its concentration is decreased with interfering RNA the repression of the signal due to *GRK2* is reduced. There are 17 experiments on the menu and we choose to do 100 experiments allocated according the experiment design. For each experiment we are able measure the transient calcium spike peak height using a fluorescent calcium dye. We are concerned with estimating three C5A receptor parameters: K_1, k_p, k_{deg} which are detailed in (Lemon et al., 2003). We have selected the initial parameter estimates based on a least-squares fit to a separate data set of 67 experiments on a wild-type cell line with a ligand concentration of 250nM. We have estimated, from experimental data, the mean and variance for all of the experiments in our menu. Observations are simulated from these data

to obtain the least-squares parameter estimate for the optimal, robust ($\rho = 1.5 \times 10^{-6}$) and uniform experiment designs.

Figure 5.3 shows the model fits with associated 95% confidence bands for the wild-type and knockdown cell lines for the parameter estimates from the three experiment designs. A separate validation data set is generated uniformly across the design menu. Compared to the optimal design, the parameter estimates based on the robust design provide a better fit across the whole dose range for both cell types as measured by mean-squared residual error.

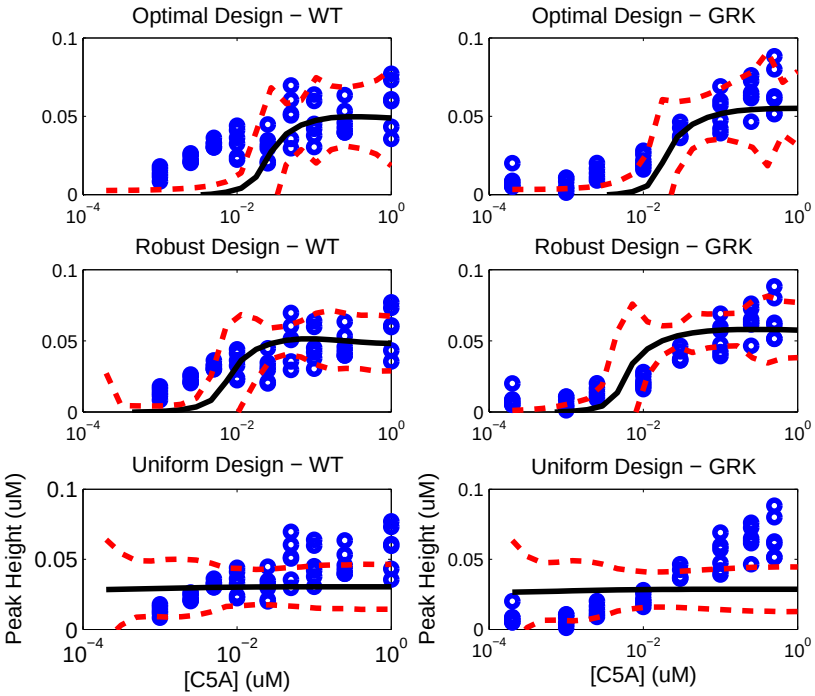

Figure 5.3: Model predictions based on the least squares parameter estimate using data observed from the optimal, robust and uniform design. The predicted peak height curve (black line) based on the robust design data is shifted to the left compared to the peak height curve based on the optimal design data and matches the validation sample (shown as blue dots) more accurately.

Note also that the measured response at high ligand concentration is better fit

with parameters estimated from the robust design. Near 1μM of C5a concentration the peak height is predicted to decrease slightly in the wild-type cell line, but plateaus for the *GRK2* knockdown cell line. This matches the biochemical understanding that *GRK2* acts as a repressor of signaling.

5.4 Discussion

The methodology of optimal experiment design leads to efficient algorithms for the construction of designs in general nonlinear situations (Atkinson, 1996). However, these variance-minimizing designs fail to account for uncertainty in the nominal parameter estimate and the model. We present a methodology, based on recent advances in semidefinite programming, that retains the advantages of the general purpose algorithm while explicitly incorporating uncertainty.

We demonstrated this robust experiment design method on two example systems. In the Michaelis-Menten model, we showed that the E-optimal design is recovered for $\rho = 0$ and the uniform design is recovered as $\rho \to \rho_{\max}$. It was also shown that the robust design is more efficient than the optimal for large perturbations of the nominal parameter estimate away from the true parameter.

The second example, of a calcium signal transduction model, is a more realistic case of the need for experiment design in high-throughput biological research. The model captures some of the important kinetics of the system, but is far from complete. We require a reasonably accurate model to make further predictions about the system and drive a set of experiments to estimate critical parameters of the model more accurately. The

resulting robust design spreads some experiments across the menu, but also concentrates on experiments that will help minimize the variance of the parameter estimates.

These robust experiment designs were obtained using SeDuMi 1.05 (Sturm, 1999). The design for the calcium signal transduction model takes approximately one second on a 2GHz processor, which is less time than required to compute the Jacobian matrix for the model.

Research in machine learning has led to significant advances in computationally-efficient data analysis methods, allowing increasingly complex models to be fit to biological data. Challenges in experimental design are the flip side of this coin—for complex models to be useful in closing the loop in biological research it is essential to begin to focus on the development of computationally-efficient experimental design methods.

Chapter 6

Conclusion

The model presented is a hypothesis of the mechanism of signal integration by the $G\alpha_i$ and $G\alpha_q$-coupled receptor systems which involves calcium-dependent feedback and combinatorial activation. It has been suggested that a synergistic release of calcium is caused by G units specific to the C5a receptor simultaneously bind to PLCβ3 with $G\alpha_q$ units from the UDP receptor and cause the activity of PLCβ3 to be greater than with either G protein subunit bound alone (Werry et al., 2003). However, the mechanism hypothesized in this model does not require simultaneous binding and produces a synergistic interaction between C5a and UDP.

Intracellular calcium concentration measurements on wild-type and genetically perturbed cell lines with a variety of ligand doses is used in a Bayesian framework to estimate the posterior distribution over a set of biochemical parameters. Prediction confidence intervals for the model simulations were estimated and used to assess the consistency of the model with validation experiments. The synergistic interaction between C5a and UDP is

shown to be consistent with the model when the prediction confidence intervals are taken into account.

The calcium measurements using in this study are done on populations of RAW264.7 cells. However, it is single cells that respond to the ligand, not populations of cells. The measurement process effectively averages over all the single cell responses to produce the population measurements that we observe. We may find that the ecological correlation is present in the data. It will be interesting to show whether the population measurements do reflect events at the single cell level.

While we have attempted to capture the state of understanding in the literature regarding the mechanism for GPCR signal integration, naturally some mechanisms represented in the model are controversial or incompletely understood. The model representation of the hypothetical mechanism does not afford us the opportunity to be vague about such components and we have made specific assertions in those areas. For instance, the mechanism of IP3-mediated calcium release is still under debate (Berridge et al., 1999). In other areas of the model, we have constructed mechanisms that are simplified versions of the more complex reality which permit us and others the opportunity to extend the model as more experiments testing those areas become available (e.g. Ca^{2+} store replenishment and PIP2 regeneration). Despite these usual qualifications, we have demonstrated a novel two-receptor GPCR model which represents a feasible mechanism for signal integration from multiple GPCR systems, used Bayesian methods to construct confidence intervals on model predictions and used the model to design novel experiments which were shown to be consistent with the model predictions.

The statistical methods employed here are readily applicable to other mechanistic and phenomenological models to inform parameter values and assess the consistency of the model with novel experimental data. Further, this initial model is a substrate for many extensions. The second messenger cAMP is known to interact with Ca^{2+} and contribute to signal transduction complexity but was not included in this model. Many other ligand combinations have been shown to interact synergistically and experiments on those ligand pairs will be a valuable test for the combinatorial activation/calcium-dependent feedback mechanism hypothesized by this model.

The experiment design methodology presented in the last chapter fits well within formal application of statistical methods to complex uncertain biological systems. Parameter estimates, while improved by the posterior analysis, is still uncertain even after observing experimental data. The natural next question is: "What experiments can be done to gain the most information about the uncertain parameters." A solution of this experiment design question is presented in the form of a semidefinite program which is computationally efficient.

Bibliography

Bruce Alberts. *Molecular biology of the cell*. Garland Science, New York, 4th edition, 2002. 2, 3, 33

H. Ali, R. M. Richardson, B. Haribabu, and R. Snyderman. Chemoattractant receptor cross-desensitization. *J Biol Chem*, 274(10):6027–30, 1999. 18

M. Allegretti, A. Moriconi, A. R. Beccari, R. Di Bitondo, C. Bizzarri, R. Bertini, and F. Colotta. Targeting c5a: recent advances in drug discovery. *Curr Med Chem*, 12(2): 217–36, 2005. 2

B. Ananthanarayanan, R. V. Stahelin, M. A. Digman, and W. Cho. Activation mechanisms of conventional protein kinase c isoforms are determined by the ligand affinity and conformational flexibility of their c1 domains. *J Biol Chem*, 278(47):46886–94, 2003. 37

A. C. Atkinson. The usefulness of optimum experimental designs. *Journal of the Royal Statistical Society.Series B (Methodological)*, 58(1):59–76, 1996. 88

A. C. Atkinson and A. N. Donev. *Optimum Experiment Design*. Clarendon Press, Oxford, 1992. 77

Y. Banno, T. Asano, and Y. Nozawa. Proteolytic modification of membrane-associated

phospholipase c-beta by mu-calpain enhances its activation by g-protein beta gamma subunits in human platelets. *FEBS Lett*, 340(3):185–8, 1994. 24

Jeremy Mark Berg, John L. Tymoczko, Lubert Stryer, and National Center for Biotechnology Information (U.S.). Biochemistry, 2002. 7, 17, 19, 20, 23, 25, 35, 36, 43, 55

M. Berridge, P. Lipp, and M. Bootman. Calcium signalling. *Curr Biol*, 9(5):R157–9, 1999. 30, 91

M. J. Berridge, M. D. Bootman, and H. L. Roderick. Calcium signalling: dynamics, homeostasis and remodelling. *Nature reviews. Molecular cell biology*, 4(7):517–529, 2003. 19, 30, 31

EMD Biosciences. Inhibitor sourcebook, 2006. 55

M. D. Bootman, M. J. Berridge, and C. W. Taylor. All-or-nothing ca2+ mobilization from the intracellular stores of single histamine-stimulated hela cells. *The Journal of physiology*, 450:163–178, 1992. 33

H. R. Bourne, D. A. Sanders, and F. McCormick. The gtpase superfamily: conserved structure and molecular mechanism. *Nature*, 349(6305):117–27, 1991. 7, 16

George E. P. Box, William Gordon Hunter, and J. Stuart Hunter. *Statistics for experimenters: an introduction to design, data analysis, and model building*. Wiley, New York, 1978. 10, 77

Stephen Boyd and Lieven Vandenberghe. *Convex Optimization*. Cambridge University Press, 2003. 77, 80

E. Carafoli. Intracellular calcium homeostasis. *Annu Rev Biochem*, 56:395–433, 1987. 28, 31, 34

E. Carafoli, L. Santella, D. Branca, and M. Brini. Generation, control, and processing of cellular calcium signals. *Critical reviews in biochemistry and molecular biology*, 36(2): 107–260, 2001. 32

G. Casella and R. L. Berger. *Statistical inference*. Duxbury/Thomson Learning, Australia; Pacific Grove, CA, 2002. 64, 69

P. J. Casey and A. G. Gilman. G protein involvement in receptor-effector coupling. *J Biol Chem*, 263(6):2577–80, 1988. 17

Kathryn Chaloner and Isabella Verdinelli. Bayesian experimental design: A review. *Statistical Science*, 10(3):273–304, 1995. 79

T. T. Chuang, 3rd LeVine, H., and A. De Blasi. Phosphorylation and activation of beta-adrenergic receptor kinase by protein kinase c. *J Biol Chem*, 270(31):18660–5, 1995. 39, 40

D. E. Clapham and E. J. Neer. New roles for g-protein beta gamma-dimers in transmembrane signalling. *Nature*, 365(6445):403–6, 1993. 23

D. E. Clapham and E. J. Neer. G protein beta gamma subunits. *Annu Rev Pharmacol Toxicol*, 37:167–203, 1997. 17, 22

K. S. Cuthbertson and T. R. Chay. Modelling receptor-controlled intracellular calcium oscillators. *Cell Calcium*, 12(2-3):97–109, 1991. 10

Y. Daaka, J. A. Pitcher, M. Richardson, R. H. Stoffel, J. D. Robishaw, and R. J. Lefkowitz. Receptor and g betagamma isoform-specific interactions with g protein-coupled receptor kinases. *Proc Natl Acad Sci U S A*, 94(6):2180–5, 1997. 39

J. M. East. Sarco(endo)plasmic reticulum calcium pumps: recent advances in our understanding of structure/function and biology (review). *Mol Membr Biol*, 17(4):189–200, 2000. 30

L. El Ghaoui and Herve Lebret. Robust solutions to least-squares problems with uncertain data. *SIAM J. Matrix Anal. Appl.*, 18(4):1035–1064, 1997. 79

Laurent El Ghaoui, Francois Oustry, and Herve Lebret. Robust solutions to uncertain semidefinite programs. *SIAM Journal on Optimization*, 9(1):33–52, 1998. 79, 82

M. V. Ellis, S. R. James, O. Perisic, C. P. Downes, R. L. Williams, and M. Katan. Catalytic domain of phosphoinositide-specific phospholipase c (plc). mutational analysis of residues within the active site and hydrophobic ridge of plcdelta1. *J Biol Chem*, 273(19):11650–9, 1998. 23, 25

David Filmore. It's a gpcr world. *Modern Drug Discovery*, page 11, 2004. 2

Horst Finger and Carl Heinz Wirsing. von Koenig. Bordetella. In Samuel Baron MD, editor, *Medical Microbiology 4th edition*. The University of Texas Medical Branch at Galveston, Galveston, 1996. 55

H. Hugh Fudenberg. *Basic & clinical immunology*. Lange Medical Publications, Los Altos, Calif., 3d edition, 1980. 18

R. C. Garrad, M. A. Otero, L. Erb, P. M. Theiss, L. L. Clarke, F. A. Gonzalez, J. T. Turner, and G. A. Weisman. Structural basis of agonist-induced desensitization and sequestration of the p2y2 nucleotide receptor. consequences of truncation of the c terminus. *J Biol Chem*, 273(45):29437–44, 1998. 15, 49

Andrew Gelman and Donald B. Rubin. Inference from iterative simulation using multiple sequences. *Statistical Science*, 7(4):457–472, 1992. 70

Louis Sanford Goodman, Alfred Gilman, Laurence L. Brunton, John S. Lazo, and Keith L. Parker. *Goodman & Gilman's the pharmacological basis of therapeutics*. McGraw-Hill, New York, 11th edition, 2006. 2, 6, 7

G. Grynkiewicz, M. Poenie, and R. Y. Tsien. A new generation of ca2+ indicators with greatly improved fluorescence properties. *J Biol Chem*, 260(6):3440–50, 1985. 45

A. T. Harootunian, J. P. Kao, S. Paranjape, and R. Y. Tsien. Generation of calcium oscillations in fibroblasts by positive feedback between calcium and ip3. *Science*, 251 (4989):75–8, 1991. 11

A. C. Hindmarsh, P. N. Brown, K. E. Grant, S. L. Lee, R. Serban, D. E. Shumaker, and C. S. Woodward. Sundials: Suite of nonlinear and differential/algebraic equation solvers. *ACM Transactions on Mathematical Software*, 31(3):363–396, 2005. 46

Charles Janeway and Paul Travers. *Immunobiology: the immune system in health and disease*. Current Biology; Garland Pub., London; San Francisco New York, 2nd edition, 1996. 2

D. Y. Jhon, H. H. Lee, D. Park, C. W. Lee, K. H. Lee, O. J. Yoo, and S. G. Rhee. Cloning, sequencing, purification, and gq-dependent activation of phospholipase c-beta 3. *J Biol Chem*, 268(9):6654–61, 1993. 20

H. Jiang, D. Wu, and M. I. Simon. Activation of phospholipase c beta 4 by heterotrimeric gtp-binding proteins. *J Biol Chem*, 269(10):7593–6, 1994. 20, 21, 25

H. Jiang, Y. Kuang, Y. Wu, A. Smrcka, M. I. Simon, and D. Wu. Pertussis toxin-sensitive activation of phospholipase c by the c5a and fmet-leu-phe receptors. *J Biol Chem*, 271 (23):13430–4, 1996. 20, 23, 25

W. Jin, T. M. Lo, H. H. Loh, and S. A. Thayer. U73122 inhibits phospholipase c-dependent calcium mobilization in neuronal cells. *Brain Res*, 642(1-2):237–43, 1994. 55

A. Katz, D. Wu, and M. I. Simon. Subunits beta gamma of heterotrimeric g protein activate beta 2 isoform of phospholipase c. *Nature*, 360(6405):686–9, 1992. 24, 25

J. H. Kehrl and S. Sinnarajah. Rgs2: a multifunctional regulator of g-protein signaling. *Int J Biochem Cell Biol*, 34(5):432–8, 2002. 41

J. Keizer and G. W. De Young. Two roles of ca2+ in agonist stimulated ca2+ oscillations. *Biophys J*, 61(3):649–60, 1992. 10, 26, 27, 29, 31, 33, 34

Maurice G. Kendall, Alan Stuart, J. K. Ord, Steven F. Arnold, and Anthony O'Hagan. *Kendall's advanced theory of statistics*. Edward Arnold; Halsted Press, London New York, 6th edition, 1994. 62, 69

E. Kobayashi, H. Nakano, M. Morimoto, and T. Tamaoki. Calphostin c (ucn-1028c), a

novel microbial compound, is a highly potent and specific inhibitor of protein kinase c. *Biochem Biophys Res Commun*, 159(2):548–53, 1989. 55

W. K. Kroeze, D. J. Sheffler, and B. L. Roth. G-protein-coupled receptors at a glance. *J Cell Sci*, 116(Pt 24):4867–9, 2003. 1, 2

A. M. Krumins and A. G. Gilman. Targeted knockdown of g protein subunits selectively prevents receptor-mediated modulation of effectors and reveals complex changes in non-targeted signaling proteins. *J Biol Chem*, 2006. 7, 18, 50

P. Langkabel, J. Zwirner, and M. Oppermann. Ligand-induced phosphorylation of anaphylatoxin receptors c3ar and c5ar is mediated by "g protein-coupled receptor kinases. *Eur J Immunol*, 29(9):3035–46, 1999. 39, 40

Douglas A. Lauffenburger and Jennifer J. Linderman. *Receptors: models for binding, trafficking, and signaling*. Oxford University Press, New York, 1993. 9, 10, 16

C. W. Lee, K. H. Lee, S. B. Lee, D. Park, and S. G. Rhee. Regulation of phospholipase c-beta 4 by ribonucleotides and the alpha subunit of gq. *J Biol Chem*, 269(41):25335–8, 1994. 21, 25

R. J. Lefkowitz. G protein-coupled receptors. iii. new roles for receptor kinases and beta-arrestins in receptor signaling and desensitization. *J Biol Chem*, 273(30):18677–80, 1998. 38, 40

G. Lemon, W. G. Gibson, and M. R. Bennett. Metabotropic receptor activation, desensitization and sequestration-i: modelling calcium and inositol 1,4,5-trisphosphate dynamics following receptor activation. *J Theor Biol*, 223(1):93–111, 2003. 11, 85, 86

D. V. Lindley. On a measure of the information provided by an experiment. *The Annals of Mathematical Statistics*, 27(4):986–1005, 1956. 78

I. Litosch. Novel mechanisms for feedback regulation of phospholipase c-beta activity. *IUBMB Life*, 54(5):253–60, 2002. 19, 37

T. J. Lukas. A signal transduction pathway model prototype i: From agonist to cellular endpoint. *Biophys J*, 87(3):1406–16, 2004a. 11, 15

T. J. Lukas. A signal transduction pathway model prototype ii: Application to ca2+-calmodulin signaling and myosin light chain phosphorylation. *Biophys J*, 87(3):1417–25, 2004b. 11

T. Meyer and L. Stryer. Molecular model for receptor-stimulated calcium spiking. *Proc Natl Acad Sci U S A*, 85(14):5051–5, 1988. 10, 23

T. Meyer, D. Holowka, and L. Stryer. Highly cooperative opening of calcium channels by inositol 1,4,5-trisphosphate. *Science*, 240(4852):653–656, 1988. 29

M. D. Milcent, T. Christophe, M. J. Rabiet, M. Tardif, and F. Boulay. Overexpression of wild-type and catalytically inactive forms of grk2 and grk6 fails to alter the agonist-induced phosphorylation of the c5a receptor (cd88): evidence that grk6 is autophosphorylated in cos-7 cells. *Biochem Biophys Res Commun*, 259(1):224–9, 1999. 39

J. Mishra and U. S. Bhalla. Simulations of inositol phosphate metabolism and its interaction with insp(3)-mediated calcium release. *Biophys J*, 83(3):1298–316, 2002. 11

K. S. Murthy, D. H. Coy, and G. M. Makhlouf. Somatostatin receptor-mediated signaling

in smooth muscle. activation of phospholipase c-beta3 by gbetagamma and inhibition of adenylyl cyclase by galphai1 and galphao. *J Biol Chem*, 271(38):23458–63, 1996. 25

Philip Charles Nelson, Marko Radosavljevic, and Sarina Bromberg. *Biological physics: energy, information, life*. W.H. Freeman and Co., New York, 2004. 10, 14, 28

A. C. Newton. Protein kinase c: structure, function, and regulation. *J Biol Chem*, 270(48): 28495–8, 1995. 35, 36

D. Y. Noh, S. H. Shin, and S. G. Rhee. Phosphoinositide-specific phospholipase c and mitogenic signaling. *Biochim Biophys Acta*, 1242(2):99–113, 1995. 19, 20

D. Park, D. Y. Jhon, C. W. Lee, K. H. Lee, and S. G. Rhee. Activation of phospholipase c isozymes by g protein beta gamma subunits. *J Biol Chem*, 268(7):4573–6, 1993a. 20, 21

D. Park, D. Y. Jhon, C. W. Lee, S. H. Ryu, and S. G. Rhee. Removal of the carboxyl-terminal region of phospholipase c-beta 1 by calpain abolishes activation by g alpha q. *J Biol Chem*, 268(5):3710–4, 1993b. 23, 24

P. Penela, C. Ribas, and Jr. Mayor, F. Mechanisms of regulation of the expression and function of g protein-coupled receptor kinases. *Cell Signal*, 15(11):973–81, 2003. 39

Luc Pronzato and Eric Walter. Robust experiment design via maximin optimization. *Mathematical Biosciences*, 89:161–176, 1988. 78

U. Quitterer and M. J. Lohse. Crosstalk between galpha(i)- and galpha(q)-coupled receptors is mediated by gbetagamma exchange. *Proc Natl Acad Sci U S A*, 96(19):10626–31, 1999. 7

S. G. Rhee. Regulation of phosphoinositide-specific phospholipase c. *Annu Rev Biochem*, 70:281–312, 2001. 19, 20, 23

Christian P. Robert and George Casella. *Monte Carlo statistical methods*. Springer texts in statistics. Springer, New York, 2nd edition, 2004. 70

E. M. Ross and T. M. Wilkie. Gtpase-activating proteins for heterotrimeric g proteins: regulators of g protein signaling (rgs) and rgs-like proteins. *Annu Rev Biochem*, 69: 795–827, 2000. 17, 41

L. W. Runnels and S. F. Scarlata. Determination of the affinities between heterotrimeric g protein subunits and their phospholipase c-beta effectors. *Biochemistry*, 38(5):1488–96, 1999. 23

S. H. Ryu, K. S. Cho, K. Y. Lee, P. G. Suh, and S. G. Rhee. Purification and characterization of two immunologically distinct phosphoinositide-specific phospholipases c from bovine brain. *J Biol Chem*, 262(26):12511–8, 1987. 23

M. Schmidt, M. Frings, M. L. Mono, Y. Guo, P. A. Weernink, S. Evellin, L. Han, and K. H. Jakobs. G protein-coupled receptor-induced sensitization of phospholipase c stimulation by receptor tyrosine kinases. *J Biol Chem*, 275(42):32603–10, 2000. 22

G. A. F. Seber and C. J. Wild. *Nonlinear regression*. Wiley series in probability and statistics. Wiley-Interscience, Hoboken, NJ, 2003. 77

L. A. Segel and M. Slemrod. The quasi-steady-state assumption: A case study in perturbation. *SIAM Review*, 31(3):446–477, 1989. 83

L. A. Segel, A. Goldbeter, P. N. Devreotes, and B. E. Knox. A mechanism for exact sensory adaptation based on receptor modification. *Journal of theoretical biology*, 120(2):151–179, 1986. 9, 33

Lee A. Segel. *Biological kinetics*. Cambridge studies in mathematical biology. Cambridge University Press, Cambridge, England; New York, 12 edition, 1991. 14

S. K. Shenoy and R. J. Lefkowitz. Trafficking patterns of beta-arrestin and g protein-coupled receptors determined by the kinetics of beta-arrestin deubiquitination. *J Biol Chem*, 278 (16):14498–506, 2003. 39, 40

T. Shinomura, Y. Asaoka, M. Oka, K. Yoshida, and Y. Nishizuka. Synergistic action of diacylglycerol and unsaturated fatty acid for protein kinase c activation: its possible implications. *Proc Natl Acad Sci U S A*, 88(12):5149–53, 1991. 36, 37

George J. Siegel, R. Wayne Albers, Scott Brady, and Donald L. Price. *Basic neurochemistry: molecular, cellular, and medical aspects*. Elsevier Academic, Burlington; London, 7th edition, 2006. 15

S. D. Silvey. *Optimal Design*. Chapman & Hall, London, 1980. 78, 79

A. V. Smrcka and P. C. Sternweis. Regulation of purified subtypes of phosphatidylinositol-specific phospholipase c beta by g protein alpha and beta gamma subunits. *J Biol Chem*, 268(13):9667–74, 1993. 20, 22

M. Spitaler and D. A. Cantrell. Protein kinase c and beyond. *Nat Immunol*, 5(8):785–90, 2004. 35

P. C. Sternweis and A. V. Smrcka. G proteins in signal transduction: the regulation of phospholipase c. *Ciba Found Symp*, 176:96–106; discussion 106–11, 1993. 20

Jos F. Sturm. Using sedumi 1.02, a matlab toolbox for optimization over symmetric cones. *Optimization Methods and Software*, 11(12):625–653, 1999. 89

S. Swillens and D. Mercan. Computer simulation of a cytosolic calcium oscillator. *Biochem J*, 271(3):835–8, 1990. 11

T. Tamaoki, I. Takahashi, E. Kobayashi, H. Nakano, S. Akinaga, and K. Suzuki. Calphostin (ucn1028) and calphostin related compounds, a new class of specific and potent inhibitors of protein kinase c. *Adv Second Messenger Phosphoprotein Res*, 24:497–501, 1990. 55

R. Y. Tsien. Fluorescent indicators of ion concentrations. *Methods Cell Biol*, 30:127–56, 1989. 45

L. Vandenberghe and S. Boyd. Semidefinite programming. *SIAM Review*, 1996. 79

M. Warny, S. Aboudola, S. C. Robson, J. Sevigny, D. Communi, S. P. Soltoff, and C. P. Kelly. P2y(6) nucleotide receptor mediates monocyte interleukin-8 production in response to udp or lipopolysaccharide. *J Biol Chem*, 276(28):26051–6, 2001. 3

T. D. Werry, G. F. Wilkinson, and G. B. Willars. Mechanisms of cross-talk between g-protein-coupled receptors resulting in enhanced release of intracellular ca2+. *Biochem J*, 374(Pt 2):281–96, 2003. 90

G. B. Willars, S. R. Nahorski, and R. A. Challiss. Differential regulation of muscarinic

acetylcholine receptor-sensitive polyphosphoinositide pools and consequences for signaling in human neuroblastoma cells. *J Biol Chem*, 273(9):5037–46, 1998. 42

D. Wu, A. Katz, and M. I. Simon. Activation of phospholipase c beta 2 by the alpha and beta gamma subunits of trimeric gtp-binding protein. *Proc Natl Acad Sci U S A*, 90(11): 5297–301, 1993. 21, 25

H. J. Xia and G. Yang. Inositol 1,4,5-trisphosphate 3-kinases: functions and regulations. *Cell Res*, 15(2):83–91, 2005. 43

K. Yoshioka, O. Saitoh, and H. Nakata. Heteromeric association creates a p2y-like adenosine receptor. *Proc Natl Acad Sci U S A*, 98(13):7617–22, 2001. 15, 19

C. Yue, C. Y. Ku, M. Liu, M. I. Simon, and B. M. Sanborn. Molecular mechanism of the inhibition of phospholipase c beta 3 by protein kinase c. *J Biol Chem*, 275(39):30220–5, 2000. 37, 38

X. Zhu and L. Birnbaumer. G protein subunits and the stimulation of phospholipase c by gs-and gi-coupled receptors: Lack of receptor selectivity of galpha(16) and evidence for a synergic interaction between gbeta gamma and the alpha subunit of a receptor activated g protein. *Proc Natl Acad Sci U S A*, 93(7):2827–31, 1996. 23

Appendix A

Model Implementation

A.1 Model Equations

$$
\begin{aligned}
\mathrm{d[C5aR]} = \; & -k_{101\mathrm{f}}[\mathrm{C5a}][\mathrm{C5aR}] + k_{101\mathrm{r}}[\mathrm{C5aC}] + k_{104\mathrm{f}}[\mathrm{C5aC_p}] \\
\mathrm{d[C5aC]} = \; & -k_{101\mathrm{r}}[\mathrm{C5aC}] + k_{101\mathrm{f}}[\mathrm{C5a}][\mathrm{C5aR}] - k_{102\mathrm{af}}[\mathrm{GRK_p} \bullet \mathrm{G}\beta\gamma][\mathrm{C5aC}] \\
& + k_{102\mathrm{ar}}[\mathrm{GRK_p} \bullet \mathrm{G}\beta\gamma \bullet \mathrm{C5aC}] \\
\mathrm{d[GRK_p \bullet G}\beta\gamma] = \; & -k_{102\mathrm{af}}[\mathrm{GRK_p} \bullet \mathrm{G}\beta\gamma][\mathrm{C5aC}] + k_{102\mathrm{ar}}[\mathrm{GRK_p} \bullet \mathrm{G}\beta\gamma \bullet \mathrm{C5aC}] \\
& + k_{102\mathrm{bf}}[\mathrm{GRK_p} \bullet \mathrm{G}\beta\gamma \bullet \mathrm{C5aC}] - k_{37\mathrm{r}}[\mathrm{GRK_p} \bullet \mathrm{G}\beta\gamma] + k_{37\mathrm{f}}[\mathrm{GRK_p}][\mathrm{G}\beta\gamma] \\
\mathrm{d[GRK_p \bullet G}\beta\gamma \bullet \mathrm{C5aC}] = \; & -k_{102\mathrm{ar}}[\mathrm{GRK_p} \bullet \mathrm{G}\beta\gamma \bullet \mathrm{C5aC}] + k_{102\mathrm{af}}[\mathrm{GRK_p} \bullet \mathrm{G}\beta\gamma][\mathrm{C5aC}] \\
& - k_{102\mathrm{bf}}[\mathrm{GRK_p} \bullet \mathrm{G}\beta\gamma \bullet \mathrm{C5aC}] \\
\mathrm{d[C5aC_p]} = \; & +k_{102\mathrm{bf}}[\mathrm{GRKp} \bullet \mathrm{Gbg} \bullet \mathrm{C5aC}] - k_{104\mathrm{f}}[\mathrm{C5aC_p}] \\
\mathrm{d[P2YR]} = \; & -k_{108\mathrm{f}}[\mathrm{UDP}][\mathrm{P2YR}] + k_{108\mathrm{r}}[\mathrm{UDPC}] \\
\mathrm{d[UDPC]} = \; & -k_{108\mathrm{r}}[\mathrm{UDPC}] + k_{108\mathrm{f}}[\mathrm{UDP}][\mathrm{P2YR}] - k_{109\mathrm{f}}[\mathrm{UDPC}][\mathrm{G}\beta\gamma \bullet \mathrm{G}\alpha_\mathrm{q}\mathrm{GDP}] \\
& + k_{109\mathrm{f}}[\mathrm{UDPC}][\mathrm{G}\beta\gamma \bullet \mathrm{G}\alpha_\mathrm{q}\mathrm{GDP}] \\
\mathrm{d[G}\beta\gamma \bullet \mathrm{G}\alpha_\mathrm{i}\mathrm{GDP}] = \; & -k_{105\mathrm{f}}[\mathrm{C5aC}][\mathrm{G}\beta\gamma \bullet \mathrm{G}\alpha_\mathrm{i}\mathrm{GDP}] + k_{11\mathrm{f}}[\mathrm{G}\alpha_\mathrm{i}\mathrm{GDP}][\mathrm{G}\beta\gamma] \\
\mathrm{d[G}\beta\gamma] = \; & +k_{105\mathrm{f}}[\mathrm{C5aC}][\mathrm{G}\beta\gamma \bullet \mathrm{G}\alpha_\mathrm{i}\mathrm{GDP}] + k_{109\mathrm{f}}[\mathrm{UDPC}][\mathrm{G}\beta\gamma \bullet \mathrm{G}\alpha_\mathrm{q}\mathrm{GDP}] \\
& - k_{11\mathrm{f}}[\mathrm{G}\alpha_\mathrm{i}\mathrm{GDP}][\mathrm{G}\beta\gamma] - k_{113\mathrm{f}}[\mathrm{G}\alpha_\mathrm{q}\mathrm{GDP}][\mathrm{G}\beta\gamma] - k_{20\mathrm{f}}[\mathrm{G}\beta\gamma][\mathrm{PLC}\beta 3 \bullet \mathrm{Ca}^{2+}] \\
& + k_{20\mathrm{r}}[\mathrm{PLC}\beta 3 \bullet \mathrm{Ca}^{2+} \bullet \mathrm{G}\beta\gamma] - k_{37\mathrm{f}}[\mathrm{GRK_p}][\mathrm{G}\beta\gamma] + k_{37\mathrm{r}}[\mathrm{GRK_p} \bullet \mathrm{G}\beta\gamma] \\
\mathrm{d[G}\alpha_\mathrm{i}\mathrm{GTP}] = \; & +k_{105\mathrm{f}}[\mathrm{C5aC}][\mathrm{G}\beta\gamma \bullet \mathrm{G}\alpha_\mathrm{i}\mathrm{GDP}] - k_{106\mathrm{f}}[\mathrm{G}\alpha_\mathrm{i}\mathrm{GTP}] - k_{9\mathrm{af}}[\mathrm{RGS_a}][\mathrm{G}\alpha_\mathrm{i}\mathrm{GTP}]
\end{aligned}
$$

$$
\begin{aligned}
& +k_{9ar}[\mathrm{RGS_a} \bullet \mathrm{G}\alpha_i\mathrm{GTP}] \\
\mathrm{d}[\mathrm{G}\alpha_i\mathrm{GDP}] = \; & +k_{106f}[\mathrm{G}\alpha_i\mathrm{GTP}] + k_{9bf}[\mathrm{RGS_a} \bullet \mathrm{G}\alpha_i\mathrm{GTP}] - k_{11f}[\mathrm{G}\alpha_i\mathrm{GDP}][\mathrm{G}\beta\gamma] \\
\mathrm{d}[\mathrm{G}\beta\gamma \bullet \mathrm{G}\alpha_q\mathrm{GDP}] = \; & -k_{109f}[\mathrm{UDPC}][\mathrm{G}\beta\gamma \bullet \mathrm{G}\alpha_q\mathrm{GDP}] + k_{113f}[\mathrm{G}\alpha_q\mathrm{GDP}][\mathrm{G}\beta\gamma] \\
\mathrm{d}[\mathrm{G}\alpha_q\mathrm{GTP}] = \; & +k_{109f}[\mathrm{UDPC}][\mathrm{G}\beta\gamma \bullet \mathrm{G}\alpha_q\mathrm{GDP}] - k_{110f}[\mathrm{G}\alpha_q\mathrm{GTP}] \\
& -k_{111af}[\mathrm{RGS_a}][\mathrm{G}\alpha_q\mathrm{GTP}] + k_{111ar}[\mathrm{RGS_a} \bullet \mathrm{G}\alpha_q\mathrm{GTP}] \\
& -k_{13f}[\mathrm{PLC}\beta4 \bullet \mathrm{Ca}^{2+}][\mathrm{G}\alpha_q\mathrm{GTP}] + k_{13r}[\mathrm{PLC}\beta4 \bullet \mathrm{Ca}^{2+} \bullet \mathrm{G}\alpha_q\mathrm{GTP}] \\
& -k_{17f}[\mathrm{PLC}\beta3 \bullet \mathrm{Ca}^{2+}][\mathrm{G}\alpha_q\mathrm{GTP}] + k_{17r}[\mathrm{PLC}\beta3 \bullet \mathrm{Ca}^{2+} \bullet \mathrm{G}\alpha_q\mathrm{GTP}] \\
\mathrm{d}[\mathrm{G}\alpha_q\mathrm{GDP}] = \; & +k_{110f}[\mathrm{G}\alpha_q\mathrm{GTP}] + k_{111bf}[\mathrm{RGS_a} \bullet \mathrm{G}\alpha_q\mathrm{GTP}] - k_{113f}[\mathrm{G}\alpha_q\mathrm{GDP}][\mathrm{G}\beta\gamma] \\
& +k_{15bf}[\mathrm{PLC}\beta4 \bullet \mathrm{Ca}^{2+} \bullet \mathrm{G}\alpha_q\mathrm{GTP} \bullet \mathrm{PIP2}] \\
& +k_{19bf}[\mathrm{PLC}\beta3 \bullet \mathrm{Ca} \bullet \mathrm{G}\alpha_q\mathrm{GTP} \bullet \mathrm{PIP2}] \\
\mathrm{d}[\mathrm{RGS_a}] = \; & -k_{9af}[\mathrm{RGS_a}][\mathrm{G}\alpha_i\mathrm{GTP}] + k_{9ar}[\mathrm{RGS_a} \bullet \mathrm{G}\alpha_i\mathrm{GTP}] + k_{9bf}[\mathrm{RGS_a} \bullet \mathrm{G}\alpha_i\mathrm{GTP}] \\
& -k_{111af}[\mathrm{RGS_a}][\mathrm{G}\alpha_q\mathrm{GTP}] + k_{111ar}[\mathrm{RGS_a} \bullet \mathrm{G}\alpha_q\mathrm{GTP}] \\
& +k_{111bf}[\mathrm{RGS_a} \bullet \mathrm{G}\alpha_q\mathrm{GTP}] \\
\mathrm{d}[\mathrm{RGS_a} \bullet \mathrm{G}\alpha_i\mathrm{GTP}] = \; & -k_{9ar}[\mathrm{RGS_a} \bullet \mathrm{G}\alpha_i\mathrm{GTP}] + k_{9af}[\mathrm{RGS_a}][\mathrm{G}\alpha_i\mathrm{GTP}] \\
& -k_{9bf}[\mathrm{RGS_a} \bullet \mathrm{G}\alpha_i\mathrm{GTP}] \\
\mathrm{d}[\mathrm{RGS_a} \bullet \mathrm{G}\alpha_q\mathrm{GTP}] = \; & -k_{111ar}[\mathrm{RGS_a} \bullet \mathrm{G}\alpha_q\mathrm{GTP}] + k_{111af}[\mathrm{RGS_a}][\mathrm{G}\alpha_q\mathrm{GTP}] \\
& -k_{111bf}[\mathrm{RGS_a} \bullet \mathrm{G}\alpha_q\mathrm{GTP}] \\
\mathrm{d}[\mathrm{PLC}\beta4] = \; & -k_{12f}[\mathrm{PLC}\beta4][\mathrm{Ca}^{2+}] + k_{12r}[\mathrm{PLC}\beta4 \bullet \mathrm{Ca}^{2+}] \\
\mathrm{d}[\mathrm{Ca}^{2+}] = \; & -k_{12f}[\mathrm{PLC}\beta4][\mathrm{Ca}^{2+}] + k_{12r}[\mathrm{PLC}\beta4 \bullet \mathrm{Ca}^{2+}] - k_{16f}[\mathrm{PLC}\beta3][\mathrm{Ca}^{2+}] \\
& +k_{16r}[\mathrm{PLC}\beta3 \bullet \mathrm{Ca}^{2+}] - k_{2f}[\mathrm{IP3R} \bullet \mathrm{IP3}][\mathrm{Ca}^{2+}] + k_{2r}[\mathrm{IP3R} \bullet \mathrm{IP3} \bullet \mathrm{Ca}^{2+}] \\
& -k_{3f}[\mathrm{IP3R}][\mathrm{Ca}^{2+}] + k_{3r}[\mathrm{IP3R} \bullet \mathrm{Ca}^{2+}] - k_{6f}[\mathrm{Ca}^{2+}][\mathrm{Buf}] \\
& +k_{6r}[\mathrm{Ca}^{2+} \bullet \mathrm{Buf}] - k_{34f}[\mathrm{PKC} \bullet \mathrm{DAG}][\mathrm{Ca}^{2+}]] + k_{34r}[\mathrm{PKC} \bullet \mathrm{DAG} \bullet \mathrm{Ca}^{2+}] \\
& -k_{35f}[\mathrm{PKC}][\mathrm{Ca}^{2+}] + k_{35r}[\mathrm{PKC} \bullet \mathrm{Ca}^{2+}] + \mathrm{c}_2 \\
& -(\mathrm{v}_1[\mathrm{IP3R} \bullet \mathrm{IP3}]^4 + \mathrm{v}_8)([\mathrm{Ca}^{2+}_{\mathrm{ER}}] - [\mathrm{Ca}^{2+}]) - \mathrm{v}_4 \tfrac{[\mathrm{Ca}^{2+}]^2}{[\mathrm{Ca}^{2+}]^2 + \mathrm{k}_4^2} \\
& +\mathrm{a}_1 - \mathrm{V}_{\mathrm{ex}} \tfrac{[\mathrm{Ca}^{2+}]}{\mathrm{K}_{\mathrm{ex}} + [\mathrm{Ca}^{2+}]} \\
\mathrm{d}[\mathrm{PLC}\beta4 \bullet \mathrm{Ca}^{2+}] = \; & -k_{12r}[\mathrm{PLC}\beta4 \bullet \mathrm{Ca}^{2+}] + k_{12f}[\mathrm{PLC}\beta4][\mathrm{Ca}^{2+}] \\
& -k_{13f}[\mathrm{PLC}\beta4 \bullet \mathrm{Ca}^{2+}][\mathrm{G}\alpha_q\mathrm{GTP}] \\
& +k_{13r}[\mathrm{PLC}\beta4 \bullet \mathrm{Ca}^{2+} \bullet \mathrm{G}\alpha_q\mathrm{GTP}] \\
& +k_{15bf}[\mathrm{PLC}\beta4 \bullet \mathrm{Ca}^{2+} \bullet \mathrm{G}\alpha_q\mathrm{GTP} \bullet \mathrm{PIP2}] \\
& -k_{24af}[\mathrm{PKC} \bullet \mathrm{DAG} \bullet \mathrm{Ca}^{2+}][\mathrm{PLC}\beta4 \bullet \mathrm{Ca}^{2+}] \\
& +k_{24ar}[\mathrm{PKC} \bullet \mathrm{DAG} \bullet \mathrm{Ca}^{2+} \bullet \mathrm{PLC}\beta4 \bullet \mathrm{Ca}^{2+}] + k_{115f}[\mathrm{PLC}\beta4 \bullet \mathrm{Ca}^{2+}_{\mathrm{p}}] \\
\mathrm{d}[\mathrm{PLC}\beta4 \bullet \mathrm{Ca}^{2+} \bullet \mathrm{G}\alpha_q\mathrm{GTP}] = \; & -k_{13r}[\mathrm{PLC}\beta4 \bullet \mathrm{Ca}^{2+} \bullet \mathrm{G}\alpha_q\mathrm{GTP}] + k_{13f}[\mathrm{PLC}\beta4 \bullet \mathrm{Ca}^{2+}][\mathrm{G}\alpha_q\mathrm{GTP}]
\end{aligned}
$$

$$
\begin{aligned}
& & & -k_{15af}[\mathrm{PLC}\beta4 \bullet \mathrm{Ca}^{2+} \bullet \mathrm{G}\alpha_q\mathrm{GTP}][\mathrm{PIP2}] \\
& & & +k_{15ar}[\mathrm{PLC}\beta4 \bullet \mathrm{Ca}^{2+} \bullet \mathrm{G}\alpha_q\mathrm{GTP} \bullet \mathrm{PIP2}] \\
& \mathrm{d}[\mathrm{PIP2}] = & & -k_{15af}[\mathrm{PLC}\beta4 \bullet \mathrm{Ca}^{2+} \bullet \mathrm{G}\alpha_q\mathrm{GTP}][\mathrm{PIP2}] \\
& & & +k_{15ar}[\mathrm{PLC}\beta4 \bullet \mathrm{Ca}^{2+} \bullet \mathrm{G}\alpha_q\mathrm{GTP} \bullet \mathrm{PIP2}] \\
& & & -k_{19af}[\mathrm{PLC}\beta3 \bullet \mathrm{Ca}^{2+} \bullet \mathrm{G}\alpha_q\mathrm{GTP}][\mathrm{PIP2}] \\
& & & +k_{19ar}[\mathrm{PLC}\beta3 \bullet \mathrm{Ca}^{2+} \bullet \mathrm{G}\alpha_q\mathrm{GTP} \bullet \mathrm{PIP2}] \\
& & & -k_{21af}[\mathrm{PLC}\beta3 \bullet \mathrm{Ca}^{2+} \bullet \mathrm{G}\beta\gamma][\mathrm{PIP2}] \\
& & & +k_{21ar}[\mathrm{PLC}\beta3 \bullet \mathrm{Ca}^{2+} \bullet \mathrm{G}\beta\gamma \bullet \mathrm{PIP2}] + k_{55f}[\mathrm{IP5}] \\
& \mathrm{d}[\mathrm{PLC}\beta4 \bullet \mathrm{Ca}^{2+} & & \\
& \bullet \mathrm{G}\alpha_q\mathrm{GTP} \bullet \mathrm{PIP2}] = & & -k_{15ar}[\mathrm{PLC}\beta4 \bullet \mathrm{Ca}^{2+} \bullet \mathrm{G}\alpha_q\mathrm{GTP} \bullet \mathrm{PIP2}] \\
& & & +k_{15af}[\mathrm{PLC}\beta4 \bullet \mathrm{Ca}^{2+} \bullet \mathrm{G}\alpha_q\mathrm{GTP}][\mathrm{PIP2}] \\
& & & -k_{15bf}[\mathrm{PLC}\beta4 \bullet \mathrm{Ca}^{2+} \bullet \mathrm{G}\alpha_q\mathrm{GTP} \bullet \mathrm{PIP2}] \\
& \mathrm{d}[\mathrm{IP3}] = & & +k_{15bf}[\mathrm{PLC}\beta4 \bullet \mathrm{Ca}^{2+} \bullet \mathrm{G}\alpha_q\mathrm{GTP} \bullet \mathrm{PIP2}] \\
& & & +k_{19bf}[\mathrm{PLC}\beta3 \bullet \mathrm{Ca}^{2+} \bullet \mathrm{G}\alpha_q\mathrm{GTP} \bullet \mathrm{PIP2}] \\
& & & +k_{21bf}[\mathrm{PLC}\beta3 \bullet \mathrm{Ca}^{2+} \bullet \mathrm{G}\beta\gamma \bullet \mathrm{PIP2}] \\
& & & -k_{1f}[\mathrm{IP3R}][\mathrm{IP3}] + k_{1r}[\mathrm{IP3R} \bullet \mathrm{IP3}] \\
& & & -k_{4f}[\mathrm{IP3R} \bullet \mathrm{Ca}^{2+}][\mathrm{IP3}] + k_{4r}[\mathrm{IP3R} \bullet \mathrm{IP3} \bullet \mathrm{Ca}^{2+}] - \mathrm{V}_{qssk}\frac{[\mathrm{IP3K_a}][\mathrm{IP3}]}{\mathrm{Kqssk}+[\mathrm{IP3}]} \\
& \mathrm{d}[\mathrm{DAG}] = & & +k_{15bf}[\mathrm{PLC}\beta4 \bullet \mathrm{Ca}^{2+} \bullet \mathrm{G}\alpha_q\mathrm{GTP} \bullet \mathrm{PIP2}] \\
& & & +k_{19bf}[\mathrm{PLC}\beta3 \bullet \mathrm{Ca}^{2+} \bullet \mathrm{G}\alpha_q\mathrm{GTP} \bullet \mathrm{PIP2}] \\
& & & +k_{21bf}[\mathrm{PLC}\beta3 \bullet \mathrm{Ca}^{2+} \bullet \mathrm{G}\beta\gamma \bullet \mathrm{PIP2}] \\
& & & -k_{33f}[\mathrm{PKC}][\mathrm{DAG}] + k_{33r}[\mathrm{PKC} \bullet \mathrm{DAG}] - k_{36f}[\mathrm{PKC} \bullet \mathrm{Ca}^{2+}][\mathrm{DAG}] \\
& & & +k_{36r}[\mathrm{PKC} \bullet \mathrm{DAG} \bullet \mathrm{Ca}^{2+}] - k_{49f}[\mathrm{DAG}] \\
& \mathrm{d}[\mathrm{PLC}\beta3] = & & -k_{16f}[\mathrm{PLC}\beta3][\mathrm{Ca}^{2+}] + k_{16r}[\mathrm{PLC}\beta3 \bullet \mathrm{Ca}^{2+}] \\
& \mathrm{d}[\mathrm{PLC}\beta3 \bullet \mathrm{Ca}^{2+}] = & & -k_{16r}[\mathrm{PLC}\beta3 \bullet \mathrm{Ca}^{2+}] + k_{16f}[\mathrm{PLC}\beta3][\mathrm{Ca}^{2+}] \\
& & & -k_{17f}[\mathrm{PLC}\beta3 \bullet \mathrm{Ca}^{2+}][\mathrm{G}\alpha_q\mathrm{GTP}] + k_{17r}[\mathrm{PLC}\beta3 \bullet \mathrm{Ca}^{2+} \bullet \mathrm{G}\alpha_q\mathrm{GTP}] \\
& & & +k_{19bf}[\mathrm{PLC}\beta3 \bullet \mathrm{Ca}^{2+} \bullet \mathrm{G}\alpha_q\mathrm{GTP} \bullet \mathrm{PIP2}] \\
& & & -k_{20f}[\mathrm{G}\beta\gamma][\mathrm{PLC}\beta3 \bullet \mathrm{Ca}^{2+}] + k_{20r}[\mathrm{PLC}\beta3 \bullet \mathrm{Ca}^{2+} \bullet \mathrm{G}\beta\gamma] \\
& & & -k_{25af}[\mathrm{PKC} \bullet \mathrm{DAG} \bullet \mathrm{Ca}^{2+}][\mathrm{PLC}\beta3 \bullet \mathrm{Ca}^{2+}] \\
& & & +k_{25ar}[\mathrm{PKC} \bullet \mathrm{DAG} \bullet \mathrm{Ca}^{2+} \bullet \mathrm{PLC}\beta3 \bullet \mathrm{Ca}^{2+}] + k_{117f}[\mathrm{PLC}\beta3 \bullet \mathrm{Ca}_p^{2+}] \\
& \mathrm{d}[\mathrm{PLC}\beta3 \bullet \mathrm{Ca}^{2+} \bullet \mathrm{G}\alpha_q\mathrm{GTP}] = & & -k_{17r}[\mathrm{PLC}\beta3 \bullet \mathrm{Ca}^{2+} \bullet \mathrm{G}\alpha_q\mathrm{GTP}] + k_{17f}[\mathrm{PLC}\beta3 \bullet \mathrm{Ca}^{2+}][\mathrm{G}\alpha_q\mathrm{GTP}] \\
& & & -k_{19af}[\mathrm{PLC}\beta3 \bullet \mathrm{Ca}^{2+} \bullet \mathrm{G}\alpha_q\mathrm{GTP}][\mathrm{PIP2}] \\
& & & +k_{19ar}[\mathrm{PLC}\beta3 \bullet \mathrm{Ca}^{2+} \bullet \mathrm{G}\alpha_q\mathrm{GTP} \bullet \mathrm{PIP2}]
\end{aligned}
$$

$$
\begin{aligned}
\mathrm{d}[\mathrm{PLC}\beta 3 \bullet \mathrm{Ca}^{2+} \bullet & \\
\mathrm{G}\alpha_\mathrm{q}\mathrm{GTP} \bullet \mathrm{PIP2}] = \; & -k_{19\mathrm{ar}}[\mathrm{PLC}\beta 3 \bullet \mathrm{Ca}^{2+} \bullet \mathrm{G}\alpha_\mathrm{q}\mathrm{GTP} \bullet \mathrm{PIP2}] \\
& +k_{19\mathrm{af}}[\mathrm{PLC}\beta 3 \bullet \mathrm{Ca}^{2+} \bullet \mathrm{G}\alpha_\mathrm{q}\mathrm{GTP}][\mathrm{PIP2}] \\
& -k_{19\mathrm{bf}}[\mathrm{PLC}\beta 3 \bullet \mathrm{Ca}^{2+} \bullet \mathrm{G}\alpha_\mathrm{q}\mathrm{GTP} \bullet \mathrm{PIP2}] \\
\mathrm{d}[\mathrm{PLC}\beta 3 \bullet \mathrm{Ca}^{2+} \bullet \mathrm{G}\beta\gamma] = \; & -k_{20\mathrm{r}}[\mathrm{PLC}\beta 3 \bullet \mathrm{Ca}^{2+} \bullet \mathrm{G}\beta\gamma] + k_{20\mathrm{f}}[\mathrm{G}\beta\gamma][\mathrm{PLC}\beta 3 \bullet \mathrm{Ca}^{2+}] \\
& -k_{21\mathrm{af}}[\mathrm{PLC}\beta 3 \bullet \mathrm{Ca}^{2+} \bullet \mathrm{G}\beta\gamma][\mathrm{PIP2}] + k_{21\mathrm{ar}}[\mathrm{PLC}\beta 3 \bullet \mathrm{Ca}^{2+} \bullet \mathrm{G}\beta\gamma \bullet \mathrm{PIP2}] \\
& +k_{21\mathrm{bf}}[\mathrm{PLC}\beta 3 \bullet \mathrm{Ca}^{2+} \bullet \mathrm{G}\beta\gamma \bullet \mathrm{PIP2}] \\
\mathrm{d}[\mathrm{PLC}\beta 3 \bullet \mathrm{Ca}^{2+} \bullet \mathrm{G}\beta\gamma \bullet \mathrm{PIP2}] = \; & -k_{21\mathrm{ar}}[\mathrm{PLC}\beta 3 \bullet \mathrm{Ca}^{2+} \bullet \mathrm{G}\beta\gamma \bullet \mathrm{PIP2}] + k_{21\mathrm{af}}[\mathrm{PLC}\beta 3 \bullet \mathrm{Ca}^{2+} \bullet \mathrm{G}\beta\gamma][\mathrm{PIP2}] \\
& -k_{21\mathrm{bf}}[\mathrm{PLC}\beta 3 \bullet \mathrm{Ca}^{2+} \bullet \mathrm{G}\beta\gamma \bullet \mathrm{PIP2}] \\
\mathrm{d}[\mathrm{PKC} \bullet \mathrm{DAG} \bullet \mathrm{Ca}^{2+}] = \; & -k_{24\mathrm{af}}[\mathrm{PKC} \bullet \mathrm{DAG} \bullet \mathrm{Ca}^{2+}][\mathrm{PLC}\beta 4 \bullet \mathrm{Ca}^{2+}] \\
& +k_{24\mathrm{ar}}[\mathrm{PKC} \bullet \mathrm{DAG} \bullet \mathrm{Ca}^{2+} \bullet \mathrm{PLC}\beta 4 \bullet \mathrm{Ca}^{2+}] \\
& +k_{24\mathrm{bf}}[\mathrm{PKC} \bullet \mathrm{DAG} \bullet \mathrm{Ca}^{2+} \bullet \mathrm{PLC}\beta 4 \bullet \mathrm{Ca}^{2+}] \\
& -k_{25\mathrm{af}}[\mathrm{PKC} \bullet \mathrm{DAG} \bullet \mathrm{Ca}^{2+}][\mathrm{PLC}\beta 3 \bullet \mathrm{Ca}^{2+}] \\
& +k_{25\mathrm{ar}}[\mathrm{PKC} \bullet \mathrm{DAG} \bullet \mathrm{Ca}^{2+} \bullet \mathrm{PLC}\beta 3 \bullet \mathrm{Ca}^{2+}] \\
& +k_{25\mathrm{bf}}[\mathrm{PKC} \bullet \mathrm{DAG} \bullet \mathrm{Ca}^{2+} \bullet \mathrm{PLC}\beta 3 \bullet \mathrm{Ca}^{2+}] \\
& -k_{34\mathrm{r}}[\mathrm{PKC} \bullet \mathrm{DAG} \bullet \mathrm{Ca}^{2+}] \\
& +k_{34\mathrm{f}}[\mathrm{PKC} \bullet \mathrm{DAG}][\mathrm{Ca}^{2+}] \\
& -k_{36\mathrm{r}}[\mathrm{PKC} \bullet \mathrm{DAG} \bullet \mathrm{Ca}^{2+}] \\
& +k_{36\mathrm{f}}[\mathrm{PKC} \bullet \mathrm{Ca}^{2+}][\mathrm{DAG}] \\
& -k_{28\mathrm{af}}[\mathrm{PKC} \bullet \mathrm{DAG} \bullet \mathrm{Ca}^{2+}][\mathrm{GRK}] \\
& +k_{28\mathrm{ar}}[\mathrm{PKC} \bullet \mathrm{DAG} \bullet \mathrm{Ca}^{2+} \bullet \mathrm{GRK}] \\
& +k_{28\mathrm{bf}}[\mathrm{PKC} \bullet \mathrm{DAG} \bullet \mathrm{Ca}^{2+} \bullet \mathrm{GRK}] \\
\mathrm{d}[\mathrm{PKC} \bullet \mathrm{DAG} \bullet & \\
\mathrm{Ca}^{2+} \bullet \mathrm{PLC}\beta 4 \bullet \mathrm{Ca}^{2+}] = \; & -k_{24\mathrm{ar}}[\mathrm{PKC} \bullet \mathrm{DAG} \bullet \mathrm{Ca}^{2+} \bullet \mathrm{PLC}\beta 4 \bullet \mathrm{Ca}^{2+}] \\
& +k_{24\mathrm{af}}[\mathrm{PKC} \bullet \mathrm{DAG} \bullet \mathrm{Ca}^{2+}][\mathrm{PLC}\beta 4 \bullet \mathrm{Ca}^{2+}] \\
& -k_{24\mathrm{bf}}[\mathrm{PKC} \bullet \mathrm{DAG} \bullet \mathrm{Ca}^{2+} \bullet \mathrm{PLC}\beta 4 \bullet \mathrm{Ca}^{2+}] \\
\mathrm{d}[\mathrm{PLC}\beta 4 \bullet \mathrm{Ca}^{2+}_\mathrm{p}] = \; & +k_{24\mathrm{bf}}[\mathrm{PKC} \bullet \mathrm{DAG} \bullet \mathrm{Ca}^{2+} \bullet \mathrm{PLC}\beta 4 \bullet \mathrm{Ca}^{2+}] \\
& -k_{115\mathrm{f}}[\mathrm{PLC}\beta 4 \bullet \mathrm{Ca}^{2+} \bullet \mathrm{p}] \\
\mathrm{d}[\mathrm{PKC} \bullet \mathrm{DAG} \bullet & \\
\mathrm{Ca}^{2+} \bullet \mathrm{PLC}\beta 3 \bullet \mathrm{Ca}^{2+}] = \; & -k_{25\mathrm{ar}}[\mathrm{PKC} \bullet \mathrm{DAG} \bullet \mathrm{Ca}^{2+} \bullet \mathrm{PLC}\beta 3 \bullet \mathrm{Ca}^{2+}] \\
& +k_{25\mathrm{af}}[\mathrm{PKC} \bullet \mathrm{DAG} \bullet \mathrm{Ca}^{2+}][\mathrm{PLC}\beta 3 \bullet \mathrm{Ca}^{2+}] \\
& -k_{25\mathrm{bf}}[\mathrm{PKC} \bullet \mathrm{DAG} \bullet \mathrm{Ca}^{2+} \bullet \mathrm{PLC}\beta 3 \bullet \mathrm{Ca}^{2+}]
\end{aligned}
$$

$$
\begin{aligned}
\mathrm{d}[\mathrm{PLC}\beta 3 \bullet \mathrm{Ca}_{\mathrm{p}}^{2+}] = \; & +k_{25\mathrm{bf}}[\mathrm{PKC} \bullet \mathrm{DAG} \bullet \mathrm{Ca}^{2+} \bullet \mathrm{PLC}\beta 3 \bullet \mathrm{Ca}^{2+}] \\
& -k_{117\mathrm{f}}[\mathrm{PLC}\beta 3 \bullet \mathrm{Ca}^{2+} \bullet \mathrm{p}] \\
\mathrm{d}[\mathrm{IP3R}] = \; & -k_{1\mathrm{f}}[\mathrm{IP3R}][\mathrm{IP3}] \\
& +k_{1\mathrm{r}}[\mathrm{IP3R} \bullet \mathrm{IP3}] - k_{3\mathrm{f}}[\mathrm{IP3R}][\mathrm{Ca}^{2+}] \\
& +k_{3\mathrm{r}}[\mathrm{IP3R} \bullet \mathrm{Ca}^{2+}] \\
\mathrm{d}[\mathrm{IP3R} \bullet \mathrm{IP3}] = \; & -k_{1\mathrm{r}}[\mathrm{IP3R} \bullet \mathrm{IP3}] \\
& +k_{1\mathrm{f}}[\mathrm{IP3R}][\mathrm{IP3}] - k_{2\mathrm{f}}[\mathrm{IP3R} \bullet \mathrm{IP3}][\mathrm{Ca}^{2+}] \\
& +k_{2\mathrm{r}}[\mathrm{IP3R} \bullet \mathrm{IP3} \bullet \mathrm{Ca}^{2+}] \\
\mathrm{d}[\mathrm{IP3R} \bullet \mathrm{IP3} \bullet \mathrm{Ca}^{2+}] = \; & -k_{2\mathrm{r}}[\mathrm{IP3R} \bullet \mathrm{IP3} \bullet \mathrm{Ca}^{2+}] \\
& +k_{2\mathrm{f}}[\mathrm{IP3R} \bullet \mathrm{IP3}][\mathrm{Ca}^{2+}] - k_{4\mathrm{r}}[\mathrm{IP3R} \bullet \mathrm{IP3} \bullet \mathrm{Ca}^{2+}] \\
& +k_{4\mathrm{f}}[\mathrm{IP3R} \bullet \mathrm{Ca}^{2+}][\mathrm{IP3}] \\
\mathrm{d}[\mathrm{IP3R} \bullet \mathrm{Ca}^{2+}] = \; & -k_{3\mathrm{r}}[\mathrm{IP3R} \bullet \mathrm{Ca}^{2+}] \\
& +k_{3\mathrm{f}}[\mathrm{IP3R}][\mathrm{Ca}^{2+}] - k_{4\mathrm{f}}[\mathrm{IP3R} \bullet \mathrm{Ca}^{2+}][\mathrm{IP3}] \\
& +k_{4\mathrm{r}}[\mathrm{IP3R} \bullet \mathrm{IP3} \bullet \mathrm{Ca}^{2+}] \\
\mathrm{d}[\mathrm{Buf}] = \; & -k_{6\mathrm{f}}[\mathrm{Ca}^{2+}][\mathrm{Buf}] + k_{6\mathrm{r}}[\mathrm{Ca}^{2+} \bullet \mathrm{Buf}] \\
\mathrm{d}[\mathrm{Ca}^{2+} \bullet \mathrm{Buf}] = \; & -k_{6\mathrm{r}}[\mathrm{Ca}^{2+} \bullet \mathrm{Buf}] + k_{6\mathrm{f}}[\mathrm{Ca}^{2+}][\mathrm{Buf}] \\
\mathrm{d}[\mathrm{Ca}_{\mathrm{ER}}^{2+}] = \; & -(\mathrm{v}_1[\mathrm{IP3R} \bullet \mathrm{IP3}]^4 + \mathrm{v}8)([\mathrm{Ca}_{\mathrm{ER}}^{2+}] - [\mathrm{Ca}^{2+}]) \\
& +(1/c2)v_4 \tfrac{[\mathrm{Ca}^{2+}]^2}{[\mathrm{Ca}^{2+}]^2 + k_4^2} \\
\mathrm{d}[\mathrm{PKC}] = \; & -k_{33\mathrm{f}}[\mathrm{PKC}][\mathrm{DAG}] + k_{33\mathrm{r}}[\mathrm{PKC} \bullet \mathrm{DAG}] \\
& -k_{35\mathrm{f}}[\mathrm{PKC}][\mathrm{Ca}^{2+}] + k_{35\mathrm{r}}[\mathrm{PKC} \bullet \mathrm{Ca}^{2+}] \\
\mathrm{d}[\mathrm{PKC} \bullet \mathrm{DAG}] = \; & -k_{33\mathrm{r}}[\mathrm{PKC} \bullet \mathrm{DAG}] \\
& +k_{33\mathrm{f}}[\mathrm{PKC}][\mathrm{DAG}] - k_{34\mathrm{f}}[\mathrm{PKC} \bullet \mathrm{DAG}][\mathrm{Ca}^{2+}] \\
& +k_{34\mathrm{r}}[\mathrm{PKC} \bullet \mathrm{DAG} \bullet \mathrm{Ca}^{2+}] \\
\mathrm{d}[\mathrm{PKC} \bullet \mathrm{Ca}^{2+}] = \; & -k_{35\mathrm{r}}[\mathrm{PKC} \bullet \mathrm{Ca}^{2+}] \\
& +k_{35\mathrm{f}}[\mathrm{PKC}][\mathrm{Ca}^{2+}] - k_{36\mathrm{f}}[\mathrm{PKC} \bullet \mathrm{Ca}^{2+}][\mathrm{DAG}] \\
& +k_{36\mathrm{r}}[\mathrm{PKC} \bullet \mathrm{DAG} \bullet \mathrm{Ca}^{2+}] \\
\mathrm{d}[\mathrm{GRKp}] = \; & -k_{37\mathrm{f}}[\mathrm{GRKp}][\mathrm{G}\beta\gamma] + k_{37\mathrm{r}}[\mathrm{GRKp} \bullet \mathrm{G}\beta\gamma] \\
& +k_{28\mathrm{bf}}[\mathrm{PKC} \bullet \mathrm{DAG} \bullet \mathrm{Ca}^{2+} \bullet \mathrm{GRK}] \\
\mathrm{d}[\mathrm{GRK}] = \; & -k_{28\mathrm{af}}[\mathrm{PKC} \bullet \mathrm{DAG} \bullet \mathrm{Ca}^{2+}][\mathrm{GRK}] + k_{28\mathrm{ar}}[\mathrm{PKC} \bullet \mathrm{DAG} \bullet \mathrm{Ca}^{2+} \bullet \mathrm{GRK}] \\
\mathrm{d}[\mathrm{PKC} \bullet \mathrm{DAG} \bullet \mathrm{Ca}^{2+} \bullet \mathrm{GRK}] = \; & -k_{28\mathrm{ar}}[\mathrm{PKC} \bullet \mathrm{DAG} \bullet \mathrm{Ca}^{2+} \bullet \mathrm{GRK}] + k_{28\mathrm{af}}[\mathrm{PKC} \bullet \mathrm{DAG} \bullet \mathrm{Ca}^{2+}][\mathrm{GRK}] \\
& -k_{28\mathrm{bf}}[\mathrm{PKC} \bullet \mathrm{DAG} \bullet \mathrm{Ca}^{2+} \bullet \mathrm{GRK}] \\
\mathrm{d}[\mathrm{DAG}_{\mathrm{d}}] = \; & +k_{49\mathrm{f}}[\mathrm{DAG}]
\end{aligned}
$$

$$
\begin{aligned}
\mathrm{d}[\mathrm{IP3K_a}] &= \quad 0 \\
\mathrm{d}[\mathrm{IP4}] &= \quad +\mathrm{Vqssk50}\frac{[\mathrm{IP3K_a}][\mathrm{IP3}]}{\mathrm{K_{qssk50}}+[\mathrm{IP3}]} - \mathrm{V_{maxk54}}\frac{[\mathrm{IP4}]}{\mathrm{K_{mk54}}+[\mathrm{IP4}]} \\
\mathrm{d}[\mathrm{IP5}] &= \quad +\mathrm{V_{maxk54}}\frac{[\mathrm{IP4}]}{\mathrm{K_{mk54}}+[\mathrm{IP4}]} - k_{55\mathrm{f}}[\mathrm{IP5}]
\end{aligned}
$$

Table A.1: Model Equations

A.2 Model Parameters

Constant	Prior	MAP	Unit	Description
k108f*	1.628	13.20	$\mu M^{-1}\ s^{-1}$	UDP + p2yr → UDPC
k108r*	0.165	3.62	s^{-1}	UDP + p2yr ← UDPC
k101f*	12.14	92.41	$\mu M^{-1}\ s^{-1}$	c5a + c5aR → c5aC
k101r*	0.0378	0.376	s^{-1}	c5a + c5aR ← c5aC
k102af	591.5	591.5	$\mu M^{-1} s^{-1}$	GRKp-G$\beta\gamma$ + c5aC → GRKp-G$\beta\gamma$-c5aC
k102ar	12.37	12.37	s^{-1}	GRKp-G$\beta\gamma$ + c5aC ← GRKp-G$\beta\gamma$-c5aC
k102bf*	123.3	199.3	s^{-1}	GRKp-G$\beta\gamma$-c5aC → GRKp-G$\beta\gamma$ + c5aCp
k104f	0.0001	0.0001	s^{-1}	c5aCp → c5aR + c5a
k105f*	0.0946	0.0129	$\mu M^{-1}\ s^{-1}$	c5aC + G$\beta\gamma$-Gα_i-GDP → c5aC + G$\beta\gamma$ + Gα_i-GTP
k106f	0.022	0.022	s^{-1}	Gα_i-GTP → Gα_i-GDP
k109f*	0.269	0.137	$\mu M^{-1}\ s^{-1}$	UDPC + G$\beta\gamma$-Gα_q-GDP → UDPC + G$\beta\gamma$ + Gα_q-GTP
k110f	0.022	0.022	s^{-1}	Gα_q-GTP → Gα_q-GDP
k11f	7000	7000	$\mu M^{-1}\ s^{-1}$	Gα_i-GDP + G$\beta\gamma$ → G$\beta\gamma$-Gα_i-GDP
k113f	7000	7000	$\mu M^{-1}\ s^{-1}$	Gα_q-GDP + G$\beta\gamma$ → G$\beta\gamma$-Gα_q-GDP
k9af	100	100	$\mu M^{-1}\ s^{-1}$	RGS$_a$ + Gα_i-GTP → RGS$_a$-Gα_i-GTP
k9ar	0.1	0.1	s^{-1}	RGS$_a$ + Gα_i-GTP ← RGS$_a$-Gα_i-GTP
k9bf	100	100	s^{-1}	RGS$_a$-Gα_i-GTP → RGS$_a$ + Gα_i-GDP
k111af	100	100	$\mu M^{-1}\ s^{-1}$	RGS$_a$ + Gα_q-GTP → RGS$_a$-Gα_q-GTP
k111ar	0.1	0.1	s^{-1}	RGS$_a$ + Gα_q-GTP ← RGS$_a$-Gα_q-GTP
k111bf	100	100	s^{-1}	RGS$_a$-Gα_q-GTP → RGS$_a$ + Gα_q-GDP
k12f	20	20	$\mu M^{-1}\ s^{-1}$	PLCβ4 + Ca → PLCβ4-Ca^{2+}
k12r	8	8	s^{-1}	PLCβ4 + Ca^{2+} ← PLCβ4-Ca^{2+}
k13f	62.55	62.55	$\mu M^{-1}\ s^{-1}$	PLCβ4-Ca^{2+} + Gα_q-GTP → PLCβ4-Ca^{2+}-Gα_q-GTP
k13r	10.63	10.63	s^{-1}	PLCβ4-Ca^{2+} + Gα_q-GTP ← PLCβ4-Ca^{2+}-Gα_q-GTP
k15af*	100	1238.7	$\mu M^{-1}\ s^{-1}$	PLCβ4-Ca^{2+}-Gα_q-GTP + PIP2 → PLCβ4-Ca^{2+}-Gα_q-GTP-PIP2
k15ar	1	1	s^{-1}	PLCβ4-Ca^{2+}-Gα_q-GTP + PIP2 ← PLCβ4-Ca^{2+}-Gα_q-GTP-PIP2

Constant	Prior	MAP	Unit	Description
k15bf*	3	22.85	s^{-1}	PLCβ4-Ca^{2+}-Gα_q-GTP-PIP2 → PLCβ4-Ca^{2+} + Gα_q-GDP + IP3 + DAG
k16f	20	20	μM^{-1} s^{-1}	PLCβ3 + Ca^{2+} → PLCβ3-Ca^{2+}
k16r	8	8	s^{-1}	PLCβ3 + Ca^{2+} ← PLCβ3-Ca^{2+}
k17f	50	50	μM^{-1} s^{-1}	PLCβ3-Ca^{2+} + Gα_q-GTP → PLCβ3-Ca^{2+}-Gα_q-GTP
k17r	0.1	0.1	s^{-1}	PLCβ3-Ca^{2+} + Gα_q-GTP ← PLCβ3-Ca^{2+}-Gα_q-GTP
k19af*	100	70.88	μM^{-1} s^{-1}	PLCβ3-Ca^{2+}-Gα_q-GTP + PIP2 → PLCβ3-Ca^{2+}-Gα_q-GTP-PIP2
k19ar	1	1	s^{-1}	PLCβ3-Ca^{2+}-Gα_q-GTP + PIP2 ← PLCβ3-Ca^{2+}-Gα_q-GTP-PIP2
k19bf*	3	27.90	s^{-1}	PLCβ3-Ca^{2+}-Gα_q-GTP-PIP2 → PLCβ3-Ca^{2+} + Gα_q-GDP + IP3 + DAG
k20f	8.35	8.35	μM^{-1} s^{-1}	G$\beta\gamma$ + PLCβ3-Ca^{2+} → PLCβ3-Ca^{2+}-G$\beta\gamma$
k20r	0.388	0.388	s^{-1}	G$\beta\gamma$ + PLCβ3-Ca^{2+} ← PLCβ3-Ca^{2+}-G$\beta\gamma$
k21af*	80	165.83	μM^{-1} s^{-1}	PLCβ3-Ca^{2+}-G$\beta\gamma$ + PIP2 → PLCβ3-Ca^{2+}-G$\beta\gamma$-PIP2
k21ar	8	8	s^{-1}	PLCβ3-Ca^{2+}-G$\beta\gamma$ + PIP2 ← PLCβ3-Ca^{2+}-G$\beta\gamma$-PIP2
k21bf*	1	0.931	s^{-1}	PLCβ3-Ca^{2+}-G$\beta\gamma$-PIP2 → PLCβ3-Ca^{2+}-G$\beta\gamma$ + IP3 + DAG
k24af*	10	5.42	μM^{-1} s^{-1}	PKC-DAG-Ca^{2+} + PLCβ4-Ca^{2+} → PKC-DAG-Ca^{2+}-PLCβ4-Ca^{2+}
k24ar	11	11	s^{-1}	PKC-DAG-Ca^{2+} + PLCβ4-Ca^{2+} ← PKC-DAG-Ca^{2+}-PLCβ4-Ca^{2+}
k24bf*	1	0.93	s^{-1}	PKC-DAG-Ca^{2+}-PLCβ4-Ca^{2+} → PKC-DAG-Ca^{2+} + PLCβ4-Ca^{2+} p
k25af*	110	830.44	μM^{-1} s^{-1}	PKC-DAG-Ca^{2+} + PLCβ3-Ca^{2+} → PKC-DAG-Ca^{2+}-PLCβ3-Ca^{2+}
k25ar	11	11	s^{-1}	PKC-DAG-Ca^{2+} + PLCβ3-Ca^{2+} ← PKC-DAG-Ca^{2+}-PLCβ3-Ca^{2+}
k25bf*	1	11.69	s^{-1}	PKC-DAG-Ca^{2+}-PLCβ3-Ca^{2+} → PKC-DAG-Ca^{2+} + PLCβ3-Ca^{2+} p
k115f	0.12	0.12	s^{-1}	PLCβ4-Ca^{2+} p → PLCβ4-Ca^{2+}

Constant	Prior	MAP	Unit	Description
k117f	0.12	0.12	s^{-1}	PLCβ3-Ca^{2+} p → PLCβ3-Ca^{2+}
k1f	177.47	177.47	μM^{-1} s^{-1}	IP3R + IP3 → IP3R-IP3
k1r	2.2	2.2	s^{-1}	IP3R + IP3 ← IP3R-IP3
k2f	0.411	0.411	μM^{-1} s^{-1}	IP3R-IP3 + Ca^{2+} → IP3R-IP3-Ca^{2+}
k2r	0.0434	0.0434	s^{-1}	IP3R-IP3 + Ca^{2+} ← IP3R-IP3-Ca^{2+}
k3f	0.9	0.9	μM^{-1} s^{-1}	IP3R + Ca^{2+} → IP3R-Ca^{2+}
k3r	0.806	0.806	s^{-1}	IP3R + Ca^{2+} ← IP3R-Ca^{2+}
k4f	20	20	μM^{-1} s^{-1}	IP3R-Ca^{2+} + IP3 → IP3R-IP3-Ca^{2+}
k4r	0.029	0.029	s^{-1}	IP3R-Ca^{2+} + IP3 ← IP3R-IP3-Ca^{2+} (thermcycle)
k6f	10	10	μM^{-1} s^{-1}	Ca^{2+} + Buf → CaBuf
k6r	7	7	s^{-1}	Ca^{2+} + Buf ← CaBuf
k33f	100	100	μM^{-1} s^{-1}	PKC + DAG → PKC-DAG
k33r	0.05	0.05	s^{-1}	PKC + DAG ← PKC-DAG
k34f	10	10	μM^{-1} s^{-1}	PKC-DAG + Ca^{2+} → PKC-DAG-Ca^{2+}
k34r	6	6	s^{-1}	PKC-DAG + Ca^{2+} ← PKC-DAG-Ca^{2+} (thermcycle)
k35f	0.01	0.01	μM^{-1} s^{-1}	PKC + Ca^{2+} → PKC-Ca^{2+}
k35r	0.01	0.01	s^{-1}	PKC + Ca^{2+} ← PKC-Ca^{2+}
k36f	1000	1000	μM^{-1} s^{-1}	PKC-Ca^{2+} + DAG → PKC-DAG-Ca^{2+}
k36r	0.0001	0.0001	s^{-1}	PKC-Ca^{2+} + DAG ← PKC-DAG-Ca^{2+}
k37f*	1	4.98	μM^{-1} s^{-1}	GRKp + G$\beta\gamma$ → GRKp-G$\beta\gamma$
k37r	0.05	0.05	s^{-1}	GRKp + G$\beta\gamma$ ← GRKp-G$\beta\gamma$
k28af*	158.49	77.52	μM^{-1} s^{-1}	PKC-DAG-Ca^{2+} + GRK → PKC-DAG-Ca^{2+}-GRK
k28ar	10	10	s^{-1}	PKC-DAG-Ca^{2+} + GRK ← PKC-DAG-Ca^{2+}-GRK
k28bf*	10	18.35	s^{-1}	PKC-DAG-Ca^{2+}-GRK → PKC-DAG-Ca^{2+} + GRKp
k49f	0.35	0.35	s^{-1}	DAG → DAG-d
Vqssk50	13.9	13.9	s^{-1}	IP3 + IP3K-a → IP4 + IP3K-a (Vmax)
Kqssk50	0.0557	0.0557	μM	IP3 + IP3K-a → IP4 + IP3K-a (Km)
Vmaxk54	100	100	$\mu M s^{-1}$	IP4 → IP5
Kmk54	1.4	1.4	μM	IP4 → IP5
k55f	0.008	0.008	s^{-1}	IP5 → PIP2
c2	0.185	0.185	none	ratio of ER volume/cell: de young

Constant	Prior	MAP	Unit	Description
v1	1×10^8	1×10^8	s^{-1}	Ca^{2+} channel flux constant
v8	0.15	0.15	s^{-1}	leak flux constant
v4	20	20	$\mu M s^{-1}$	maximum Ca^{2+} uptake rate
k4	0.65	0.65	μM	activation constant of pump
a1	0.0055	0.0055	s^{-1}	Ca^{2+} leak into the cell from outside
Kex	0.25	0.25	μM	Na/Ca^{2+} exchange activation const
Vex	0.023	0.023	$\mu M s^{-1}$	maximum Ca^{2+} exchange rate

Table A.2: Model Parameters

A.3 Initial State Values

Name	Initial Value (μM)	Molecules	Description
C5aR	5.00E-02	30100	C5a receptor concentration
p2yr	1.00E-01	60200	P2YX receptor concentration
G$\beta\gamma$	7.14E+00	430000	Gbg concentration
Gα_{i} GDP	6.64E+00	4000000	Gai concentration
Gα_{q} GDP	4.98E-01	30000	Gaq concentration
PLCβ3	1.16E-01	70000	PLCb3 concentration
PLCβ4	6.64E-02	40000	PLCb4 concentration
PIP2	5.00E-01	301000	Phosphoinositol (1,4,5) phosphate
IP3	1.80E-03	1084	Free IP3 concentration
DAG	1.00E-03	602	Free DAG concentration
IP3R	2.08E-02	12492	IP3 receptor concentration
IP3R-IP3	1.75E-03	1054	
IP3R-IP3-Ca	2.30E-03	1385	
IP3R-Ca	2.00E-04	120	
Ca^{2+}	7.86E-02	47317	Cytosolic Calcium concentration
Ca^{2+}_{ER}	1.04E+01	6231302	IP3 sensitive stored calcium concentration
PKC	2.49E-02	15000	Protein Kinase C
GRK	2.31E-02	13880	GRK concentration
RGS_{a}	2.31E-02	13880	Regulator of G protein Signaling
Buf	4.50E-01	270599	
Ca^{2+}-Buf	5.05E-02	30401	
$IP3K_{\mathrm{a}}$	1.66E-03	1000	
IP4	1.00E-01	60200	
IP5	1.00E-01	60200	

Table A.3: Initial State Values

Appendix B

Supplementary Simulations

B.1 Toxin Response

B.1.1 Pertussis Toxin

B.1.2 U-73122 Toxin

B.1.3 Calphostin-C Toxin

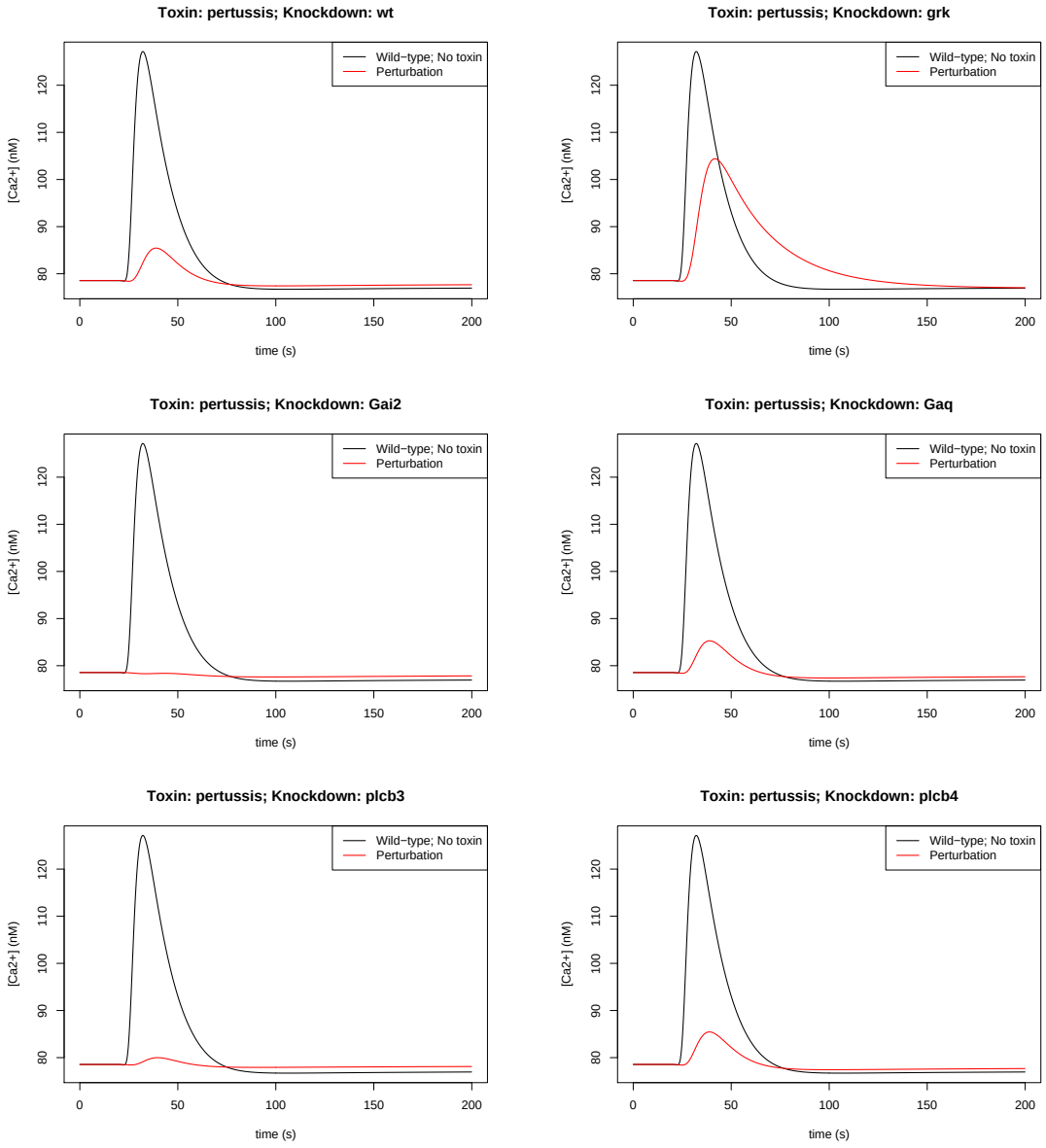

Figure B.1: These simulations show the effect of pretreatment with pertussis toxin on wild-type and knockdown cell lines in the model when stimulated by 250nM C5a.

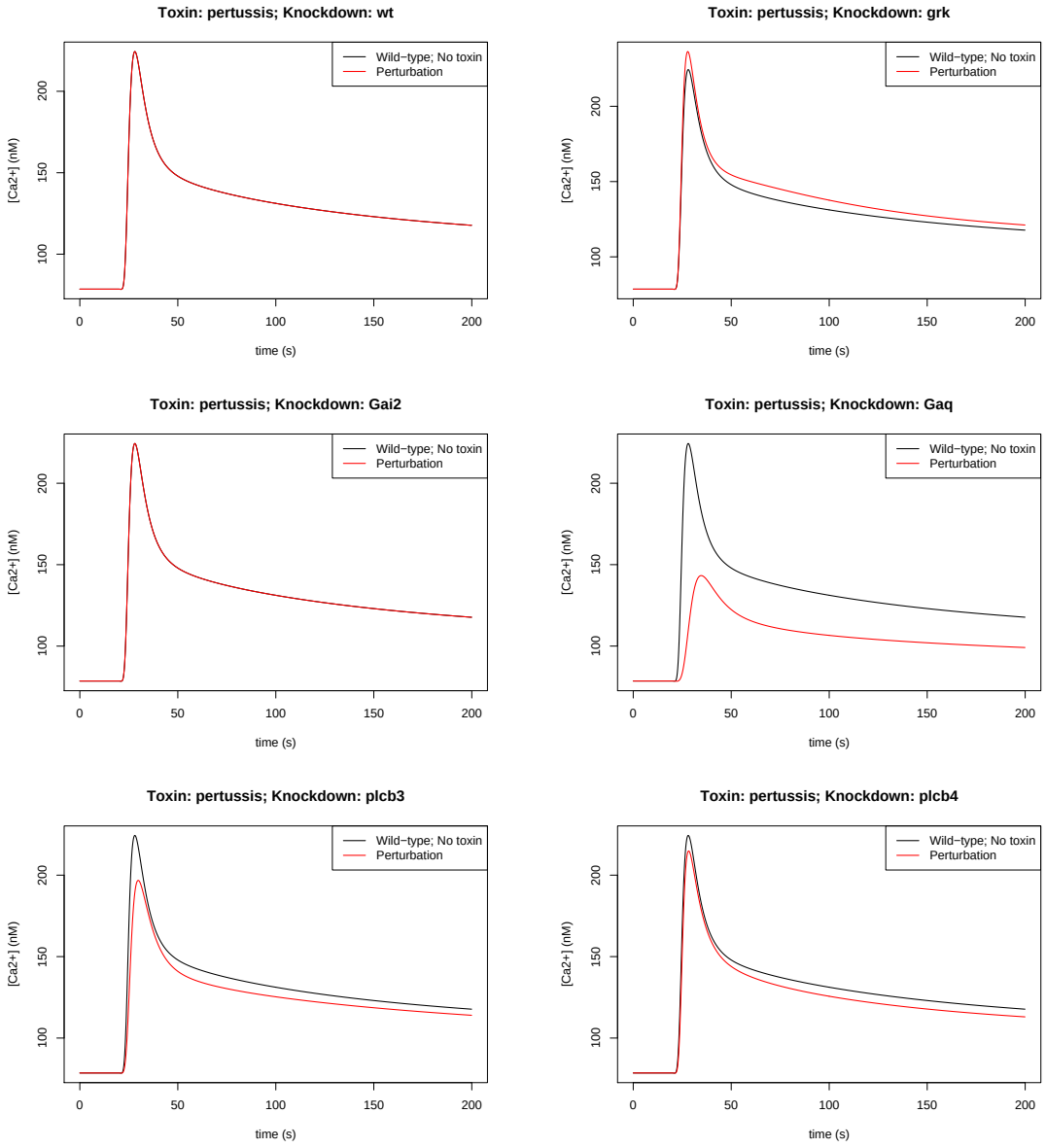

Figure B.2: These simulations show the effect of pretreatment with pertussis toxin on wild-type and knockdown cell lines in the model when stimulated by 25μM UDP.

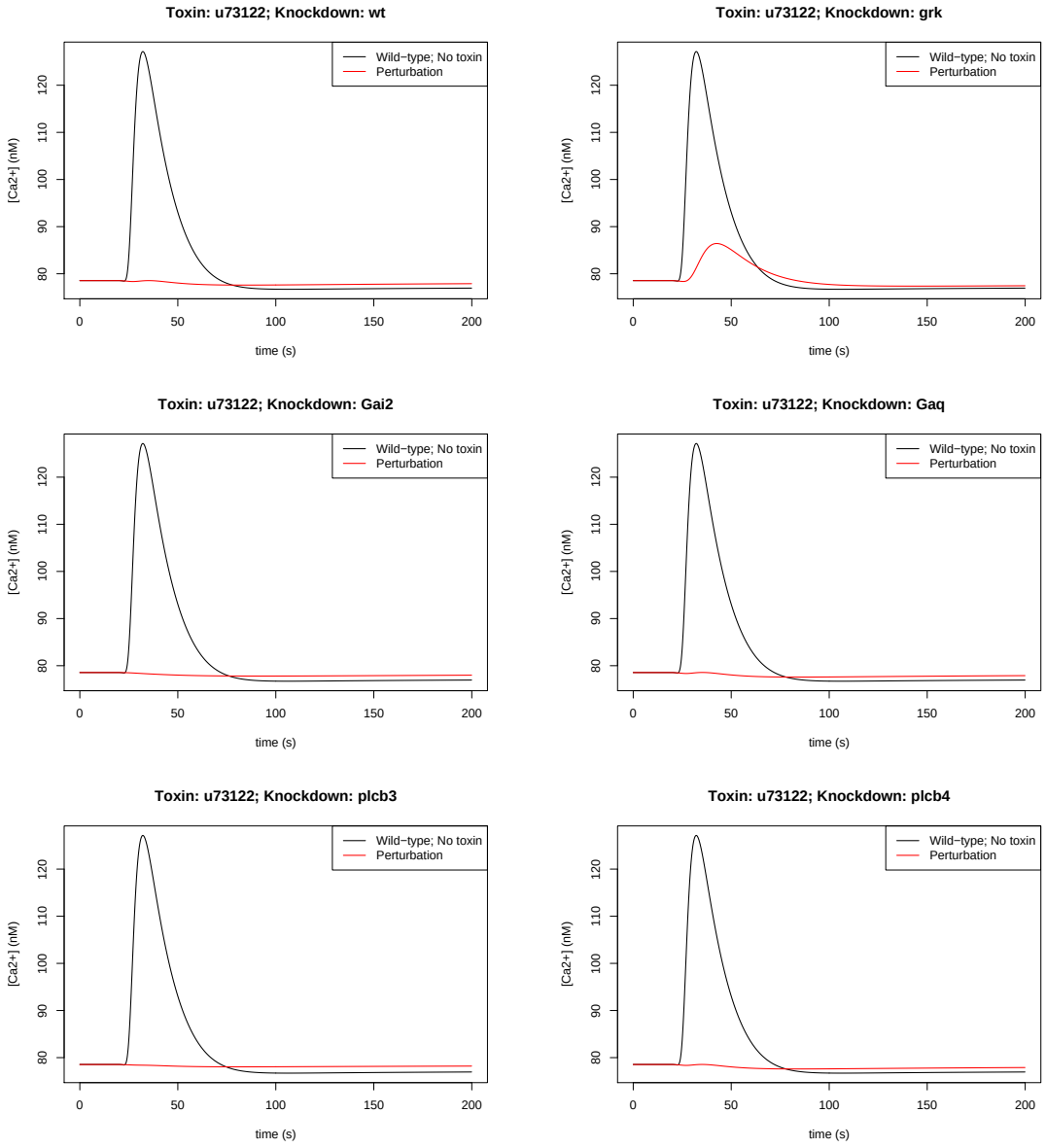

Figure B.3: These simulations show the effect of pretreatment with U-73122 toxin on wild-type and knockdown cell lines in the model when stimulated by 250nM C5a.

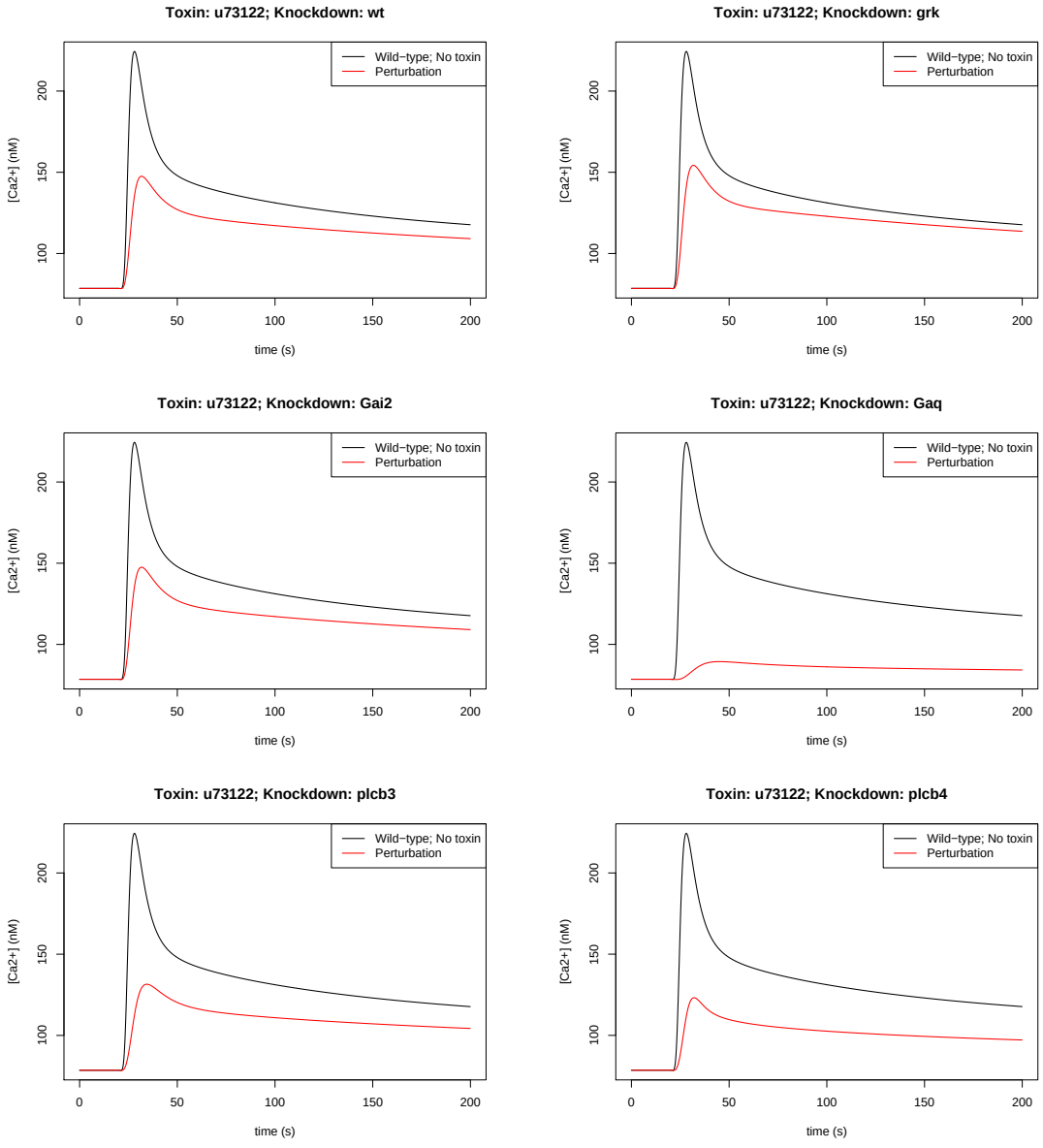

Figure B.4: These simulations show the effect of pretreatment with U-73122 toxin on wild-type and knockdown cell lines in the model when stimulated by 25μM UDP.

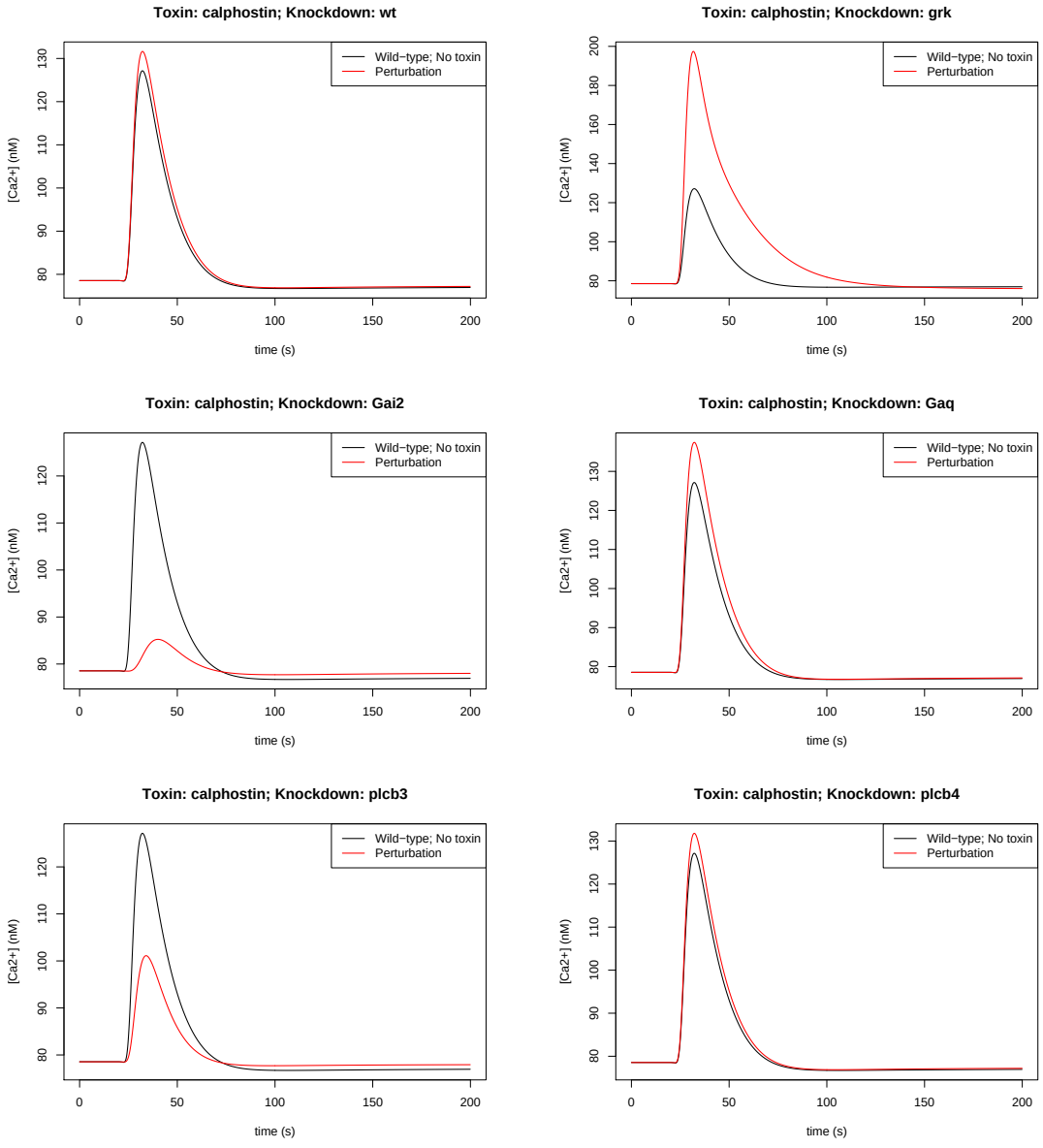

Figure B.5: These simulations show the effect of pretreatment with Calphostin-C toxin on wild-type and knockdown cell lines in the model when stimulated by 250nM C5a.

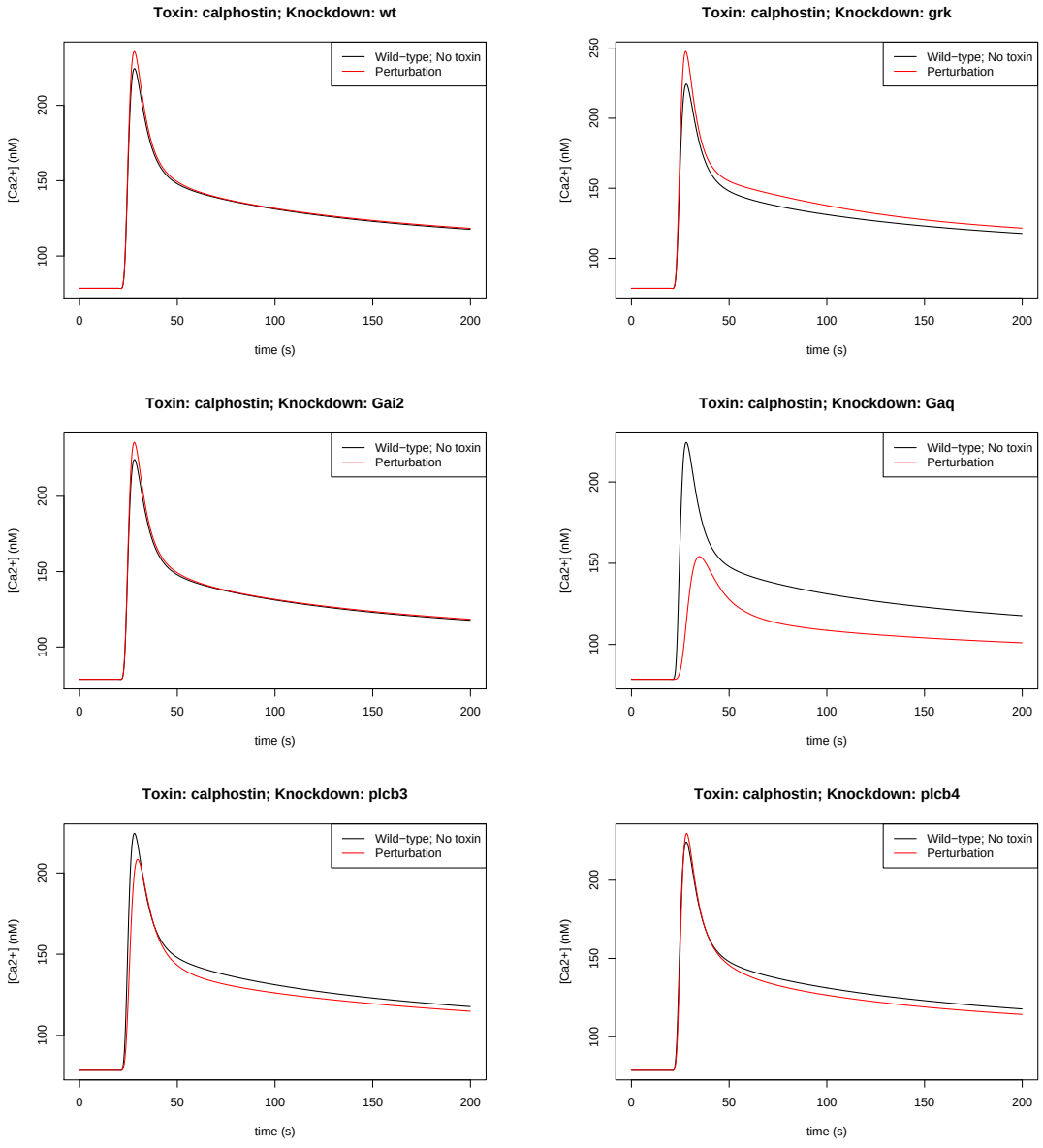

Figure B.6: These simulations show the effect of pretreatment with Calphostin-C toxin on wild-type and knockdown cell lines in the model when stimulated by 25μM UDP.